UNIVERSITÀ DEGLI STUDI DI GENOVA

SCUOLA POLITECNICA

DIPARTIMENTO DI INGEGNERIA NAVALE, ELETTRICA, ELETTRONICA E DELLE TELECOMUNICAZIONI (DITEN)

TESI DI DOTTORATO DI RICERCA IN SCIENZE E TECNOLOGIE PER L'INGEGNERIA ELETTRICA, L'INGEGNERIA NAVALE, I SISTEMI COMPLESSI PER LA MOBILITÀ
CURRICULUM INGEGNERIA NAVALE
CICLO XXXI

Analisi di strutture vetrate a bordo di super e mega yacht

SETTORE SCIENTIFICO-DISCIPLINARE: **ING-IND/02**

CANDIDATO: **Gianmarco Vergassola**

TUTOR: **Prof. Dario Boote**

COORDINATORE: **Prof. Mario Marchesoni**

ANNO ACCADEMICO: 2017/2018

UNIVERSITÀ DEGLI STUDI DI GENOVA

POLITECHNICAL SCHOOL

DEPARTMENT OF MARINE, ELECTRICAL, ELECTRONIC AND TELECOMMUNICATIONS ENGINEERING (DITEN)

PHILOSOPHY DOCTORATE IN DOCTORAL THESIS IN SCIENCE AND TECHONOLOGY FOR ELECTRICAL ENGINEERING, MARINE ENGINEERING, COMPLEX SYSTEMS FOR MOBILITY
CURRICULUM MARINE ENGINEERING
XXXI CYCLE

Analysis of window structures for super and megayachts

SUBJECT AREA: **ING-IND/02**

CANDIDATE: **Gianmarco Vergassola**

TUTOR: **Prof. Dario Boote**

COORDINATOR: **Prof. Mario Marchesoni**

ACADEMICAL YEAR: 2017/2018

Table of contents

Nomenclature

ABN	Air borne noise
CFM	Circle fit method
DEET	Dynamic effective enhanced thickness
DLF	Damping loss factor
EDT	Early decay time
EET	Effective enhanced thickness
ERP	Effective radiated power
FE/FEA/FEM	Finite Element (Method/Analysis
FFT	Fast Fourier Transform
FRF	Frequency response function
GT	Gross tonnage
HPBM	Half power bandwidth method
NVH	Noise, Vibration and Harshness
ISO	International Organization for Standardization
LDM	Logarithmic decrement method
MD	Main deck
PVB	Polyvinyl butyral

RT	Reverberation time
SBN	Structure borne noise
SEA	Statistical energy analysis
SPL	Sound pressure level
SIF	Semi-infinite fluid
UD	Upper deck

Abstract

In the last years, after the economic crisis that modified the super and megayacht market and construction, the project focus of shipyards and owners has been moved from the research of higher performances and whimsical exteriors to more classic aesthetics and higher level of onboard comfort.

This first aspect has led to the use of larger openings on superstructures' sides in order to enlarge windows and bring more natural light onboard vessels. The request of more comfortable units has granted a strong effort to find new solutions in order to reduce the noise and vibration level, dealing in particular to the structural elements that with higher noise radiations, such as dampers, pillars and windows.

The aforementioned trends is reflected on a more intensive use of glazed windows onboard, that have led to non-trivial problem of both structural response (since the structural component are reduced in order to enlarge opening) and NVH assessment, considering that glued glass panes act as an harmonic speakers, having natural frequencies closed to ones of the main superyacht excitations.

In this PhD thesis, the use of glass onboard superyacht has been focused with particular attention to finding new, simpler numerical and experimental procedure to take into account the vibroacustic properties of glass, that are actually ignored by Classification Societies, during their structural scantling and mounting. The proposed simplified methods has been tested also in two different global models, for the assessment of the vertical hull girder vibration at low frequency and for the NVH assessment in the mid-high frequency respectively. Moreover, the role of openings has also been tested from a

structural point of view, as a first step of a wider research that should verify the stress transfer mechanisms between metallic structures and glazed windows.

Introduction

Since 2008, the shipbuilding of large pleasure craft has faced an important economic crisis, which has revolutionized the sector, changing the focus in the design of super and megayachts [1].

Until 2008, the recreational market pushed to the search for higher performance and speed, increasing the installed power on board and revolutionizing the traditional propulsion systems; this trend, however, has raised both production and design costs and those related to the maintenance of these units.

In order to cope with the problems of the global economic crisis, which led to the closure of several shipyards, the level and quality of the production of large pleasure craft has had to grow exponentially and this has changed the design philosophies. The demand for extreme speeds has been replaced by a greater attention to environmental problems and comfort on board. This last aspect in particular appears as one of the main challenges for the designers, driven towards more silent and comfortable units both by the demands of the classification societies, which release increasingly stricter regulations in terms of noise and vibration limits, and the ship owners, which in turn require standards that are often more restrictive than the CSs themselves. This trend has been confirmed by the ISSC committees, that are recognizing the importance of comfort in the design of structural layouts of ships [2]–[4].

The secondary but not negligible effect of changing the nautical market is a different interior and architectural design. While in the pre-crisis period, the interior designer pushed to extravagant solutions to attract the attention of new customers and win the competition, today the designers are returning to more

classic tastes, abandoning any extravagance in favour of more sober furnishings and a greater use of natural furniture and lighting.

The use of glazed structures in the design of large pleasure craft is one of the aspects that has faced both the above mentioned aspects [5], [6]; in particular, the large windows have replaced small portholes on the walls of hulls and superstructures in order to bring as much natural light as possible into the interior living spaces, arriving at extreme deck-to-deck solutions with long windows up to 5 meters [7].

From a more structural point of view, these openings have significantly reduced the structural elements on the walls of super and megayachts, raising non-trivial problems of longitudinal strength and compression (buckling) on the uprights of the windows, often made in aluminium light alloy. In this perspective, some studies [8]–[11] on the contribution of large openings on superstructures' sides on different vessels, especially regarding cruise ships. In those cases, the openings are somehow small if compared to traditional superyacht in the range of 30-60 meter in length; for this type of units, windows could cover even the 90% of the superstructure effective length, they are usually mounted deck to deck and the length of the glazed surface could be over then 3 meters. Even though, the gluing system should guarantee that no stresses are transferred to the glass, as it happens for cruise ships, the behaviour of windows with such dimensions have to be analysed in detail in order to verify if they are structurally disconnected from the metallic structure or if it should be possible to consider them as partially collaborative to the primary response to global loads.

Nowadays, shipyards project windows only in order to be complaint with the regulation in terms of fire insulation and structural resistance, but no importance is given in the layering sequence of laminated glass and in the use of different interlayers, following the principle of "less cost and less weight, better". As it will be addressed in the first Chapter of this thesis, this philosophy is completely

backed up by Classification Societies, which considers laminated windows as equivalent to monolithic ones with a different thickness.

This approach does not take into consideration the effect of laminated windows in the noise and vibration propagations inside superyachts. As a matter of facts, the large glass panes, which are currently glued to the structure [12], behave like real harmonic speakers [13], [14], with natural frequencies very close to those of the main sources of noise and vibration on board [15], i.e. the main engines, gearboxes, gensets and blade passing frequencies [16]. This has led in many cases to not comply with the limits imposed on both the ship owner's side and that of the classification companies and a consequent economic loss on the part of the shipyard, in terms of contractual penalties and replacement of glass that do not lead to problems of resonance.

Several method are proposed in literature for the estimation of dynamic parameter (in particular natural frequencies and damping loss factor) of laminated glass and viscoelastic materials in order to cover up this problem. For what concerns the natural frequencies [17]–[19], different definition of dynamic equivalent thickness are given, but they requires a long computational times since they are based on a iterative procedures. Moreover, the application of this procedure has to be tested on a global model of superyacht for the NVH assessment even by using SEA for higher frequency ranges and then compared with experimental data obtained by sea trials.

Dealing with damping loss factor, a fully numerical approach should be avoided since the complex shear transfer mechanism between glass plies and interlayers. Nowadays, the common practice for the estimation of damping loss factor is to use the Oberst test [20], but it requires the use of a shaker, that , since it has to swipe a wide frequency range, is very heavy and it cannot be used during normal shipyard operations. So, a procedure for the direct assessment of damping loss factor with simpler instrumentations is still missing.

The research on the careful use of glazed structures on board super and megayachts has therefore undergone an important acceleration in the very last few years, and has therefore been chosen as the theme of this PhD thesis.

In the first part of the thesis, a study on the state of the art of using glass on board large recreational craft was carried out. In particular, the main texts of classification societies have been analysed to understand their design philosophy and highlight any differences and criticisms. Furthermore, the models of glass, monolithic or multilayer, currently developed in the literature have been studied with particular attention to the use of equivalent models for numerical analysis. From the state of art analysis, it appears clear that a simpler procedure for the use of equivalent models, that takes into account the vibroacustic characteristics of laminated glass, has to be developed, by simplifying the proposed analytical solutions.

The second part of the monograph focuses on the structural problems caused by large openings and on the collaboration of the windows to the longitudinal strength of the hull girder. Through FEM analysis on a megayacht, it was possible to evaluate the contribution of the different types of windows and how they are glued to the structural components of superstructures. By this analysis, the equivalent thickness method has been tested and it has been verified the behaviour of large opening even for shorter superyacht, if compared to the literature background.

In the third and final part of the thesis, the vibro-acoustic impact of windows has been studied, using numerical FEA and SEA, with particular attention to how they propagate noise and vibration. In particular, a new, simpler method for the evaluation of the total coefficient of glass damping is proposed, validated by experimental tests carried out also on viscoelastic materials (which samples are more available on construction sites and less expensive than multi-layered glass), and has been studied how to simplify, even from the dynamic point of

view, the multilayer glazed structures with monolithic equivalent elements in the numerical models.

The thesis therefore concludes with the analysis of two pleasure boats; in the first study, carried out in collaboration with the Technical University of Hamburg, the FE model of a megayacht was realized and the effect of the glazed structures was studied in the first vertical hull girder vibration mode through the use of superelements. The second case study is instead focused on the propagation of noise on board; a SEA model of an under construction superyacht was then created where the equivalent modelling techniques of multilayer glazing and their effect in noise propagation were tested and compared with full scale experimental data at the end of the vessel construction.

Chapter 1

REGULATORY STATE OF ART

In this Chapter, a comprehensive analysis of the rules and regulations regarding the use of glazing windows in pleasure craft design has been carried out. The SOLAS [21] convention has been studied as well as the rules proposed by the main Classification Societies [22]–[24]; the ISO standards11336-1[25] has been deepened as well, even if it concerns only to bonded windows, that, by the way, it is the solution preferred in super and megayacht shipyards.

1.1 – SOLAS

The International Convention for the Safety of Life at Sea (SOLAS) [21] is an international maritime safety treaty. It ensures that ships flagged by signatory States comply with minimum safety standards in construction, equipment and operation. This Regulation apply only to ships engaged on international voyages and it must be obligatorily applied to passenger ships, with different rules according to the number of passengers, and to cargo ships of more than 500 tons gross tonnage.

The present Regulations, unless expressly provided otherwise, do not apply to:

- Ships of war and troopships;
- Cargo ships of less than 500 tons gross tonnage;
- Ships not propelled by mechanical means;
- Wooden ships of primitive build;
- Pleasure yachts not engaged in trade;
- Fishing vessels.

What is interesting about glass is provided in "Chapter II-2 - Construction - Fire protection, fire detection and fire extinction - Part C - Suppression of fire - Regulation 9 - Containment of fire - 4 Protection of openings in fire-resisting divisions".

In Paragraph 4.1, summarizing, it is stated that:

- Windows and side-scuttles in bulkheads within accommodation and service spaces and control stations shall be so constructed as to preserve the integrity requirements of the type of bulkheads in which they are fitted, this being determined in accordance with the Fire Test Procedures Code.
- The requirements for "A" and "B" class integrity of the outer boundaries of a ship shall not apply to exterior doors, except for those in superstructures and deckhouses facing lifesaving appliances, embarkation and external assembly station areas, external stairs and open decks used.
- Windows located in the ship's side below the lifeboat embarkation area shall have fire integrity at least equal to "A-0" class.

It must be remembered that:

Class A divisions: decks and bulkheads satisfying the following criteria:

- They shall be constructed of steel or other equivalent material;
- They shall be suitably stiffened;
- They shall be insulated so that the average temperature on the unexposed side will not rise more than 140°C above the original temperature, nor the temperature, at any one point, including any joint, will rise more than 180°C above the original temperature during the following fire protection time:
    - A-60 class……..60 minutes

  - A-30 class……..30 minutes
  - A-15 class……..15 minutes
  - A-0 class……..……0 minutes;
- They shall be so constructed as to be capable of preventing the passage of smoke and flame up to the end of the fire protection time of one hour;
- A test of a prototype bulkhead or deck in accordance with the Fire Test Procedures Code shall be required by the Class Society to ensure that it meets the above requirements.

Class B divisions: decks, bulkheads ceilings or linings satisfying the following criteria:

- They shall be constructed of approved non combustible materials;
- They shall be insulated so that the average temperature on the unexposed side will not rise more than 140°C above the original temperature, nor the temperature, at any one point, including any joint, will rise more than 225°C above the original temperature during the following fire protection time:
  - B-15 class……..15 minutes
  - B-0 class……0 minutes;
- They shall be so constructed as to be capable of preventing the passage of smoke and flame up to the end of the fire protection time of half an hour;
- A test of a prototype bulkhead or deck in accordance with the Fire Test Procedures Code shall be required by the Class Society to ensure that it meets the above requirements.

Class C divisions: they shall be constructed of approved non combustible materials.

1.2 – LARGE YACHT CODE

The Large Commercial Yacht Code [26], introduced in 1998 by the UK's Maritime and Coastguard Agency (MCA), is a set of requirements more suited to yachts than other regulations like Solas.

The Code applies to a motor or sailing vessel of 24 meters in load line length and over or, if built before 21 July 1968, which is of 150 tons gross tonnage and over and which, at the time, is in commercial use for sport or pleasure and carries no cargo and no more than 12 passengers. The Code only applies to vessels of less than 3000 GT. Sail training vessels are included in this application.

In this Code general requirements about weather-tight integrity, safety of escape routes etc., are provided for every openings type (skylights, port-lights, windows, doorways etc.).

Some fundamental paragraphs are:

- Paragraphs 5.3.4, 5.4.1 and 5.5.1, which are about glazing skylight, port-lights and windows respectively. They state that the glazing material and its method of securing within the frame should meet an appropriate national or international standard like Recognized Classification Society rules for "ships". For Short Range Yachts, Classification Society rules for "pleasure vessels" or "yachts" can be considered appropriate. Paragraph 5.4.1 also states that windows should be of strength appropriate to their location in the vessel and meet the requirements of BSMA 25 or equivalent international standard;
- Paragraphs 5.4.2 and 5.4.3, which include requirement about port-lights fitted in the hull of the vessel. They should be provided with permanently attached deadlight (which are to be capable of securing the opening watertight in the event of a breakage of the glazing) and they should be positioned above a minimum height from the all-season load line depending on vessel breadth;

- Paragraph from 5.5.2 to 5.5.8, which are about windows requirement. If glazing material, glazing thickness, or fixing of the windows does not meet the requirements of a recognized standard, windows may be tested at a minimum of 4 times the required design pressure derived from an appropriate national or international standard. Additionally, as a minimum, calculated thicknesses should meet Classification Society requirements for pleasure vessels or yachts. If the BSMA 25 is used, the minimum design head pressures are provided. There are also some requirements about glass type. In fact toughened safety glass type is required for superstructure or weather-tight deckhouses windows. If chemically toughened safety glass is used, windows are to be of the laminated type with a minimum depth of chemical toughening. In addition, for all vessels, other than Short Range Yachts, storm shutters are required for all windows in the front and sides of first tier and front windows of the second tier of superstructures or weather-tight deckhouses above the freeboard deck. Where windows are of laminated construction and their equivalent toughened safety glass thickness exceeds the requirements of the applied standard by a minimum of 30%, storm shutters need not be carried, but a blanking plate is to be provided so that any window opening may be sealed in the event of glass failure. Finally, it is claimed that side and front windows to the navigating position should not be constructed of polarized or tinted glass and the visibility should comply with SOLAS Chapter V.

In section 14B, the Code provides requirements about structural fire protection. For windows and port-lights the SOLAS's requirements are kept. In fact, it is stated that all windows and port-lights in bulkheads within accommodation spaces, service spaces and control stations should be so constructed to preserve the integrity requirements of the type of bulkheads in which they are fitted. In addition glass is not to be installed as an interior main vertical zone, stairway enclosure bulkhead, or within machinery space boundaries.

1.3 – REGISTRO ITALIANO NAVALE

RINA rule [24] provides general requirement about side-scuttles and windows in Pt. B, Ch. 1, Sec.1.

It should be distinguish between:

- Side-scuttles and windows of yachts not more than 24m, for which the requirements of ISO STANDARD 12216 are to be applied;
- Side-scuttles and windows of yachts more than 24m, for which the Register provides the design requirements.
- For the scantlings of side-scuttles and rectangular windows, the yacht may be subdivided into zones which differ in their position to the waterline:
- Zone A: zone between the full load waterline and a line drawn parallel to the sheer profile and having its lowest point not less than 500 mm or 2,5% B, whichever is greater, above the full load waterline;
- Zone B: zone above zone A bounded at the top by the deck from which the freeboard is calculated;
- Zone C: Zone corresponding to the 1st tier of superstructures and above.

First the windows and side-scuttles classes that could be installed in each zone are indicated.

Then the guidelines for the calculation of tempered glass thickness are provided, distinguishing between rectangular windows and side-scuttles having surface above or below 0,16 m^2:

- For the thickness of toughened glass panes of side-scuttles and rectangular windows, having surfaces not exceeding 0,16 m^2, and fitted below the weather deck, see the following Table 1.1:

Table 1.1: Side scuttles' thicknesses [24]

Clear light diameter [mm]	Thickness of toughened glass [mm]	
	Type B side scuttles (medium series)	Type C side scuttles (light series series)
200	8	6
250	8	6
300	10	6
350	12	8
400	12	8
450	15	8

Different thickness may be accepted on the basis of a hydraulic pressure test, performed on a mock-up representative of the arrangement, the result of which confirms that the proposed thickness is able to ensure watertight integrity at a pressure not less than 4 times the design pressure of the hull in that zone.

- For the thickness of toughened glass panes of side-scuttles and rectangular windows, having surfaces exceeding 0,16 m^2 and positioned below the weather deck, the thickness of the glass is given by the following formula:

$$t = 0.015b\sqrt{\beta p} > 15\ mm \tag{1.1}$$

where p is the design pressure and β is a coefficient depending on window aspect ratio defined by the following relations:

$$\beta = \begin{cases} 0.54\Lambda - 0.078\Lambda^2 - 0.17 & for\ \Lambda < 3 \\ 0.75 & for\ \Lambda > 3 \end{cases} \tag{1.2}$$

where Λ is the aspect ratio of the window, defined as a/b ratio, where a is the bigger side of the window and b the smaller one.

If the windows are above the weather deck the required thickness is as from Table 1.2.

Table 1.2: Required thickness for windows above weather deck [24]

Normal sizes (clear light) of rectangular window [mm]	Thickness of toughened glass [mm]	Total minimum number of closing appliances of opening type of rectangular window
300x500	6	4
355x500	6	4
400x560	6	4
450x630	6	4
500x710	6	6
560x800	7	6
900x630	8	6
1000x710	8	8
1100x800	9	8

or, for other sizes:

$$t = 0.0.5b\sqrt{\beta p} > 15\ mm \tag{1.3}$$

Even in this case different thickness may be accepted on the basis of a hydraulic pressure test.

Materials other than toughened glass may be used for side-scuttles and windows above and below the weather deck. The thickness of the sheets may be obtained by multiplying the Rule thickness for toughened glass by 1.3 in the case of polycarbonate sheets and 1.5 in the case of acrylic sheets. The thickness of laminated glass is to be such that:

$$t_e^2 = \sum_i t_i^2 \tag{1.4}$$

where t_e is the equivalent thickness of the single sheet glass pane, t_i is the thickness of the single sheet in the laminate and n is the number of sheets in the laminate.

The design pressure p, in kN/m^2, for the scantlings of side windows is to be taken as equal to the value P1, defined as follows:

$$p_1\left[\frac{kN}{m^2}\right] = 66.25(a + 0.024)(0.15L - h_0) > 20\ \left[\frac{kN}{m^2}\right] \tag{1.5}$$

where:

- h_o is the vertical distance, in m, from pdr to the full load waterline;
- a is a coefficient function of the longitudinal position of pdr, equal to:

$$a = \begin{cases} 0.036\ \ aft\ of\ 0.5L \\ \frac{0.04}{C_B} - 0.024\ \ in\ way\ of\ P_{PFW} \\ \text{values for intermediate positions obtained by linear interpolation} \end{cases} \tag{1.6}$$

- L is the scantling length, in m, on the full load waterline, assumed to be equal to the length on the full load waterline with the yacht at rest.

1.4 – LLOYD'S REGISTER

Lloyd's Register [22] provides all the regulations about positions, dimensions, shapes, materials and thickness of windows, portholes, side-scuttles and sliding glass doors in Section 7.

The regulation requires a plan showing the location of all the port-lights and windows to be submitted, and accepts recognized national standards for materials and fire resistance, depending on the location of the ship.

A differentiation based on areas between side-scuttles and windows is then introduced: all openings of round or oval shape with an area not exceeding 0,16

m^2 shall be treated as side-scuttle, while all openings with an area exceeding 0,16 m^2 are treated as windows.

A hydrostatic test is to be carried out in order to examine the capability of the frame, and glass retaining arrangements. A design pressure 4p, where p is the design pressure, is to be applied. Alternatively, this test may be carried out using a steel plate in place of the glass. Ideally, the steel plate thickness should be of a suitable reduced thickness to simulate the flexural performance of the glass.

No windows are to be fitted in the following locations:

- below the freeboard deck;
- in the first tier end bulkheads or sides of enclosed superstructures;
- in first tier deckhouses that are considered buoyant in the stability calculations.

The regulation then moves on thickness, stating that the thickness t of toughened safety glass:

$$t = max \begin{cases} 0.0.5b\sqrt{\beta p} \\ 0.00559r\sqrt{p} \\ 6\ mm \end{cases} \tag{1.7}$$

Depending on the rectangular or circular shape of glazing, where:

- r = radius of the glazing in mm;
- b = length of shorter side of glazing in mm;
- p = design pressure in kN/m2;
- $\beta = \begin{cases} 0.54\Lambda - 0.078\Lambda^2 - 0.17 & for\ \Lambda < 3 \\ 0.75 & for\ \Lambda > 3 \end{cases}$ (1.8)

Then, a formulation for laminated glass is introduced, where the whole thickness is considered as a composition of the thicknesses of all layers. Laminated

toughened safety glass may be used having a thickness greater than the single plate toughened safety glass for the same size window, as given by:

$$t_s^2 = \sum_i t_i^2 \tag{1.9}$$

Storm covers or deadlights are required for all windows and port-lights in the front of the deckhouse on the weather deck and also the sides, except where these are interchangeable port and starboard; in this case a sufficient number to fit any one side are to be provided. Additionally a storm cover or deadlight is to be provided for each different size of window or port-light respectively. A glazing equivalent may be fitted in lieu of deadlights or storm covers on the weather deck and above. The equivalent minimum thickness in lieu of storm covers is presented in Fig. 1.1.

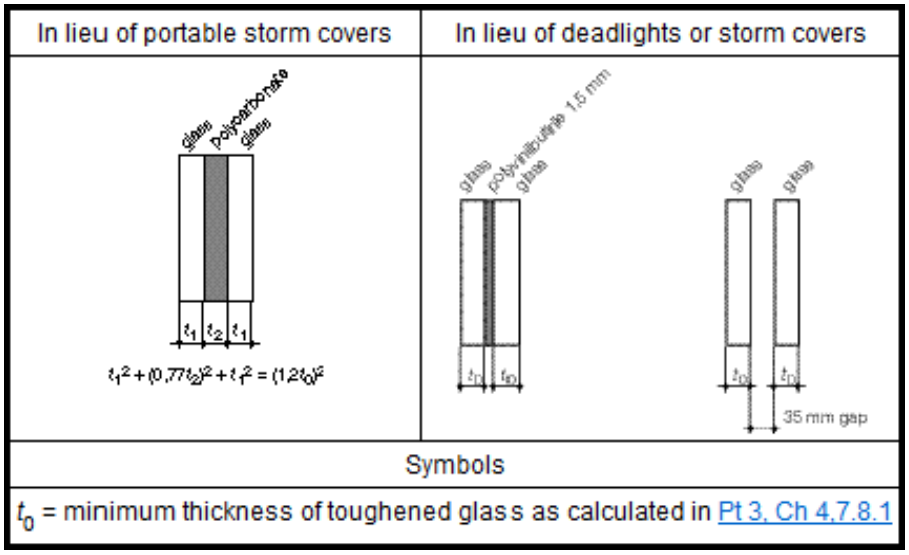

Figure 1.1: Equivalent minimum thicknesses in lieu of storm covers[22]

Finally, Lloyd's Register gives recommendations about how to identify the pressure acting on windows. It states that the pressure P_s acting on windows is composed, considering the height from the sea surface (Fig. 1.2), by different pressures as follows:

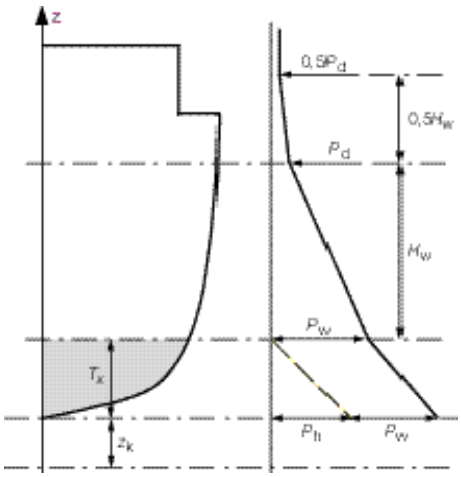

Figure 1.2: Vertical distribution of pressure head [22]

$$P_s = \begin{cases} P_h + P_w & for\ z \le T_x + z_k\ (up\ to\ the\ DWL) \\ P_D & for\ z = T_x + z_k + H_w \\ 0.5P_D & for\ z \ge T_x + z_k + 1.5H_w \\ linear\ interpolation\ for\ different\ z \end{cases} \quad (1.10)$$

where:

- H_w is the nominal wave limit height;

$$H_w\ [m] = 2H_{rm} \quad (1.11)$$

- P_h is the hydrostatic pressure, defined as:

$$P_h \left[\frac{kN}{m^2}\right] = 10(T_x - (z - z_k)) \quad (1.12)$$

- P_w is the hydrodynamic wave pressure, defined as the following:

$$P_w \left[\frac{kN}{m^2}\right] = max \begin{cases} P_m = 10 f_z H_{rm} \\ P_P = 10 H_{pm} \end{cases} \quad (1.13)$$

- P_D is the weather deck pressure, defined as (in displacement mode):

$$P_D \left[\frac{kN}{m^2}\right] = f_l(6 + 0.01 L_{WL})(1 + 0.05\Gamma) \quad (1.14)$$

- f_z is the vertical distribution factor;
- f_S is a longitudinal location factor for weather decks;
- Γ is the Taylor quotient;
- E is a factor that considers the exposition of the decks, and is taken as:

$$E \left[\frac{kN}{m^2}\right] = \frac{0.7 + 0.08 L_{WL}}{D - T} \quad (1.15)$$

- H_{rm} is the relative vertical motion, taken as:

$$H_{rm}[m] = C_{w,min}\left(1 + \frac{k_r}{C_B+0.2}\left(\frac{x_{wi}}{L_{WL}} - 1\right)\right)\sqrt{L_{WL}} \tag{1.16}$$

  where $C_{w,min}$ represents the wave head, in meters and k_r is a factor considering different hull configurations;

- H_{pm} is the pressure vertical motion, taken as:

$$H_{PM}[m] = max\begin{cases} 1.1\left(\frac{2x_{wi}}{L_{WL}} - 1\right)\sqrt{L_{WL}} \\ f_L\sqrt{L_{WL}} \end{cases} \tag{1.17}$$

  where f_L is a factor which depends on ship's length.

1.5 – AMERICAN BUREAU OF SHIPPING

The ABS regulation [23] deals with openings and windows stating some considerations about the subdivision between side-scuttles and windows, the materials to be used, the position of openings and the reinforcement needed.

In particular, windows are defined as being rectangular openings traditionally, but can be oval with an area exceeding 0.16 m^2.

Windows on first tier (front and side) and second tier (front only) to spaces within enclosed superstructure and deckhouses are to be fitted with strong steel, aluminium or other approved material, storm shutters. Windows are not to be fitted below the freeboard deck. Window frames are to be of steel or other approved material and are to be attached by through bolts or equivalent. The glazing is to be set into the frames in a suitable, approved packing or compound and mechanically secured.

The Bureau make also some consideration about glazing set up using adhesives; in particular, it states that for windows utilizing solely adhesives to secure glazing into their frames an installation procedure must be provided or approved by the manufacturer of the adhesive. The designer or shipyard, in conjunction with the adhesive manufacturer, is to provide calculations justifying the length and depth of the bond-line. A sample of the proposed installation is to be tested so that

the adhesive bonding is tested, by an external bearing pressure against the window frame and an internal pressure that puts the adhesive bonding in tension. The applied external head of water is to be at least equal to the pressure for the specific location of the window, while the internal pressure head is to be not less than an equivalent to 703,1 kgf/m^2. In lieu of an internal pressure test a separation test of the bonding may be carried out. Bonded windows are not acceptable for boundaries that are to comply with structural fire protection requirements, unless test data can be provided indicating that the joint complies with the necessary regulations.

The register provides some reductions on standard regulations for yachts limited in service range and weather conditions and not receiving a Load Line Certificate; particularly consideration will be given to the omission of storm shutters depending on the location, type and thickness of the windows.

Finally, the regulation moves on the requirements of the thickness of the window glazing material, which is not to be taken less than that obtained from the following expressions, whichever is greater:

$$t\,[mm] = max\begin{cases} s\left(\sqrt{\frac{pk}{1000\sigma_a}}\right) \\ s\left(\sqrt[3]{\frac{pk_1}{20E}}\right) \end{cases} \tag{1.18}$$

where:

- t is the required window thickness in mm;
- s is the lesser dimension of window in mm;
- p is the pressure head for window location;
- k and k1 are parameters depending on the aspect ratio of the window;
- σ_a is the 30% of the material flexural strength σ_f;
- E is the material flexural modulus.

The material characteristics, in terms of flexural modulus and strength, are given by the register (Table 1.3), but special considerations could be made with regards to design, manufacture and testing of glass specimens.

Table 1.3: Assumed glass mechanical properties [23]

Glazing	Flexural strength[MPa]	Flexural modulus [MPa]
Tempered Monolithic	119 Mpa	73'000 MPa
Laminated Glass	69 Mpa	2'620 MPa
Polycarbonate	93 MPa	2'345 MPa
Acrylic	110 MPa	3'000 MPa

The regulation also states that minimum thicknesses must be ensured form monolithic glass windows; in particular, a minimum thickness of 10 mm must be provided for front windows, while a minimum thickness of 6 mm must be provided for side and end windows.

Finally, some statements to evaluate the pressure head in different locations are given. The pressure is given by the following equation:

$$P_D \left[\frac{kN}{m^2}\right] = N_3 h \tag{1.19}$$

where:

- N_3 is a conversion factor considering the gravity acceleration;
- h is the design head in m, which has to meet the next requirements:

  $$h\,[m] = ak(bf - y)c \tag{1.20}$$

  and it should not be less than:
  - 0,015L + 3,45 [m] for unprotected fronts on the lowest tier
  - 0,0075L + 1,8 [m] for all other locations on lowest tier and second tier
  - 1,5 [m] for all other locations, third tier and above
- a is a parameter relating to bulkhead location and yacht length;

- k is the service factor, equal to 1 for yachting service and commercial yachting service, and 0,85 for restricted yachting service notation R;
- b is a factor based on longitudinal location;
- f is a factor based on yacht length;
- y is the vertical distance, in m, from the design waterline or load waterline, to the midpoint of the stiffener or panel;
- c is a parameter equal to 1 for superstructures and 0,85 for deckhouses.

1.6 – ISO 11336-1:2012

In the ISO rules [25], the International Organization for Standardization exposes the strength requirements and the design criteria of independently glued glazed openings on large yachts (over 24 meter in length and up to 3'000 GT). This standard can be considered as the first step made by the ISO, which plans to release additional regulations for ship windows integrated in adjacent structures. In this first part of the rule, only pane supported on their full perimeter and mechanically independent from the adjacent structure is considered.

According to the present rule, the strength of glass has to be considered only with reference to local loads, i.e. the external hydrostatic load due to the weather and sea state. Any effect of global loads, such as the primary longitudinal or transversal response, has to be neglected for the calculation of the pane thickness.

Moreover, the standard clarifies that the strength assessment of both monolithic and laminated glass has to be fulfilled only by the main structure section, and that any additional functional plies, such as gluing and films are not intended to fulfil the strength requirements.

The design pressure p_D has to be calculated as:

$$p_D\ [\frac{kN}{m^2}] = 10{,}05 \cdot a \cdot k_s \cdot (b \cdot f\text{-}h) \cdot c \tag{1.21}$$

where:

- a is a parameter relating to location and vessel length;
- k_s is the service factor defined as:
  - 1,00 for unrestricted range yacht;
  - 0,85 for intermediate range yacht;
  - 0,75 for short range yacht;
- b is a parameter based on the longitudinal location;
- f is a parameter based on the vessel length;
- h is the height of centre of windows from the design waterline
- c=0,85.

The basic pane thickness t_O has to be calculated as:

$$t_O\ [mm] = \begin{cases} b_P \cdot \sqrt{\frac{\beta \cdot p_D}{1000 \cdot \sigma_a}}, & rectangular\ openings \\ 0{,}5 \cdot d \cdot \sqrt{\frac{1{,}21 \cdot p_D}{1000 \cdot \sigma_a}}, & circular\ openings \end{cases} \tag{1.22}$$

where:

- b_P is the clear opening short side of the rectangular pane;
- d is the diameter of the glazed opening;
- β is the pane aspect ratio based coefficient;
- σ_A is the allowable design flexural strength of the material [MPa].

For what concerns the use of laminated glass, a slight different formulation has been adopted, if compared to other CS rules exposed in the previous paragraphs.

The equivalent thickness has to be calculated as the minimum of the j-th partial equivalent thickness as it follows:

$$t_{eq} = \min\left[\sqrt{\frac{\sum_{i=1}^{n} t_i^3}{t_j}}\right] \geq t_O, j = 1, n \tag{1.23}$$

1.7 – GENERAL CONSIDERATIONS

To complete the investigation, a summary table (Table 1.4) is given, in which a comparison between the analysed registers is proposed, particularly looking to the thickness equations adopted.

Table 1.4 Minimum glass thickness equations

Register	Monolithic glass	Laminated Glass
RINA	$t = 0.0.5b\sqrt{\beta p}$	$t_e^2 = \sum_i t_i^2$
LR	$t = 0.0.5b\sqrt{\beta p}$	$t_s^2 = \sum_i t_i^2$
ABS	$t = s\left(\sqrt{\frac{pk}{1000\sigma_a}}\right)$	--
ISO 11336-1:2012	$t = b_P \cdot \sqrt{\frac{\beta \cdot p_D}{1000 \cdot \sigma_a}}$	$t_{eq}^2 = \min\left[\frac{\sum_{i=1}^{n} t_i^3}{t_j}\right]$

As it can be seen, RINA and Lloyd's Register's regulations provide exactly the same equations to evaluate the window's thickness of monolithic glass. ABS and ISO also provide a similar equation, which depends again on smaller side of the window and on aspect ratio, but it introduces moreover a flexural strength, which in some way is able to take in account the material characteristics and behaviours.

Even for the calculation of the laminated glass thickness, RINA and Lloyd's Register present the same equation, while ABS doesn't need an additional formulation; this could be in accordance with the introduction of the flexural strength in the monolithic glass equation which, in this way, already takes into account the material characteristics. Anyway, the driving philosophy of the CSs in the framework of laminated glass is to substitute them in the structural layout

by using an equivalent monolithic glass, without paying any attention to the lamination sequence, the different type of interlayers (as defined in the next Chapter) and on the different behaviour in terms of vibro-acoustic response.

ISO standard proposes a sort of fusion between the ABS and RINA/LR approach, which reflects both the allowable strength of the material and the lamination sequence, with a more detailed formulation for the equivalent thickness.

All the four registers refer the thickness to the pressure acting on the window, which depends on the location where it is placed. The way the pressure is considered it is extremely different between the three regulations, with no, on first sight, dependencies in common.

Storm shutters are considered by both the three regulations but, while for RINA and ABS registers only some requirements about positioning and materials are given, Lloyd's Register also provides an equivalent thickness of glazing in lieu of the storm shutters, which corresponds to an increment of about the 20% of thickness.

Finally, a remark on the thickness of different layers in the laminated glass used on board has to be made. The well-known trend of using symmetric laminate is actually an unrewarding method, since this configuration gives the lower equivalent monolithic thickness with respect to the asymmetric configuration. Indeed, a very simple calculation shows that, in a two layers laminate, the more different the thicknesses of the two layers are, the higher the equivalent thickness will be. The following Table 1.5 and Fig. 1.3 clearly show this trend.

Table 1.5: Equivalent monolithic glass thickness for laminated panels as a function of layers thickness

t_1=	50%	t_{tot}	t_2=	50%	t_{tot}	t_e=	71%	t_{tot}
t_1=	45%	t_{tot}	t_2=	55%	t_{tot}	t_e=	71%	t_{tot}

t_1=	40%	t_{tot}	t_2=	60%	t_{tot}	t_e=	72%	t_{tot}
t_1=	35%	t_{tot}	t_2=	65%	t_{tot}	t_e=	74%	t_{tot}
t_1=	30%	t_{tot}	t_2=	70%	t_{tot}	t_e=	76%	t_{tot}
t_1=	25%	t_{tot}	t_2=	75%	t_{tot}	t_e=	79%	t_{tot}
t_1=	20%	t_{tot}	t_2=	80%	t_{tot}	t_e=	82%	t_{tot}
t_1=	15%	t_{tot}	t_2=	85%	t_{tot}	t_e=	86%	t_{tot}
t_1=	10%	t_{tot}	t_2=	90%	t_{tot}	t_e=	91%	t_{tot}

Where t_1 and t_2 are the thickness of the first and the second layer of the laminate, t_{tot} is the total thickness of the laminated glass panel and t_e is the equivalent monolithic thickness for RINA corresponding to t_s in Lloyd's Register.

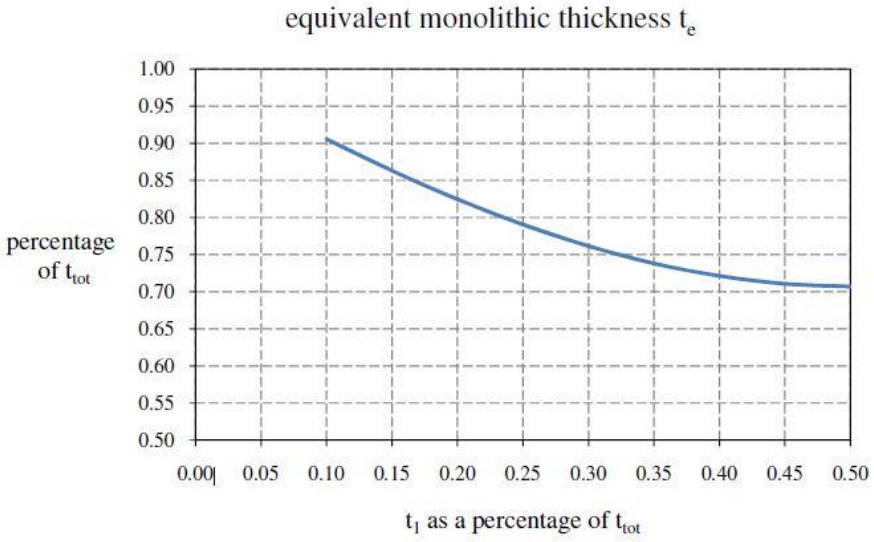

Figure 1.3: Equivalent monolithic glass thickness for laminated panels as a function of layers thickness

Therefore, using asymmetric laminates allows obtaining higher equivalent monolithic thickness that will be compared to the minimum thickness required by regulations. In this way, it is more probable to fulfil the Register requirements with the same total thickness. Nevertheless, this aspect has to be dealt carefully, since as it will be shown in the next Chapters, shifting from symmetrical to

asymmetrical glazed pane could lead to resonance problems, due to the different natural modes of the two structures and the different modal density.

Chapter 2

ANALYTICAL AND EQUIVALENT STATIC MODEL FOR LAMINATED GLASS

As defined in [27], laminated glass is an assembly consisting of one sheet of glass with one or more sheets of glass and/or plastic glazing sheet material joined together with one or more interlayers.

The adhesive contact between the glass and the interlayer is made by high pressure and heat, around 140°C. The glass plates constituting laminated glass could be made of:

- annealed glass;
- heat strengthened glass;
- tempered or heat toughened glass;
- a combination of previous types.

The interlayer is typically soft polymers like polyvinyl butyral (PVB) [28], ethyl vinyl acetate (EVA) and SentryGlass® (SGP) from the company DuPont [29].

When laminated glass shatters, this plastic interlayer keeps the pieces of glass in place. This reduces the risk of cuts caused by splinters and produces a characteristic "spider web" cracking pattern when the impact is not enough to completely pierce the glass. This is why laminated glass is considered a safety glass and it is normally used when there is a possibility of human impact or where the glass could fall if shattered.

Laminated glass is also used to increase the sound insulation rating of a window, where it significantly improves sound attenuation compared to unlaminated

glass panes of the same thickness and the attention will be focused on this fundamental property in the next Chapters.

The two main components of this material have to be introduced, i.e. glass and the viscoelastic interlayer. In fact glass is a complex material, as well as the behaviour of the viscoelastic material, so it is important to identify their mechanical and physical properties and understand how to model them.

2.1 – THE MECHANICAL CHARACTERISTICS OF LAMINATED GLASSES

2.1.1 – Glass plies

Glass is an amorphous (non-crystalline) solid material [27]. It does not have an exact melting point and it transforms from liquid to solid state over a certain temperature range, usually around 500°C. One important property of glass is its high resistance to many chemicals, which makes it a very durable material.

There are numerous types of glass with varying chemical and physical properties depending on the area of application. The most common glass is the soda-lime glass, also called soda-lime-silica glass; it contains the raw materials sand (silica), soda ash and limestone, and also a smaller amount of various additives.

Also flat glass, that is the most commonly used glass in laminated glass is typically made of soda-lime glass. Flat glass can be produced in different ways; however, the so called float glass procedure stands for 90% of the production of flat soda-lime glass. In this process, invented by Pilkington in 1959, the glass is produced by letting molten glass float on a bed of molten metal, typically tin, in order to give the sheet uniform thickness and very flat.

From the mechanical point of view, it can be stated that glass is a homogeneous and isotropic material which behaviour is linear elastic until fracture occurs, both for tension and compression. Therefore, since glass shows no plastic behaviour

there is no stress redistribution to reduce the local stress concentration as in other material such as steel. The compressive strength is usually significantly higher than the tensile strength. The tension strength is almost independent from the chemical composition but it is sensitive to environmental hygrometric conditions and to micro-cracks and flaws present on the surface after the forming process and successive treatments. In effect, the tensile strength is lower than the compression strength since stress concentrations develop in the micro-cracks and flaws for tension loading.

Therefore, the practical value for the mechanical strength is always lower due to these defects.

The glass used in civil architecture could be annealed, heat strengthened, thermally toughened or tempered, but, from the mechanical point of view, they can all be modelled in the same way, even if some differences in the tensile strength must be considered.

Common values for the mechanical properties of soda lime glass are presented in the following Table 2.1:

Table 2.1: Mechanical properties of soda lime glass [27]

Density	ϱ	2250 ÷2750	Kg/m3
Young's Modulus	E	63000 ÷ 77000	MPa
Poisson's coefficient	ν	0,20 ÷ 0,24	
Thermal expansion coefficient	α	3,1 ÷ 6	μm/(mK)
Specific heat	C_p	720	J/(kgK)
Heat conduction coefficient	λ	0.9 ÷ 1	W/(mK)
Maximum operating temperature		280	°C
Transition temperature		530	°C

2.1.2 – PVB interlayers

Today there are many interlayers on the market with a large variation in their properties. For every project, in different areas of use, it is a challenging task to

choose the most optimal interlayer. For architectural applications the most used material are:

- polyvinyl butyral (PVB),
- ethyl vinyl acetate (EVA),
- elastoplastic material, like SentryGlass® (SGP),
- polyurethane (PU).

Unlike glass, the constitutive response of these materials is not linear, it is strongly affected by many factors like the operating temperature, and the duration of loads applied.

The most common interlayer for laminated glass is the PVB. It is a polymer with viscoelastic behaviour, which means its properties are dependent on time, temperature and load. These parameters influence the properties in different ways, for example the higher the temperature, the weaker the interlayer and the material usually creeps with high loads and with long loading time, as shown in Fig. 2.1 and 2.2.

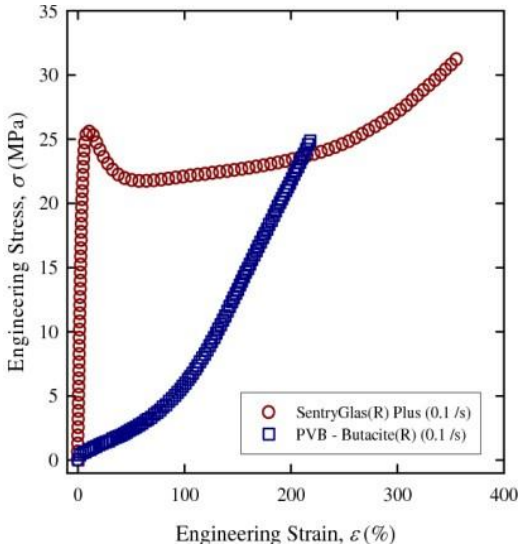

Figure 2.1: Stress-strain curves of SGP® and PVB at 20°C[27]

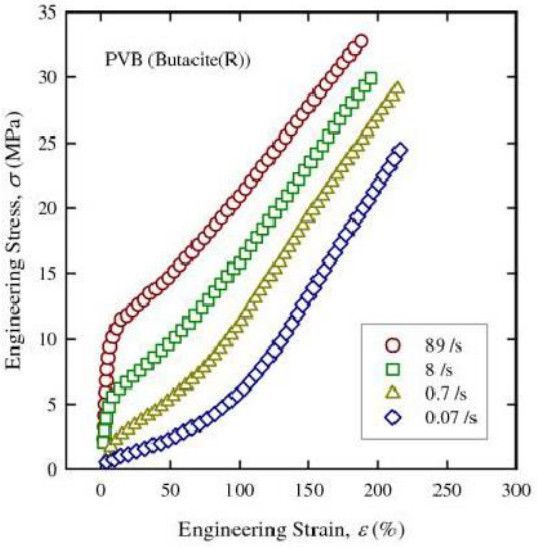

Figure 2.2: Stress strain curves for PVB for different loading velocities[27]

Viscoelastic behaviour of materials has elastic and viscous components modelled as a linear combination of spring and dashpots. In particular, the elastic component, acting as a spring, follows the Hook's law:

$$\sigma = E\varepsilon \tag{2.1}$$

Viscosity η provides the stress-strain rate relationship:

$$\sigma = \eta \frac{\partial \varepsilon}{\partial t} \tag{2.2}$$

The relationship between stress and strain can be simplified for specific stress rates. For high stress states/short time periods, the time derivative components of the stress–strain relationship is prevalent [30].

A dashpot resists to elongations, so in a high stress state it can be approximated as a rigid rod. Since a rigid rod cannot be stretched over its original length, no strain is added to the system.

Conversely, for low stress states/longer time periods, the time derivative components are negligible and the dashpot can be effectively removed from the system. As a result, only the spring component will contribute to the total strain of the system [30].

Different models have been studied in order to find the best mechanical schematization of viscoelastic materials by changing the number and the connection of elastic springs and viscous dampers.

The most accurate schematization for viscoelastic materials have been produced by Wiechert [31] and it is known as the "Generalized Maxwell-Wiechert Model", where (Fig. 2.3) a single elastic spring is parallel connected to an infinite series of spring/damper systems.

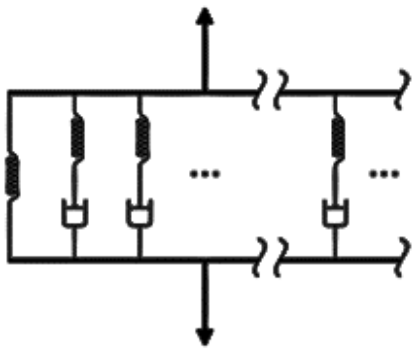

Figure 2.3: Generalized Maxwell-Wiechert model

In this schematization, the material is subject to a sudden strain that is constant over the application of the load, due to the single spring. In this schematization, the initial stress is due to the elastic response of the material and the stress relaxes over time due to viscous effects in the material.

The relaxation function of the shear modulus G can be written as:

$$G(t) = G_{\infty} + \sum_{i=1}^{n} G_i e^{-t/\tau_i} \tag{2.3}$$

where G_∞ is the long term modulus representing the totally relaxed material and τ_i terms are the relaxation times. If the elastic shear modulus G_0 is known, the relaxation function can be re-written as it follows, splitting viscous and elastic terms:

$$G(t) = G_0 - \sum_{i=1}^{n} G_i\left(1 - e^{-\frac{t}{\tau_i}}\right) \tag{2.4}$$

The following table presents the values of G_i and τ_i at 20°C for two of the most common PVB available on the market.

Table 2.2: Prony terms for two type of commercial PVB [29]

	PVB type A		PVB Type B	
	G_i/G_∞ (G_∞ = 471 MPa)	τ_i	G_i/G_∞ (G_∞ = 146.12 MPa)	τ_i
1	0.160600	3.2557·E-11	0.01550	1.0·E-5
2	0.0787770	4.9491·E-9	0.1727	1.0·E-4
3	0.2912000	7.2427·E-8	0.2111	1.0·E-3
4	0.0711550	9.8635·E-6	0.2684	1.0·E-2
5	0.2688000	2.8059·E-3	0.1988	1.0·E-1
6	0.0895860	1.6441·E-1	0.0974	1.0·E0
7	0.0301830	2.2648·E0	0.0254	1.0·E1
8	0.0076056	3.5364·E1	0.00508	1.0·E2
9	0.0009634	9.3675·E3	0.00114	1.0·E3
10	0.0004059	6.4141·E5	0.000485	1.0·E4
11	0.0006143	4.1347·E7	0.000554	1.0·E5
12			0.000752	1.0·E6
13			0.00070	1.0·E7
14			0.000985	1.0·E8

2.1 – THE WÖFEL BENNISON MODEL FOR LAMINATED GLASS BEAMS

Benninson et al. [32], [33] have proposed a model for the static calculation of laminated-glass elements based on a previous work by Wölfel [17], who analysed a sandwich structure composed of three layers, the outer ones with considerable axial stiffness but negligible bending stiffness, while the inner layer could bear shear stress with only zero axial and flexural strength. Benninson et al. [32]and Calderone et al. [33] extended the Wölfel's approach specifically for the case of laminated glass.

For the deflection of the laminated-glass beam, this model assumes a curve similar to a simply supported beam under uniformly distributed loading, and this assumption is valid for statically determined composite beams, for which the bending stiffness of the composite plies is negligible.

According to Benninson et al. [32] and Calderone et al. [33], the momentum of inertia of the entire laminated glass beam is given by the equation:

$$I_{eq} = I_1 + I_2 + \Gamma \frac{A_1 A_2}{A_{1+} A_2} H^2 \tag{2.5}$$

where

$$\Gamma = \frac{1}{1+\beta \frac{tE \quad A_1 A_2}{Gbl^2 A_{1+} A_2}} \tag{2.6}$$

The parameter Γ takes values in the range 0≤ Γ≤1 corresponding Γ=0 to the case of a layered beam and Γ=1 to a monolithic beam. The coefficient β depends upon load and boundary conditions and, for the most common cases, the corresponding values are recorded in [34] and [35].

As mentioned in [35], Wölfel-Bennison approach is accurate only for simply supported beams under uniformly distributed load and in those cases where the deflection curve is similar in type to the reference-case.

Besides, it has been verified in [36] that, when applied to a two-dimensional plate, the method is reliable only when the deformed surface is cylindrical, so that the plate response is similar to a beam.

2.2 – THE GALUPPI-ROYER CARFAGNI MODEL FOR LAMINATED GLASS BEAMS

Galuppi and Royer-Carfagni [37], based upon a variational approach, developed a model for calculating the deflection of laminated-glass beams under static loads that can be applied to a very wide range of boundary and loading conditions. The principal hypothesis are:

- the interlayer has no axial or bending stiffness, but only shear stiffness;
- shear deformation of glass is neglected;
- all materials are linear elastic;
- geometric non-linearities are not considered.

The deflection of the beam is given by:

$$w(x,t) = \frac{g(x)}{EI_R} \tag{2.7}$$

where g(x) is a shape function that takes the form of the elastic deflection of a monolithic beam having a constant cross-section under the same loading and boundary conditions as the laminated- glass beam, and I_R is the effective momentum of inertia of the laminated glass beam, comprised between the values ($I_1 + I_2 + I_3$), corresponding to the layered limit, and I_{tot}, associated with the monolithic limit.

The effective momentum of inertia I_R can be addressed as the weighted harmonic mean of this two values through the parameter η, a non-dimensional quantity tuning the plate response from the layered limit (η = 0) to the monolithic limit (η = 1):

$$\frac{1}{I_R} = \frac{\eta}{I_{TOT}} + \frac{1-\eta}{I_1 + I_2 + I_3} \tag{2.8}$$

The parameter η has been calculated by the authors as:

$$\eta = \frac{1}{1+\frac{E}{GbI_{TOT}\left(\frac{H_1^2}{t_1}+\frac{H_2^2}{t_2}\right)}(I_1 + I_2 + I_3)(A_1 d_1^2 + A_2 d_2^2 + A_3 d_3^2)\Psi} \tag{2.9}$$

where the value of Ψ depends upon the geometry, boundary and loading conditions of the beam.

2.3 – THE GALUPPI-ROYER CARFAGNI MODEL FOR LAMINATED GLASS PLATES

Based on a similar approach to the laminate glass beam, Galuppi and Royer Carfagni [18] developed a method for the effective enhanced thickness of laminated glass plates.

When considering the laminated glass plate identified by the x-y domain under distributed load p(x, y), the strain energy can be written as a function of the vertical displacement w(x, y). In order to simplify the problem, convenient shape functions for the displacement components have to be introduced [18].

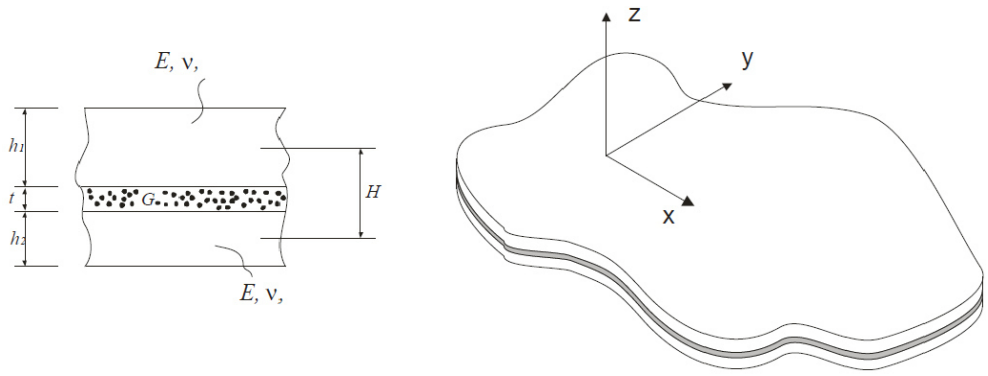

Figure 2.4: Plate composed of two glass plies bonded by a polymeric interlayer [12]

Defining the flexural rigidity of each glass ply as:

$$D_i = \frac{Eh_i^3}{12(1-\nu^2)} \tag{2.10}$$

the flexural rigidity for the layered limit is

$$D_{abs} = \sum_{i=1}^{2} D_i \tag{2.11}$$

The flexural rigidity for the monolithic limit can be written as [38]:

$$D_{full} = D_{abs} + 12\frac{D_1 D_2}{D_1 h_1^2 + D_2 h_2^2} H^2 = D_{abs} + \frac{E}{12(1-\nu^2)} \frac{h_1 h_2}{h_{1+} h_2} \tag{2.12}$$

With

$$H^2 = \frac{h_{1+} h_2}{2} + t \tag{2.13}$$

Then, the shape function w(x, y) can be selected as the elastic deformed surface of a monolithic plate with constant thickness under the same loading and boundary conditions [18].Setting, in analogy to the effective beam:

$$w(x,y) = \frac{g(x,y)}{D_{eq}} \tag{2.14}$$

where D_{eq} is the equivalent rigidity and the shape function g(x, y) is uniquely determined by the shape of the laminated glass plate in x-y plane, by the external load p(x, y) and by the geometric boundary conditions.

Assuming

$$\frac{1}{D_{eq}} = \frac{\eta_{2D}}{D_{full}} + \frac{1-\eta_{2D}}{D_{abs}} \tag{2.15}$$

where the non-dimensional weight parameter η_{2D} tunes the response from the layered limit (η_{2D} = 0) to the monolithic limit (η_{2D} = 1). Minimization of the strain energy allows to determine the best value of η_{2D} in the form:

$$\eta_{2D} = \frac{1}{1+\frac{t\,D_{abs}\quad 12D_1D_2}{GD_{full}D_1h_1^2+D_2h_2^2}\psi} \tag{2.16}$$

where ψ depends upon the plate shape, the load distribution and the boundary conditions.

It can be shown [18] that the equivalent thickness for the calculation of the maximum deflection is:

$$\hat{h}_w = \sqrt[3]{\frac{1}{\frac{\eta_{2D}}{h_1^3+h_2^3+12\frac{h_1h_2}{h_1+h_2}H^2}+\frac{1-\eta_{2D}}{h_1^3+h_2^3}}} \tag{2.17}$$

and for the calculation of the maximum stress at the interface of plate 1 and plate 2:

$$\frac{1}{\hat{h}_{1,\sigma}^2} = \frac{2\eta_{2D}\frac{h_2H}{h_1+h_2}}{h_1^3+h_2^3+12\frac{h_1h_2}{h_1+h_2}H} + \frac{h_1}{\hat{h}_w^3} \quad ; \quad \frac{1}{h_{2,\sigma}^2} = \frac{2\eta_{2D}\frac{h_1H}{h_1+h_2}}{h_1^3+h_2^3+12\frac{h_1h_2}{h_1+h_2}H} + \frac{h_2}{\hat{h}_w^3} \tag{2.18}$$

The herein presented calculation models can be easily and satisfactory used when structural numerical analysis are required, as in the next Chapter, in order to simplify the complex shear transfer mechanism of viscoelastic materials. Nevertheless, if the stress/strain distribution across the windows' thickness is required, these models cannot be adopted, since, as reported in the Section 2.3, only a deformed equivalent or stressed equivalent monolithic glass can be modelled.

Moreover, with these assumptions, the monolithic equivalent glass pane will have a completely different dynamic characteristics in terms of natural frequencies and damping loss factor, since the real damper material is the viscoelastic layer, that in the static equivalent model is completely neglected from the dynamic point of view.

Chapter 3

THE EFFECT OF LAMINATED GLASS ON THE STRUCTURAL STRENGTH OF SUPERYACHT SUPERSTRUCTURES

The role of superstructures in superyacht strength has become more and more relevant in last years because of their large extension; even if they are usually constructed in aluminum light alloy, in order to reduce the weight, their contribution to the hull strength cannot be neglected [39].

The response of upper decks to longitudinal and torsional stresses can be summarized in two typical behavior types [40]: if superstructure role is neglected, stresses acting on hull became greater, unloading higher decks, which commonly have lower ultimate strengths

On the other hand, considering a fully effective superstructure, global strains are reduced due to the greater momentum of inertia; in this case, stresses acting on the higher deck are very relevant, and they can cause several failure phenomena, i.e. yielding, buckling, vibrations, etc.

As already stated in the Introduction of this thesis, even though the superstructures in 30 to 60 meter length superyacht should extended for up to 90% of the vessel L_{oa}, the presence of large openings is a non trivial problem for naval structural architects, since they reduce the contribution of superstructure to the primary response to global loads.

Although glass has a Young modulus of the same order of magnitude of aluminum light alloy (the most used material for superyacht superstructure), the common shipyard practice to glue the windows to the metallic frame has the

result of disconnecting the glazed pane from the structural material and so they prevent glass to be stressed. From one side, this matching is able to prevent glass from brakeage due to its low ultimate stress, but, on the other side, it shouldn't enhance the effectiveness of superstructure, that, in case of cooperative windows, could lead to a reduction of side thickness and so to a reduction of weight in the upper decks.

In this Chapter, the contribution of superstructure to the primary response to global loads has been addressed, focusing on the impact of openings to the bending efficiency of superstructures. In this analysis, the aforementioned Galuppi – Royer Carfagni static equivalent model has been used in order to simplify the laminated glass panes.

3.1 –THEORETICAL APPROACH TO THE BENDING EFFICIENCY OF SUPERSTRUCTURE

3.1.1 - Hull – Superstructures interaction

The role of superstructure in the structural response to global bending moment strictly depends on the superstructure's length compared to the hull [40], [41] .

As shown in Fig. 3.1, if superstructures have a similar length compared to the hull, the longitudinal stress pattern on the entire structure can be easily compared to the classic beam theory behaviour; that is to say that longitudinal stress depends, linearly, on the distance to the neutral axis.

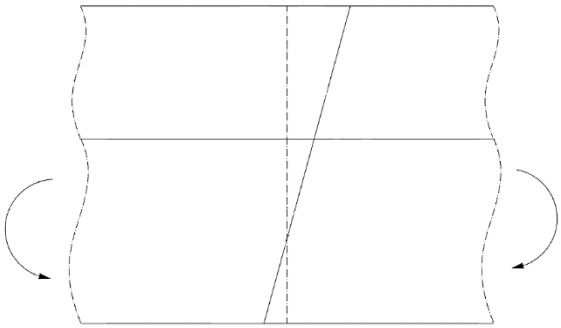

Figure 3.1: Longitudinal stress distribution in case of a superstructure's length comparable to hull

Fig. 3.2 clarifies the longitudinal stress distribution of a superstructure with reduced length; in this case, the pattern is no more globally linear with the distance to the bending neutral axis. The new stress distribution highlights an opposite in sign response to bending load between hull and superstructure [42], [43].

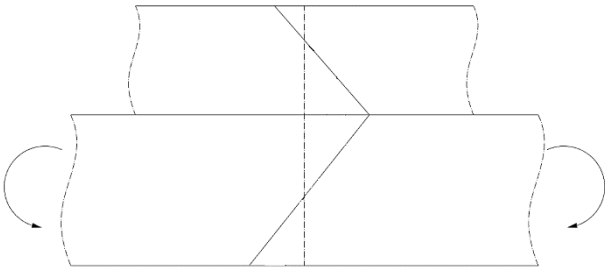

Figure 3.2: Longitudinal stress distribution in case of a superstructure's reduced length compared to hull

This behaviour, reported in Fig. 3.3, is due to the shear forces "T" and vertical reactive forces "q", generated by the primary response to global load, which tend to deform hull and superstructure with opposite curvature.

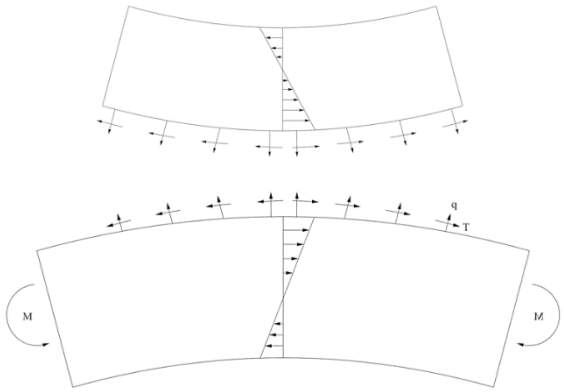

Figure 3.3: Hull-superstructure interaction forces

This phenomenon does not affect extended deckhouse.

3.1.2 - Non-linear effects in the hull-superstructures interaction

All the aforementioned aspects of hull-superstructure interaction have been deduced by the use of classic hull girder theory, which, by the way, has some restrictive hypothesis, that cannot be neglected.

The most important limitation is that longitudinal stresses depend only to the vertical distance with the neutral axis; even if this aspect is generally true for hull structures, the structural behaviour of superstructure does not accomplish this hypothesis for different reasons, as follows [40]:

- shear lag effect: as reported in Fig. 3.4, superstructures' extremities are not affected by longitudinal stresses. This aspect afflicts all frame in proximity of free ends, in which stresses are lower than theoretical ones. It can be easily deducted that in this zone, superstructures do not fully cooperate with hull to global bending moment.

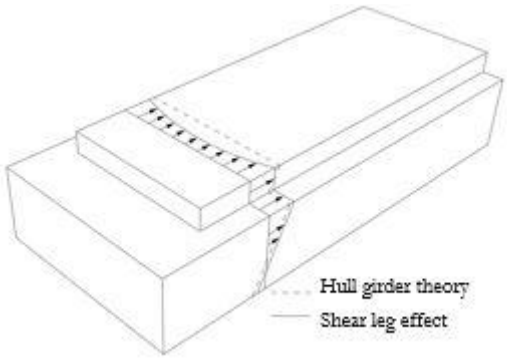

Figure 3.4: Shear leg effect on longitudinal stress

- main deck flexibility: shear and vertical forces, already defined in the previous section of this paper, cause main deck vertical deformation (Fig. 3.5), that afflicts superstructures' sides.

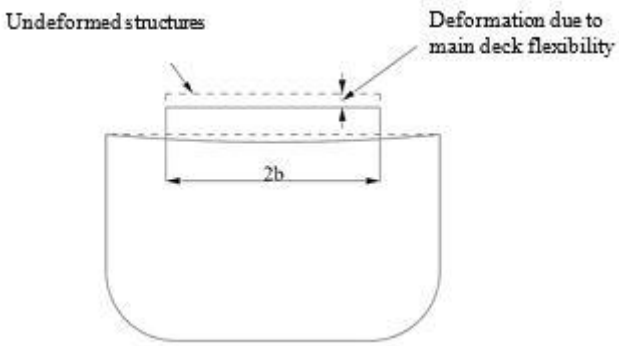

Figure 3.5: Main deck flexibility

- structural connection between hull and superstructures: in modern mega and super yacht design, the actual trend for what concerns construction material is to use steel for hulls and aluminium light alloy for superstructures, in order to reduce the global weight of vessels. Different mechanic properties of materials cause non linear distribution of stresses and deformation in the connection's area in main decks.

3.1.3 - Theoretical formulation of bending efficiency

In literature, different formulations for bending efficiency have been developed and assessed [10], [44], [45].

Caldwell [43] analysed the contribution of superstructure to the hull primary response to global loads, developing a formulation based on the reduction of longitudinal stress due to deckhouse cooperation:

$$\eta_{xs} = \frac{F_{x0} - F_x}{F_{x0} - F_{x1}} \tag{3.1}$$

where F_{x0} is the maximum stress on the hull at the main deck without superstructure, F_x is the max stress on the hull at the main deck with superstructure and F_{x1} is the max stress on the hull calculated at the main deck using the beam theory with a full effective superstructure.

In terms of structural displacement, Mackney [11], [46] has defined the efficiency ηxd:

$$\eta_{xd} = \frac{w_0}{w_s} \tag{3.2}$$

where w_0 is the maximum displacement of the plain hull (without superstructures) and w_s is the maximum displacement of section with superstructure.

3.2 –NUMERICAL APPROACH TO THE BENDING EFFICIENCY OF SUPERSTRUCTURES

3.2.1 - Creation of numerical model

The problem of the bending efficiency calculation, due to the aforementioned non-linear effect, can be achieved only by a numerical approach.

For the aim of this work, a 45 meter long megayacht has been assumed as study case and analysed by using Finite Element Analysis. The main characteristics of

the vessel has been reported in Tab. 3.1 and the main frame has been reported in Fig 3.6.

Table 3.1: Main characteristics of the vessel assumed as study case

Length overall [m]	45.14
Breadth Overall [m]	9.10
Waterline Length [m]	37.21
Height [m]	4.45
Draught [m]	2.40
Design Speed [kn]	14.50
Displacement [ton]	445

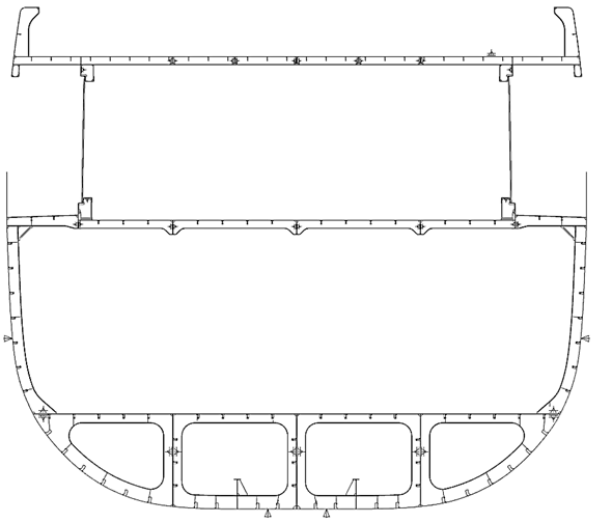

Figure 3.6: Main transversal section (frame 17)

Starting from a 3D model, a complete finite element model of the vessel up to the first order of superstructures has been realised (Fig. 3.7).

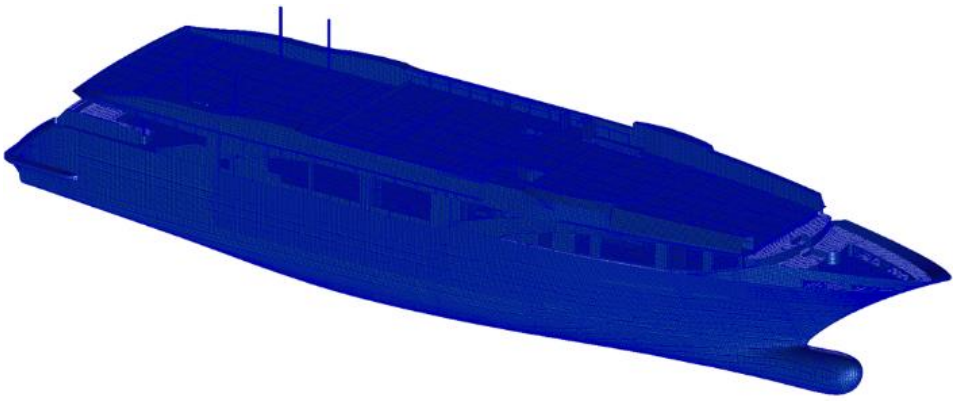

Figure 3.7: Finite element model of the vessel

Plates and primary stiffeners has been modelled using 2D shell elements, secondary stiffeners has been created by associating the characteristics of the transversal section to the 1D beam element [47].

The global model created for this work is composed by up to 700'000 elements and 1'200'000 nodes.

3.2.2 Loading and boundary conditions

In order to apply the formulation of bending efficiency, it is necessary to create pure bending moment loading scenario on the structures.

For these reasons, a 24 meter "slice" of the model has been chosen, with enough distance to the main frame in order to avoid integrations error due to free ends effect (Fig. 3.8).

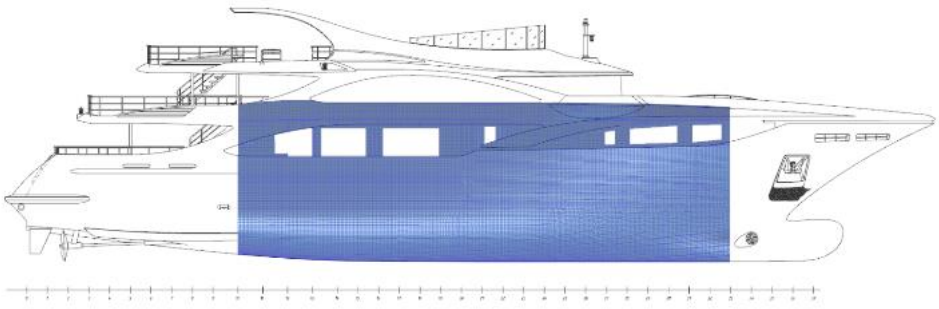

Figure 3.8: Bending efficiency calculation's numerical model

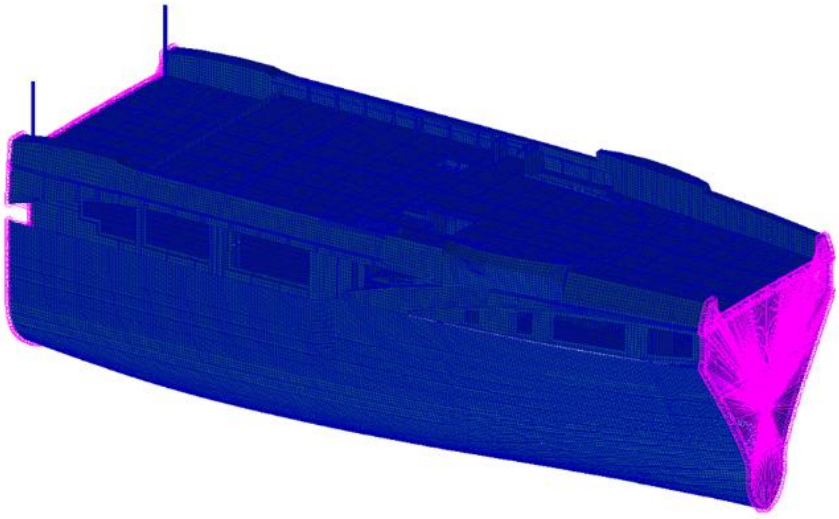

Figure 3.9: FE model used for bending efficiency calculation

In order to prevent rigid body motion of the structures, which causes finite element analysis to fail, two nodes on the neutral axis of the free end section has been constrained to the translation in the X, Y and Z direction and two nodes in the final section has been constrained at the translation in the Z direction, as it can be seen in Fig. 3.9.

All nodes in the extremity sections are connected to the bending neutral axis using rigid link [48] elements; this type of constraints allows the distribution of the bending moment applied on one node placed on the neutral axis to all nodes of the section.

The model has been loaded by pure bending moment applied on the master nodes of rigid link element. Its intensity has been calculated from RINA rules[24], in sagging condition, giving the values of 36'535 kNm.

3.3 - BENDING EFFICIENCY COMPUTATION WITHOUT GLAZING STRUCTURES

The bending efficiency numerical evaluation has been carried out by linear static analysis on the aforementioned numerical model. In Fig. 3.10, the stress plot has been reported.

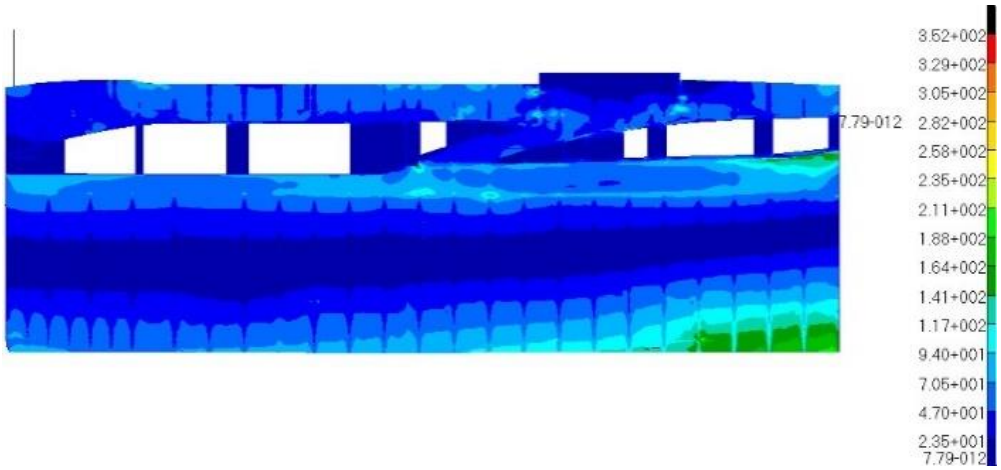

Figure 3.10: Stress plot on vessel's structure

Because of the significant variation of the momentum of inertia in each transversal frame, the calculation of the bending efficiency has been accomplished in each cross section.

This investigation allowed authors to better understand the contribution of glazing surface in a subsequent stage of this work.

In Fig. 3.11, the variation of F_x and F_{x0}, as defined in Section 3.1.3, is reported.

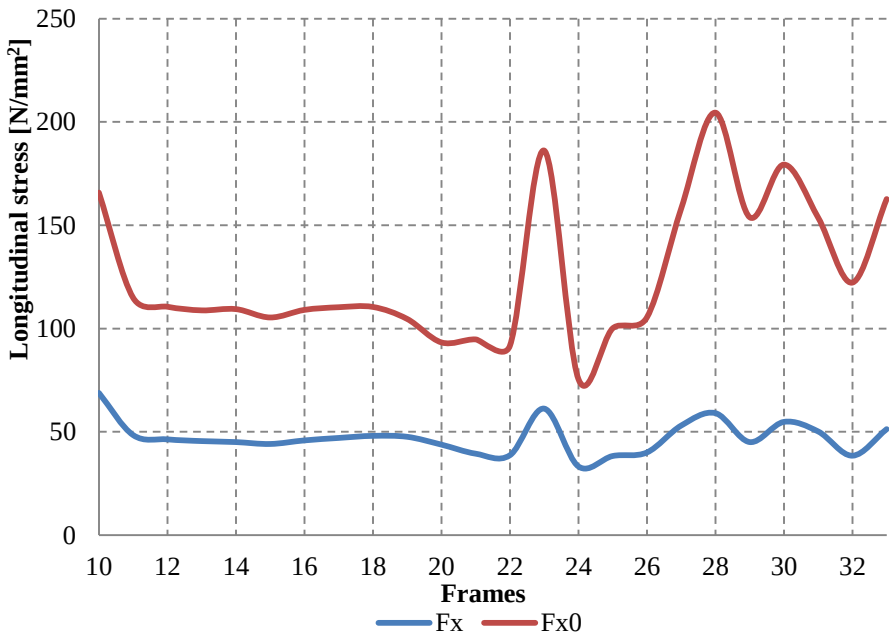

Figure 3.11: Variation of stresses values with or without superstructure

As it can be deducted from Fig. 3.11, the cooperation of superstructure reduces the level of stress on the vessel's structure. The presence of humps in correspondence of frames 23 and 28 is due to main deck's recesses.

In Fig. 3.12, bending efficiency η_{xs} values have been reported.

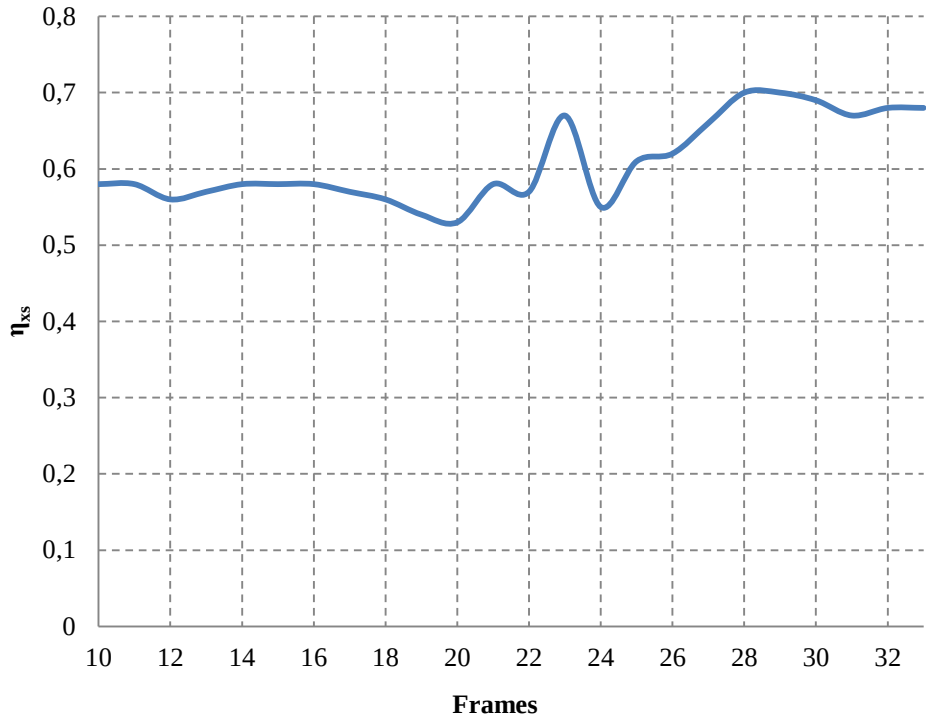

Figure 3.12: Bending efficiency η_{xs} evaluation.

From Fig. 3.12, it can be deduced that the superstructure's cooperation is included between 55% and 70%; these results are in compliance with what affirmed by Zanic [11], for what concerns bending efficiency of a cruise ship, which, by the way, is the typology of vessels that can be considered more similar to a megayacht because of their large opening in deckhouses' sides.

The mean η_{xs} value can be easily calculated by the mean values theorem;

$$\eta_{xsm} = \frac{\int_{L_0}^{L_1} \eta_{xs}(x)dx}{L_1 - L_0} = 0.62 \tag{3.3}$$

A similar evaluation has been made in order to calculate the bending efficiency ηxd and results have been reported in Fig. 3.13.

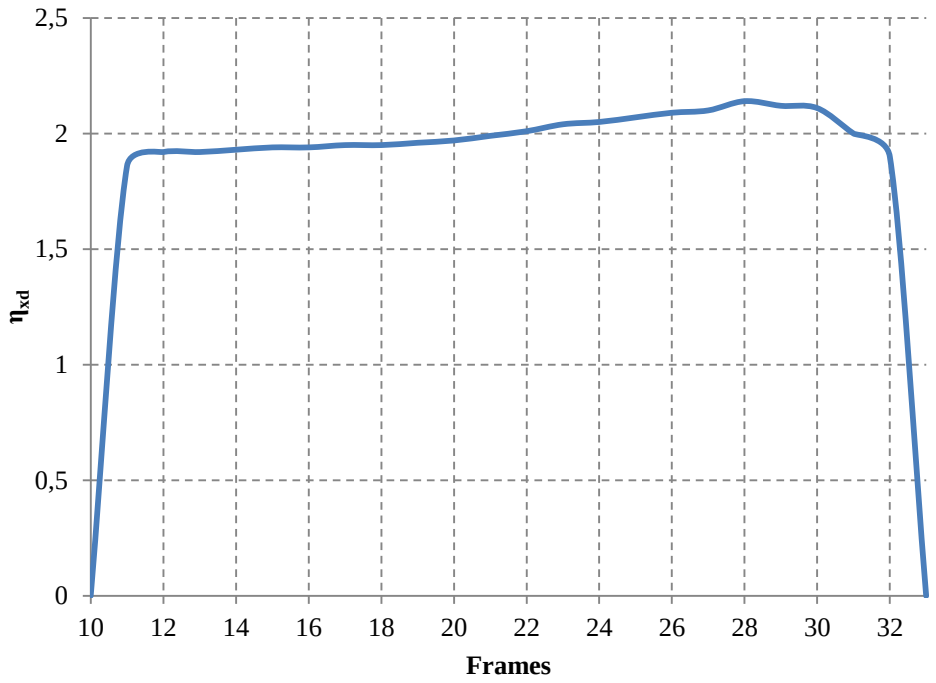

Figure 3.13: Bending efficiency η_{xd} evaluation

It must be noted that Mackney's theory [46] defines the bending efficiency η_{xd} as the reduction of displacement between the plain hull without superstructure and the complete structure, so η_{xd} values have to be grater then one.

3.4 – GLAZING STRUCTURES' NUMERICAL MODEL FOR HULL – SUPERSTRUCTURE INTERACTION

3.4.1 - *Mechanical characterization of glazing structures*

As already stated, the actual trend in super and megayacht design is to enlarge small porthole up to large windows, for aesthetic and lightning reasons.

As it can be seen in Fig. 3.14, glazing windows in superstructure's sides cannot be neglected in the primary response to global loads, because aluminium light

alloy structures have been reduced to the minimum imposed by classification societies' rules.

In order to create a correct numerical model of the vessel, a former simplified one has been developed with the same loading and boundary condition of the entire vessel and it has been reported in Fig. 3.14.

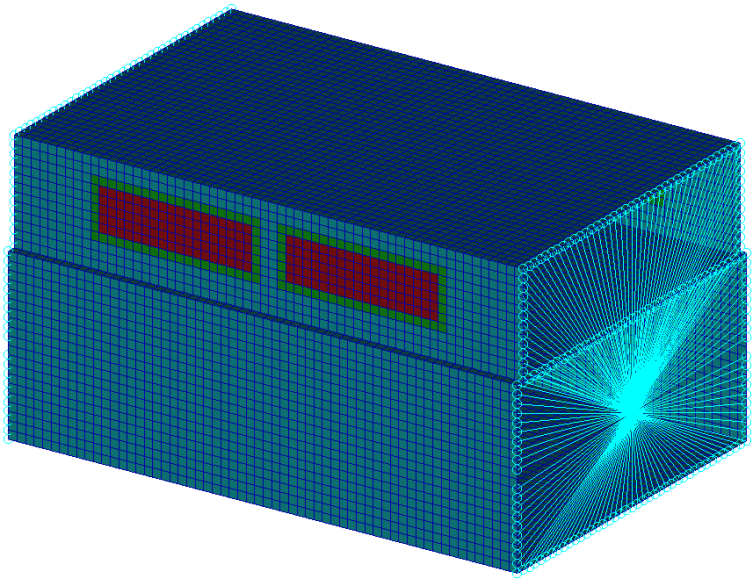

Figure 3.14: Simplified model for glazing structures' study

In the simplified model herein presented, both effects of different glazing structures (monolithic and laminated) and of the gluing system has been studied.

Adhesive materials have been modelled by using 3 solid hexahedral element through the thickness available in the FE software library with the aim to better simulate shear forces and stress distribution between aluminium light alloy and glass, which cannot be achieved by using 2D shell elements. An example of a transversal section of the window's zone can be seen in Fig. 3.15.

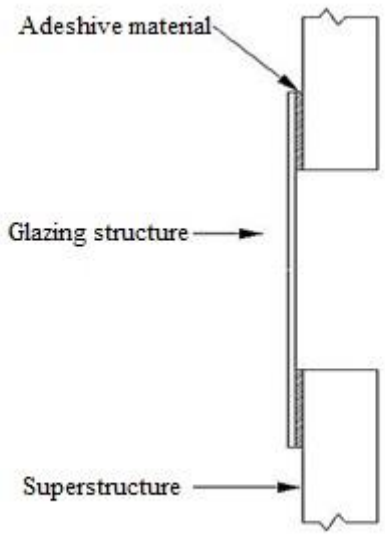

Figure 3.15: Gluing numerical model

Mechanical characteristics of the adhesive material are reported in Tab.3.2. In this case, a thickness of 5 mm has been assumed as suggested by the shipyard.

Table 3.2: Adhesive material's mechanical characteristics

	Adhesive material
E [N/mm2]	1.3
σ_u [N/mm2]	6
ν	0.22
Elongation at failure	450%

From the Table above, it is clear that the adhesive material used by the shipyard cannot be considered as a structural joint, because of its high elongation at failure and its low elastic modulus.

From the vessel's windows plan, four different simplified model has been further developed, in order to evaluate the different behaviour of the monolithic and laminated (with PVB or SGP interlayer) glass structures:

- model without windows ("Model A");
- model with equivalent monolithic windows ("Model B") according to the Galuppi – Royer Carfagni method;
- model with PVB laminated windows ("Model C");
- model with SGP laminated windows ("Model D").

As already shown in Chapter 2, it must be noted that PVB is a viscoelastic material, so its shear and bulk modulus should be defined as time variant according to the Prony series. For the aim of this work, it can be neglected because analysis are linear elastic and thus do not depend on time.

3.4.2 - Cooperation of glazing structures to longitudinal strength

Aforementioned simplified models has been deeply studied both in terms of stress distribution on the global structure and in terms of compressive forces acting on windows' strut that can collapse due to buckling phenomena.

These comparisons has been made comparing results with those obtained from the simplified model without glazing structures; stress vectors of this study case has been plotted in Fig. 3.16.

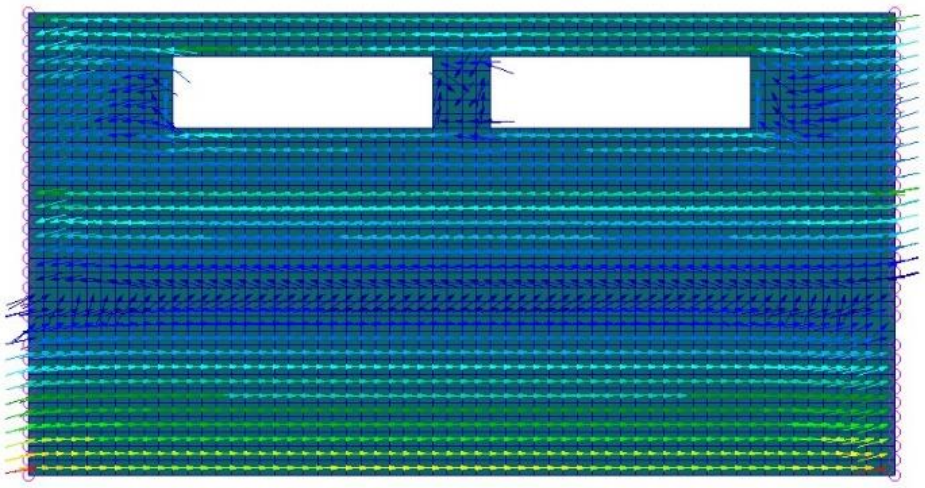

Figure 3.16: Stress vectors on "Model A"

As it can be seen, longitudinal stresses are drifted by the presence of holes replacing windows. For what concerns compressive stresses on the strut, the diagram of the FEA has been reported in Fig. 3.17.

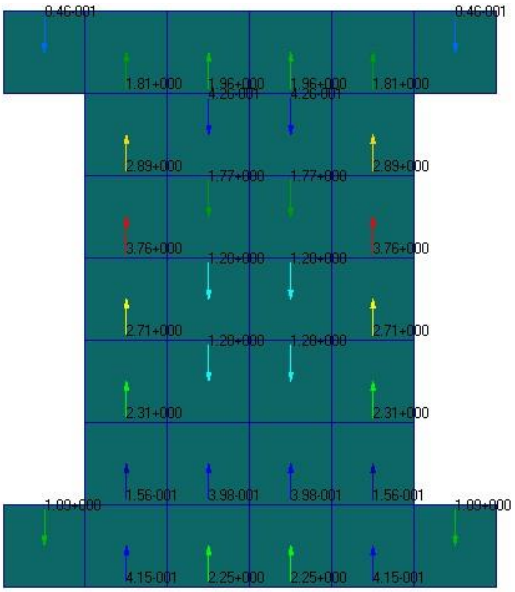

Figure 3.17: Compressive stresses on "Model A"

In Fig. 3.18, the stress distribution on the structure has been reported for "Model B", "C" and "D".

(a)

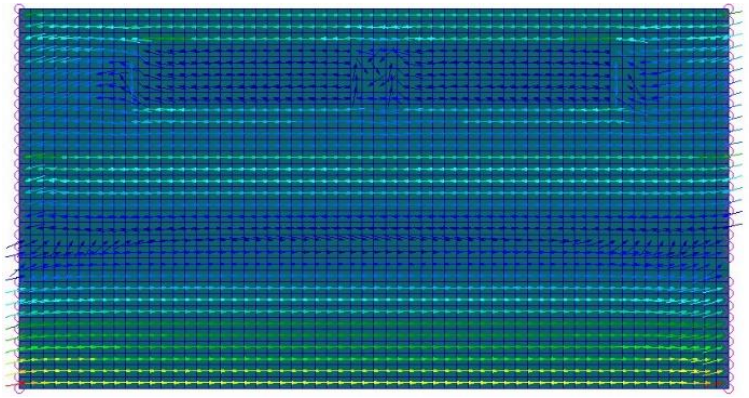

(b)

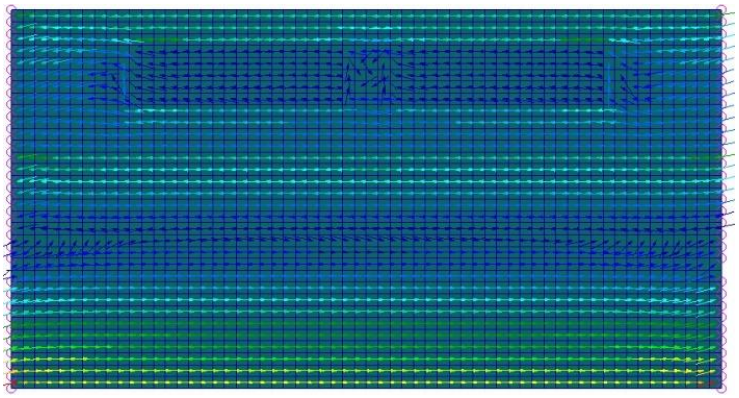

(c)

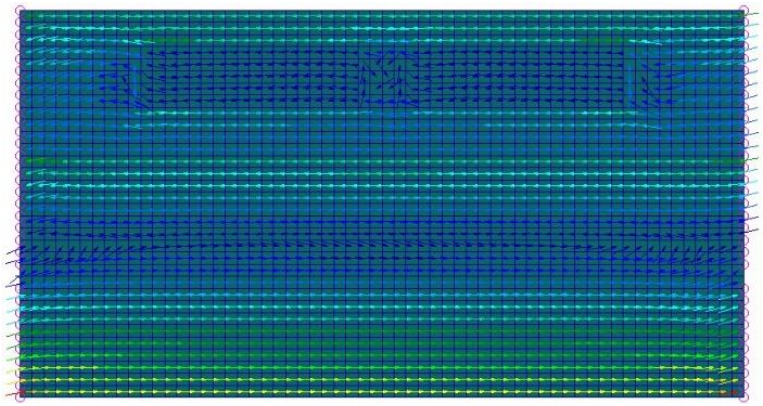

Figure 3.18: Stress distribution on (a) "Model B", (b) "Model C" and (c) "Model D".

As it can be deduced from the above figures, the stress distribution is not influenced by the presence of glazing structures glued to the superstructures.

This behaviour is due to adhesive material's mechanical characteristics, which do not achieve a correct stress transfer between superstructure and glass.

This aspect, that, by the way, cannot be considered as positive for bending efficiency, can preserve glasses from high level of stresses, which can cause windows to collapse due to their low tensile strength.

The same behaviour can be observed in Fig. 3.19, dealing with compressive stress components acting on windows' strut.

(a)

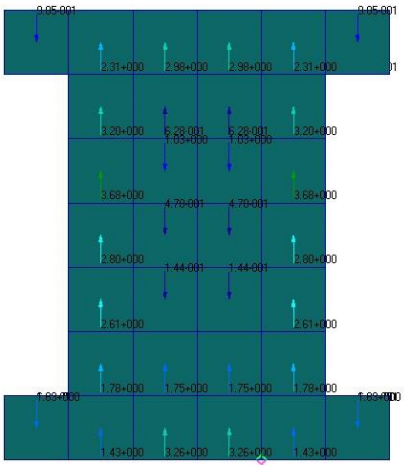
2.31+000
2.98+000
2.98+000
2.31+000
3.20+000
6.28-001
6.28-001
3.20+000
3.68+000
4.70-001
4.70-001
3.68+000
2.80+000
1.44-001
1.44-001
2.80+000
2.61+000
2.61+000
1.78+000
1.75+000
1.75+000
1.78+000
1.43+000
3.26+000
3.26+000
1.43+000

(b)

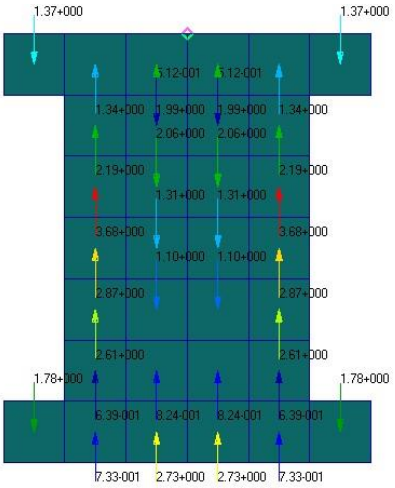
1.37+000
1.37+000
5.12-001
5.12-001
1.34+000
1.99+000
1.99+000
1.34+000
2.06+000
2.06+000
2.19+000
2.19+000
1.31+000
1.31+000
3.68+000
3.68+000
1.10+000
1.10+000
2.87+000
2.87+000
2.61+000
2.61+000
1.78+000
1.78+000
6.39-001
8.24-001
8.24-001
6.39-001
7.33-001
2.73+000
2.73+000
7.33-001

(c)

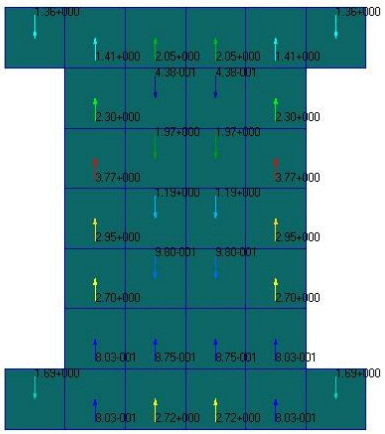

Figure 3.19: Compressive stresses on window's strut on (a) "Model B", (b) "Model C" and (c) "Model D".

As it can been observed in Fig. 3.19 and reported in Tab. 3.3, stresses acting on window's strut do not depend on glass's stratification; this behaviour is due to the fact that interlayer materials have very low mechanical characteristics, if compared to glass's ones (Tab. 3.3) and so only glass layers act as a bearing load material.

Table 3.3: Maximum compressive stress on window's strut

	Maximum compressive stress [MPa]
Model A	3.76
Model B	3.68
Model C	3.68
Model D	3.77

From these simplified analysis, it can be deduced that even though glasses has elastic modulus E comparable to the aluminium light alloy one, gluing system can avoid high level of stresses on windows, but, on the other hand, glazing

structures on superstructures' sides cannot be considered in the primary response to global loads.

Another consideration has to be clarified for monolithic and laminated glasses: in this study, the linear elastic analysis in FE software fully applies the "classic lamination theory" for laminated glasses.

The reliability of this simplification has to be deeply exanimated case by case: for what concerns vibration or structure-borne noise analysis or other non-linear analysis, it can cause trivial results, especially while using PVB as interlayer material, as declared in the previous section.

3.5 - BENDING EFFICIENCY COMPUTATION WITH GLAZING STRUCTURES

At this stage, glazing structures have been added to the vessel numerical model, according to the windows plan given by the shipyard. The final FE model (Fig. 3.20) has been developed using the consideration carried out for simplified models.

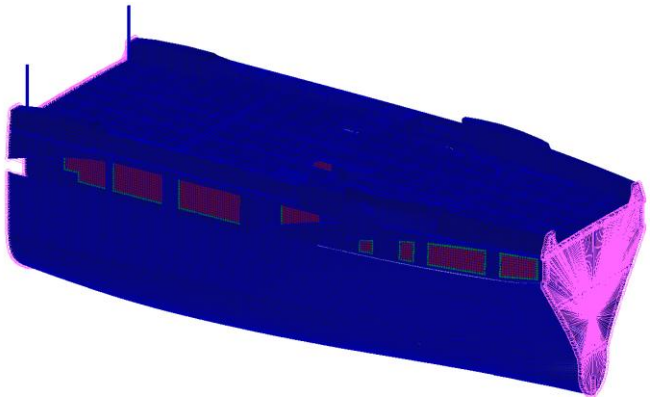

Figure 3.20: FE vessel's model with windows

Bending efficiency factor η_{xs} has been calculated for each frame and plotted in Fig. 3.21, comparing it with results obtained in Fig. 3.12.

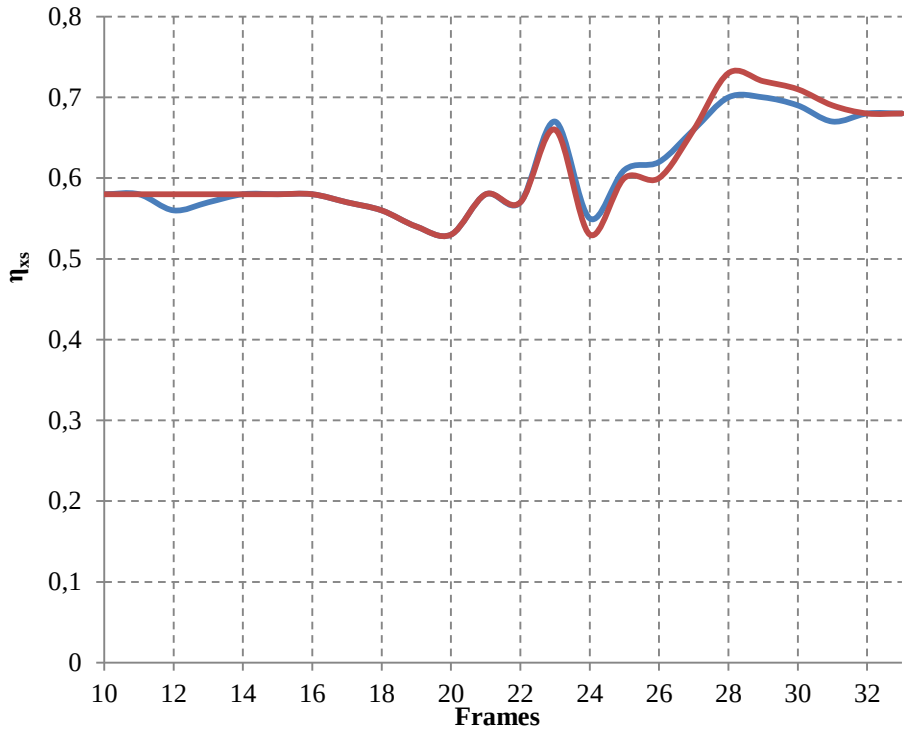

Figure 3.21: Bending efficiency n_{xs} with glazing structures (red) and without (blue) glazing structures

As it was foreseeable by considerations carried out for simplified models, glazing windows glued to sides do not cooperate with superstructure in the primary response to global loads. The role of adhesive material, which, even though they are considered as "structural", cannot assure a complete stress transfer between superstructure and glass, forestalling the collapse of glazing structures, which have low mechanical characteristics.

The mean η_{xs} value can be easily calculated by the mean value theorem, obtaining the same result of the model without windows:

$$\eta_{xsm} = \frac{\int_{L_0}^{L_1} \eta_{xs}(x)dx}{L_1 - L_0} = 0.63 \tag{3.4}$$

The negligible effect of windows to the primary response of the hull girder is mainly due to the presence of glue, that does not allow a correct transfer of shear stresses between metallic structure and windows. Moreover, the superstructure side is not transversally aligned to the window strip, and this lead to a further disconnection between structural elements and the glass [9], [12], [49].

Chapter 4

DYNAMIC EFFECTIVE THICKNESS OF LAMINATED GLASS

In addition to the non-trivial implication that laminated glasses have to the structural response of megayachts, the main implication of large openings in naval architecture is due to the vibroacoustic propagation onboard, that afflict, dramatically, the comfort perception inside the vessel.

Acting the windows as real harmonic speakers, with natural frequencies close to those of the main mechanical excitation, the problem of noise and vibration propagation through window panes has to be addressed with particular attention, since the vibroacoustic characterization of laminated glass has to be carried out carefully.[50]

In order to properly simulate the vibroacoustic characteristics of the laminated glass, especially in the Statistical Energy Analysis (SEA) and FE framework, it is necessary to simplify the classical numerical schematization (shell elements for glass plies and solid elements for interlayers [51]) in order to obtain a unique element [19], with higher modal density, that has the same dynamic properties (natural frequencies, modal density vs. wavenumber and loss factor) of the original laminated plate.

If the static equivalent model presented in Chapter 2 was for this porpoise, misleading results would be achieved, since they do not take into account the dynamic properties of glass and viscoelastic materials and so the monolithic equivalent thickness would show completely different natural modes and structural damping.

For these reasons, in this Chapter, the Lopez-Aenlle – Pelayo procedure for a more refined dynamic effective thickness (DEET) calculation has been presented; then, on that base, a simplified procedure has been developed in order to obtain an equivalent monolithic thickness having the same most effective natural frequency and vibroacoustic characteristics.

4.1 – THE LOPEZ-AENLLE – PELAYO MODEL FOR LAMINATED GLASS PLATES

Lopez-Aenlle and Pelayo [17] has extended the RKU method [52] to rectangular laminated glass plates, and a dynamic effective thickness/effective Young modulus are derived to estimate their modal parameters.

The method has been firstly developed for glass beams, by means of the relation between the static and dynamic flexural rigidity and then extended to rectangular plates. On the base of the available data, two different methodologies has been proposed:

- Stiffness based methodology: this method can be used when the wavenumber k can be calculated from the literature and a first initial frequency guess can be tried. The method consists in the steps reported in Fig. 4.1. As it can be seen from the flowchart, the Step 1 consists in the direct evaluation of the initial frequency, from which the loss factor and the dynamic equivalent rigidity are assessed in the subsequent Steps.

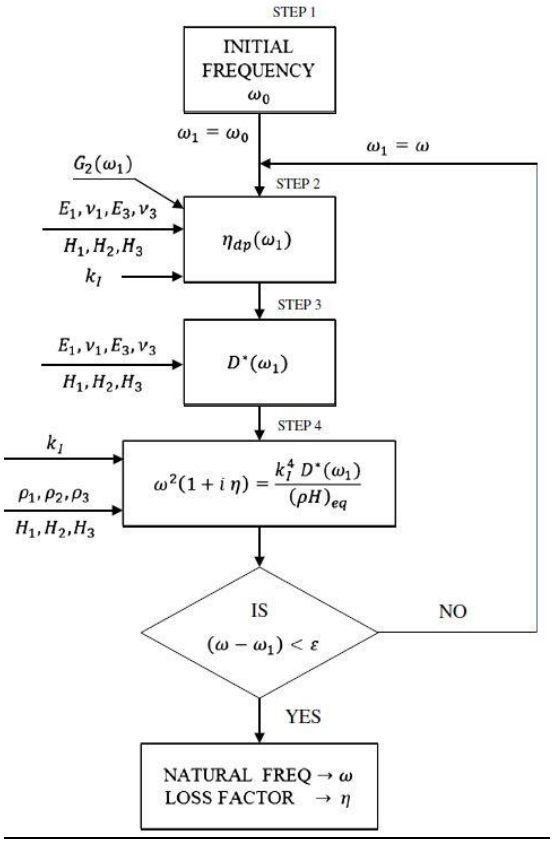

Figure 4.1: Lopez – Pelayo stiffness based method [17]

- Effective thickness based methodology: this method is based on the calculation of mode shapes and wave numbers from an initial finite element analysis on layered laminate limit and then, by averaging the natural frequency from the monolithic and layered limit as reported in Fig. 4.2, it is possible to estimate the dynamic effective thickness. In this methodology, the Step 1 and Step 2 consist in the numerical assessment of the monolithic and layered model respectively; from those results, the damping loss factor and the dynamic equivalent rigidity are evaluated by averaging the natural frequencies of the two models.

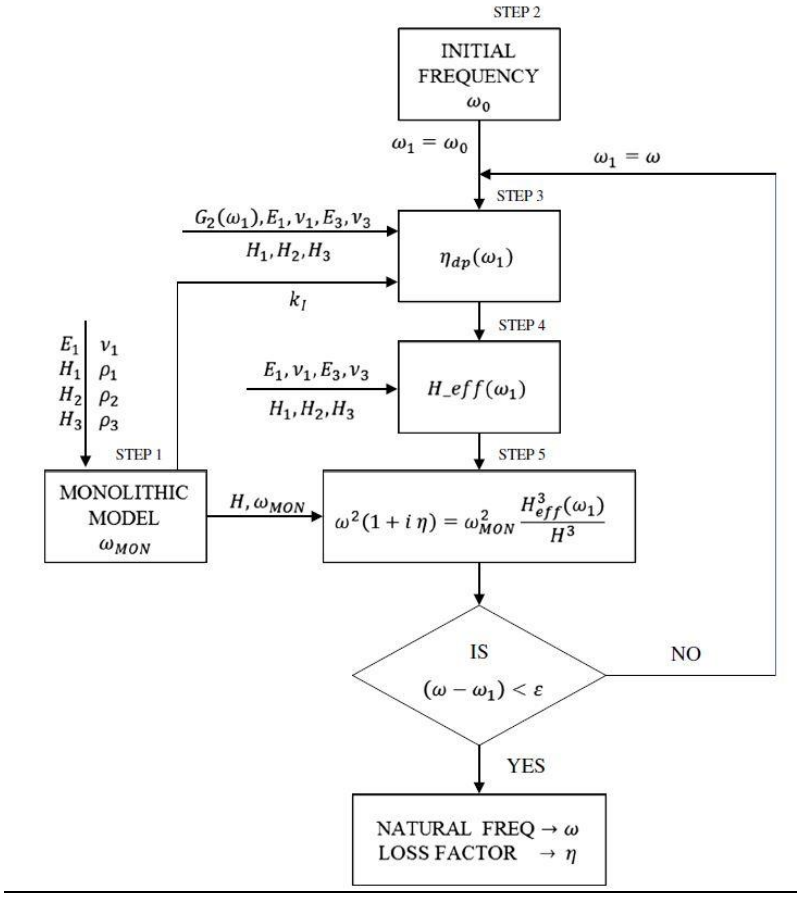

Figure 4.2: Lopez – Pelayo effective based method [17]

4.2 – A SIMPLIFIED APPROACH TO THE DYNAMIC EFFECTIVE THICKNESS OF LAMINATED GLASS

The Lopez-Pelayo methodologies are able to calculate the dynamic effective thickness of a laminated glass starting from two different steps. Nevertheless, the proposed methods require a long computational time and a trial and error procedure that cannot be carried out for each window present onboard.

Since the damping loss factor can be calculated by the experimental campaign exposed in Chapter 5 and 6, the unique aspect that has to be adequately simulated is the natural frequency. On this base, a simplified method for the estimation of the dynamic effective thickness is presented

4.2.1 – Natural mode based DEET

Once the natural frequency f_{ij} is calculated, from a numerical and/or experimental analyses, by the Timoshenko plate theory [53] it is possible to calculate the flexural rigidity D from Eq. 4.1.

$$fij = \frac{\lambda_{ij}^2}{2\pi a2} D^{1/2} \tag{4.1}$$

Substituting the obtained flexural rigidity in the Eq. 2.15, the correlation parameter η_{2D} can be easily calculated.

Moreover, from the D_{eq} previously calculated, it is possible to extract the equivalent thickness value in order to have a monolithic plate with the same starting natural frequency f_{ij}.

4.2.2 – ERP based DEET

Since the natural frequencies of a plate are infinite[54], the natural frequency, on which the simplified DEET is tuned, has to be selected carefully. For the scope of this thesis, and, more in general, in the NVH framework, the most interesting natural mode is the one that propagate the highest level of energy to the environment [55]. For this porpoise, the effective radiated power (ERP) could be considered the parameter that better reflects the capability of the structure to transmit noise and vibration.

In a mathematical sense, ERP squares the normal velocity and multiplies it with the element area. The sum over this product, multiplied with a constant yields the ERP over a panel. ERP values can be calculated for both structure and structure-fluid models. In MSC Nastran [48] it is calculated as:

$$ERP(f) = \alpha \cdot RLF \cdot \rho f \cdot c \cdot \int_{\Omega} v_n^2(f)\, ds \tag{4.2}$$

where:

- $\alpha = 1/2$ for Frequency Response analysis and $\alpha = 1$ for Transient Response analysis;
- RLF is the radiation loss factor;
- ϱ_f is the fluid density:
- c is the speed of sound in the fluid.

The card of the ERP calculation in MSC Nastran has been reported in Fig. 4.3.

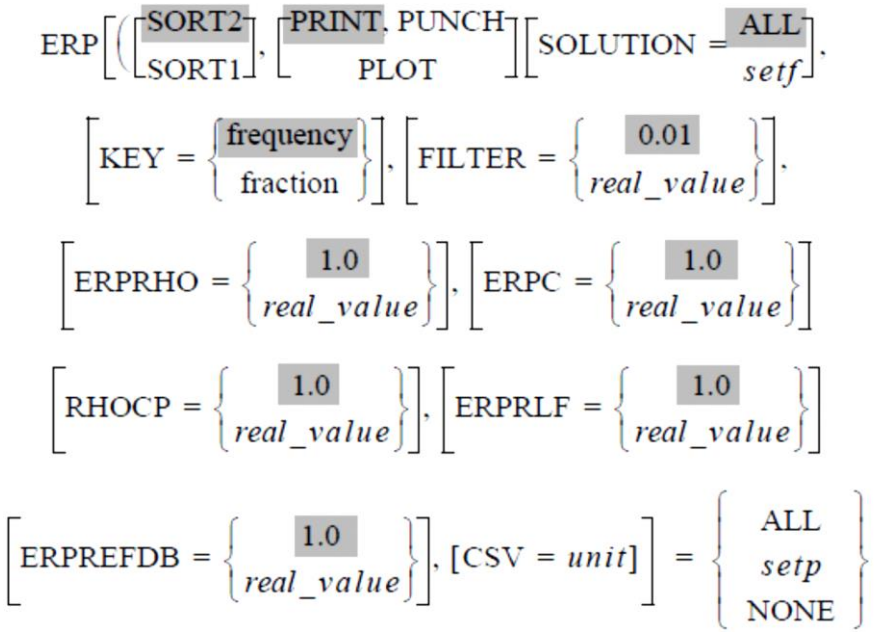

Figure 4.3: Nastran card for ERP calculation [48]

The numerical model, that has been developed for this porpoise, has been created, as in Fig. 4.4, by using shell elements for glass plies and solid elements for the interlayers. An additional window strip is created all long the net glass surface in order to represent the gluing surface between glass and metallic structures. The model has been constrained by displacement fixities all along the gluing strip and it has been loaded by applying a unitary velocity field, constant in frequency, in the same nodes, in order to simulate a pink noise propagation.

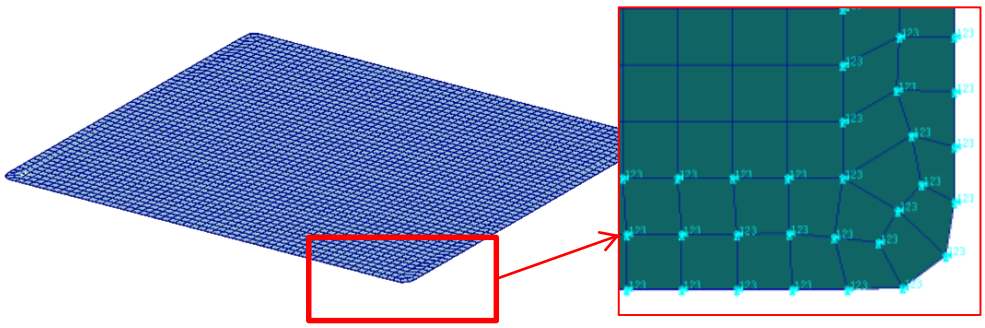

Figure 4.4: Numerical model for ERP calculation

The results of the ERP calculation of the S7 window, as it will be defined in the next Chapter 9, has been reported in Fig. 4.5.

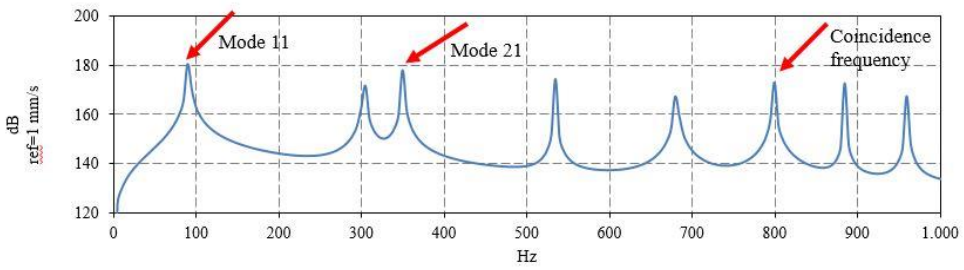

Figure 4.5: ERP results of S7 window

The main peaks in the plate response refers to the Model 11 and Mode 21 respectively and to the coincidence frequency f_C, that is defined as the frequency in which the sound celerity in the air c_0 is equal to the banding wave c_B in the plate. In particular:

$$c_B = \left(\frac{4\pi^2 f_C^2 D_{eq}}{\gamma}\right)^2 = c_0 = 343\ m/s \qquad (4.3)$$

By the way, this procedure has to be repeated for each window installed onboard, since the most effective natural frequency could change. Nevertheless, the Mode 11 can be considered the most effective in almost all the tested cases. For this scope, a parametric Nastran routine has been developed in order to calculate the ERP of each laminated window.

The script has been written in the own MSC Patran language and it is a session file *.ses that can be launched in the software by referring to an external parameter file *.dat. As it has been processed, the script could also create a gluing strip along the glass perimeter. The list of parameter for the 3 layered glass script has been reported in Table 4.1.

Table 4.1: Script parameters for the 3 layered model

Paramter	Explanation
L	Extension of the glass pane in the x direction [mm]
B	Extension of the glass pane in the y direction[mm]
T_1	Thickness of the inner glass ply[mm]
T_int	Thickness of the interlayer[mm]
T_2	Thickness of the outer glass ply[mm]
T_tot	Total thickness[mm]
E_vetro	Young modulus of glass [MPa]
Ni_vetro	Poisson's ratio of glass [MPa]
Rho_vetro	Density of glass [t/mm^3]
V_z	Velocity field (constant in frequency) on the gluing perimeter [mm/s]
Gel	Global edge length [mm]
F_inf	Frequency lower bound
F_sup	Frequency upper bound
F_step	Narrow band width
rhocp	Scale factor for the dB calculation [48]
Erpc	Speed of sound in fluid [mm/s]
Erprho	Fluid density [t/mm^3]
E_inter	Young modulus of interlayer [MPa]

Ni_inter	Poisson's ratio of interlayer [MPa]
Rho_inter	Density of interlayer [t/mm^3]

The script of the 3 layered model for the ERP calculation is reported in Annex A. In the same model, it is possible, by modifying the load case and the analysis set, to calculate the normal modes and natural frequencies of the glass pane, and it has been used in the analysis of windows proposed in Chapter

Chapter 5

RT BASED METHODOLOGY FOR THE DAMPING LOSS FACTOR CALCULATION OF VISCOELASTIC MATERIALS

Together with the estimation of the dynamic effective thickness, the other vibroacoustic parameter that reflects the capability of a material to damp or not vibration is the damping loss factor (DLF). The behaviour of viscoelastic materials in terms of damping loss factor is an open topic because of the complexity in the mechanical characterization of the material and in different configurations in which they can be used

Viscoelastic materials are largely used in ship and yacht construction when a reduction of vibration and noise levels is required. The final goal in this respect is to achieve the "acoustic black hole" [56], [57]i.e. an almost total absorption of any incident wave energy. As an example, floating floors and engine foundations are mainly based on the capability of viscoelastics to damp low frequency vibrations [58]. Moreover, modern laminated glasses use polyvinyl butyral (PVB) as interlayer in order to reduce both structural and airborne noise.

These solutions, even though not advisable to increase the structural capability to withstand loads, have been largely adopted considering the actual trend to increase comfort standards in super and megayachts. In this scenario, reliable numerical vibro-acoustic analyses, both deterministic and statistical ones, have to be adopted in the first design stages [59] , in order to reduce the economic impact of modification of structural scantlings and of the insulation plan. An accurate determination of the damping loss factor becomes mandatory in this

framework, because it could significantly affect the reliability of numerical simulations.

In this Chapter, a new methodology, lesser cost and time consuming if compared to the standard Oberst method for the estimation of the DLF of viscoelastic materials, based on experimental analysis, is proposed; in the next Chapter 6, it will be also extended to laminated glass panes.

5.1 - DAMPING LOSS FACTOR MEASUREMENT METHODS

The evaluation of the damping loss factor in structural engineering can be carried out by using several different analytical methods [60]

These techniques are used for determining DLF for each octave band fraction in order to evaluate the dynamic response of the material and of the entire structure or only in correspondence of peak values of the frequency response function (FRF), that corresponds to the natural modes of the structure[61].

It is obvious that a dynamic characterization based only on natural frequencies may over or underestimate the correct DLF value and it can carry to erroneous numerical calculations when experimental measurements are used in Finite Element based software.

In this thesis, four different DLF measurements methods have been considered[62], [63]:

- Half-Power Bandwidth Method (HPBM);
- Logarithmic Decrement Method:
- Circle Fit Method;
- Reverberation Time Method.

5.1.1 - Half power bandwidth method

By using the HPBM, it is possible to define the loss factor α only based on the amplitude plot of the FRF [64].

The HPBM defines the frequency range in which the response function is reduced by √2/2, or, in a logarithmic scale, by -3dB (Fig. 5.1). By the way, considering each resonance peak, that represents each natural modes of the structure, α_{HPBM} can be defined as it follows:

$$\alpha_{HPBM} = \frac{b}{\omega_r} = \frac{\omega_b - \omega_a}{\omega_r} \tag{5.1}$$

where ω_b-ω_a describes the above mentioned frequency range and ω_r is the resonance frequency.

This simple method is very sensitive on the accurate description of the FRF, so a closed sampling frequency is required during experimental measurements. Moreover, it cannot be accurate for very sharp peaks (small damping) and for float ones (large damping).

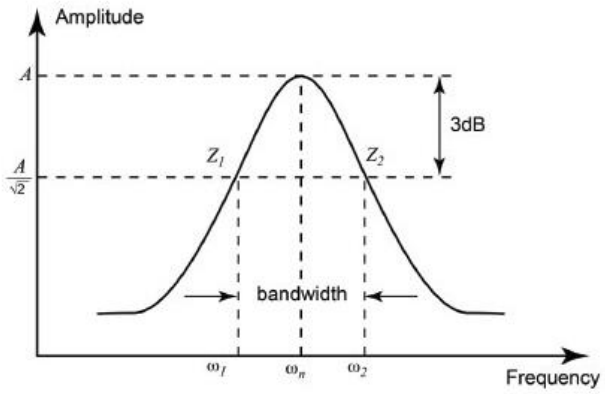

Figure 5.1: Half power bandwidth method

5.1.2 - Logarithmic decrement method

In this case, the loss factor α_{LDM} (Eq. 5.2) is calculated by analysing the logarithmic time decay of vibrations, for each resonance peak:

$$\alpha_{LDM} = \frac{1}{m} \ln \frac{x_n}{x_{n+m}} \tag{5.2}$$

where x_n is the resonance peak under consideration and x_m is the amplitude of the peak, m periods away.

The Logarithmic Decrement Method is particularly suited for measuring small damping values, while it has limitations in the case of high damping values, which implies a rapid decay in time that makes this calculation impossible to be computed.

5.1.3 - Circle fit method

The Circle Fit Method is based on a different representation of the FRF, the so-called Nyquist plot, in which frequencies around resonances identifies precise points, describing a circle.

It can be shown [65] that the inverse of the so called "sweep rate parameter" (which represents the rate at which the point representing the FRF moves along the circle for increasing frequencies) is maximum at resonance, where it provides an estimate of the DLF α_{CFM}:

$$\alpha_{CFM} = \frac{\omega_a^2 - \omega_b^2}{\omega_r^2 \left[tg\left(\frac{\theta_a}{2}\right) + tg\left(\frac{\theta_b}{2}\right) \right]} \tag{5.3}$$

where θ_a and θ_b are the phases of the FRF at points a and b respectively.

The Circle Fit Method is suitable for a wide range of damping values, giving an accurate description of DLF without remarkable approximations.

5.1.4 - Reverberation time method

All the above-mentioned damping measurements can be only used while considering resonance peaks corresponding to the natural frequencies of the structural subsystem.

In some applications, it can be useful to define the DLF as a spectrum based on a wider range of frequencies, in order to have a more accurate description of the dynamic response of materials.

For ship applications, the acoustic black hole can be only achieved by the calculation of the damping of viscoelastic materials for a very large frequency range, because of the nature of the vibration sources.

For this purpose, the Reverberation Time Method is the more reliable technique, being the most used in acoustic rooms for calculating the reverberation time (RT). It represents the rate of decay of the sound level, and it is inversely proportional to the amount of sound absorption.

The advantages of this method are the capability to define the entire DLF spectrum and the independence of the results from the input function, so a hammer impulse force is not required.

The loss factor, which is a measure of the proportion of vibrational energy that is dissipated during one cycle of vibration, is inversely proportional to RT.

The Reverberation Time Method implements different RT definitions based on the dB decay of the FRF for each octave band. So, RT15, RT30, RT60 can be defined by considering a loss of 15 dB, 30 dB and 60 dB, respectively. α_{RT60} is the DLF calculated by using RT60 and it can be calculated as it follows:

$$\alpha_{RT60} = \frac{\ln 10^6}{\omega T_{60}} = \frac{2.2}{f T_{60}} \tag{5.4}$$

5.2 - EXPERIMENTAL PRELIMINAR ANALYSIS ON A BARE STEEL PLATE

5.2.1 – Specimen set up

The first stage of this research was devoted to identify a specimen that represents a typical superyacht structure. Moreover, costs and construction time of these simplified plates should be as restrained as possible, in order to have the possibility to replicate the set up for different typology of viscoelastic materials.

The final choice has been identified in a steel stiffened plate, whose dimensions are reported in Fig. 5.2 and 5.3.

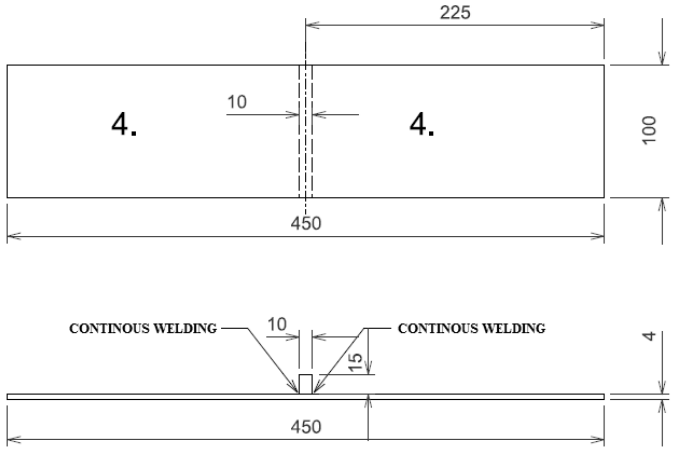

Figure 5.2: Specimen's dimensions and set up

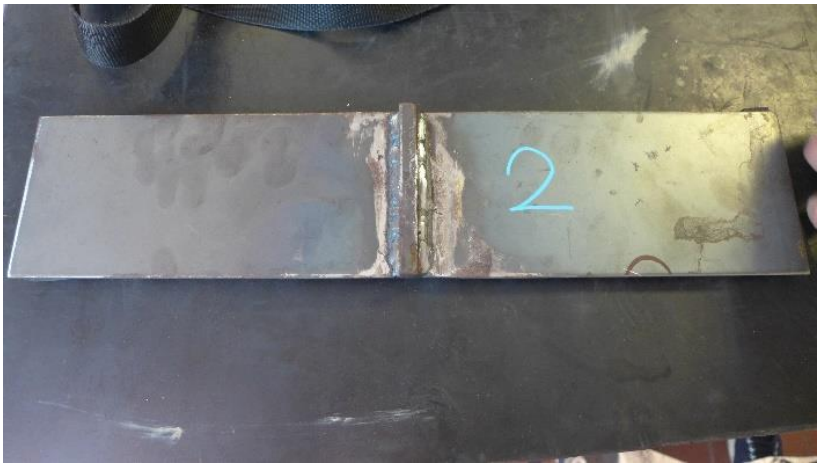

Figure 5.3: Specimen for damping loss factor calculation

The aforementioned configuration, that represent the typical thickness of a superyacht's deck , has been chosen in order to hit the central stiffener and to measure the FRF or the RT in any point of the plate. In this condition, the response function is not affected by excessive energy that could be introduced in the structural system [62]

The excitation device used in tests is an instrumented impulse hammer (PCB Impact Hammer model 086D0) with a medium Teflon tip and a weight of 0.32 kg. For what the transduction system is concerned, piezoelectric accelerometers were used (PCB accelerometers model 353B03); they are uniaxial accelerometers mounted on the centre of samples by using a thin layer of bees-wax. The analyser is a four-channel SOUNDBOOK™ system and the acquisitions have been run by the software Sinus SAMURAI™.

5.2.2 Specimen modal FE analysis

If dealing with Reverberation Time Method, it is necessary to excite the larger number of natural modes as possible.

As affirmed in [58], the piezoelectric accelerometers have to be placed in areas of plates where the relative displacements are greater; for these reasons, a former

Finite Element (FE) analysis has been carried out in order to obtain natural frequencies and modes of the stiffened plates [66],by using the eigenvalue normal mode analysis. The plate has been created by using 2D linear shell elements CQUAD4 and the central stiffeners by using 3D solid element CHEXA. The structure has not been constrained and loaded.

The final model is composed of up to 1'800 elements and 2'100 nodes. The eigenvalue extraction has been carried out by using the Lanczos method, in order to find all the eigenvalues and eigenvector that solves the normal mode equation:

$$\det([K] - \lambda[M]) = 0 \tag{5.5}$$

where [K] is the stiffness matrix, [M] the mass matrix, λ are the eigenvalues. This is the solution of the well known [58] harmonic vibration equation, excluding the trivial solutions in which the eigenvectors ϕ=0:

$$([K] - \omega^2[M])\{\phi\} = 0 \tag{5.6}$$

The Lanczos method can be considered as the best compromise between a transformation method, in which the eigenvalue problem is transformed in a simplified form from which the extraction is easier, and a tracking method, in which the eigenvalues are extracted one by one using an iterative procedure. This algorithm can be considered as the most efficient for medium-large sized model both in terms of accuracy and calculation times.

The deformation plot of the former 6 natural modes are proposed from Fig. 5.4 to Fig. 5.9. In Table 5.1, a final report of the natural frequencies of each mode have been reported.

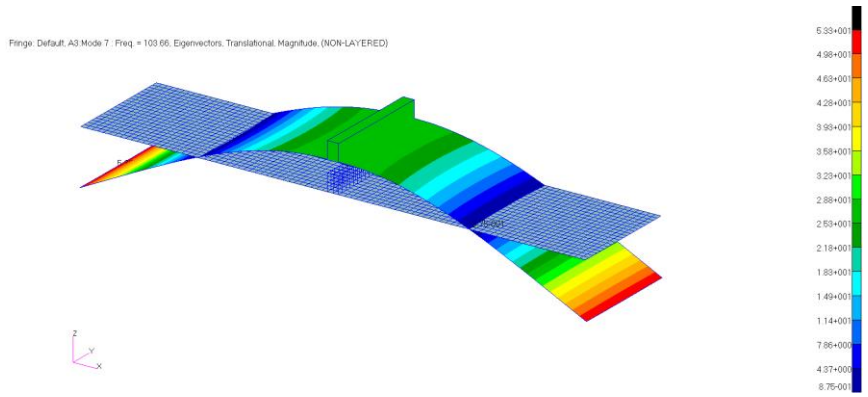

Figure 5.4: 1st natural mode of the specimen (103 Hz)

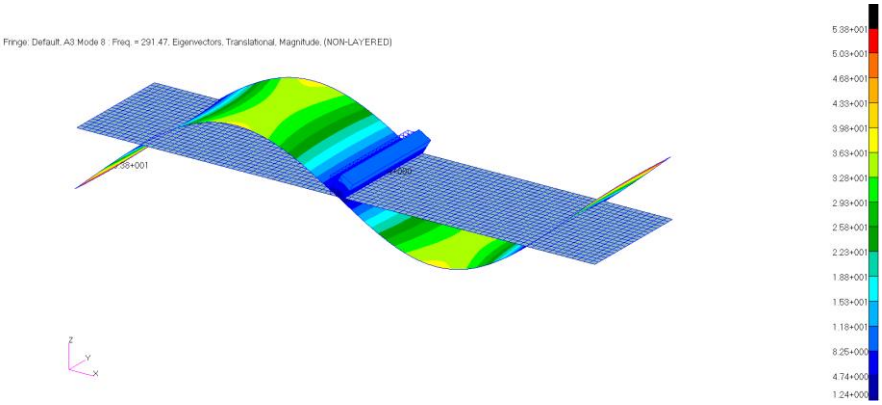

Figure 5.5: 2nd natural mode of the specimen (291 Hz)

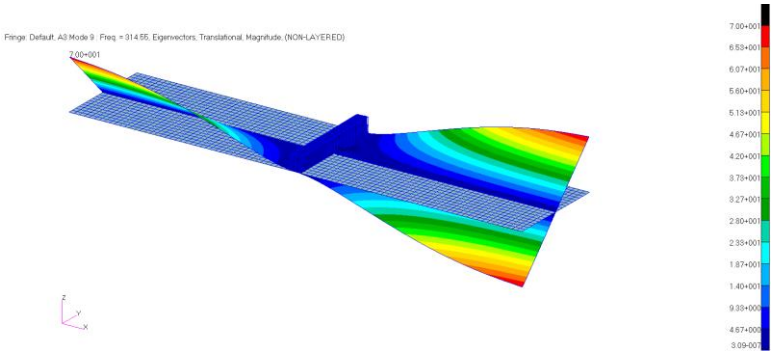

Figure 5.6: 3rd natural mode of the specimen (314 Hz)

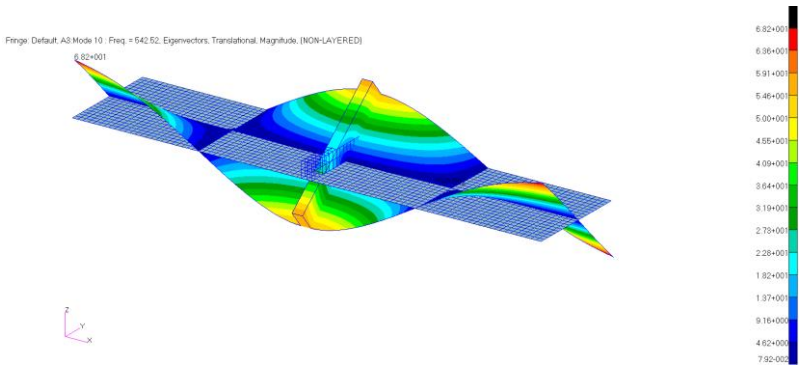

Figure 5.7: 4th natural mode of the specimen (542 Hz)

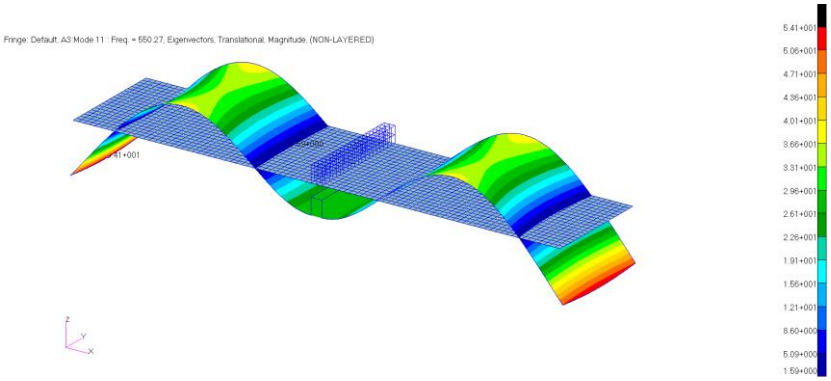

Figure 5.8: 5th natural mode of the specimen (550 Hz)

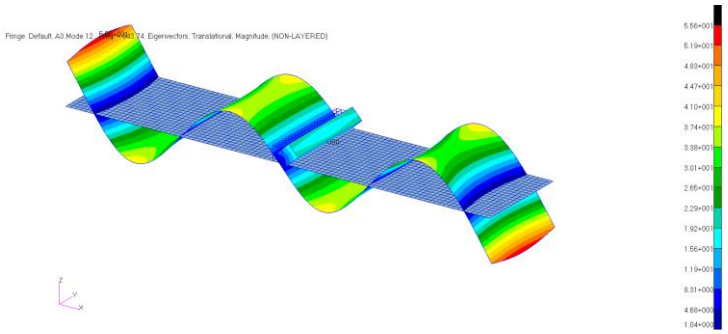

Figure 5.9: 6th natural mode of the specimen (943 Hz)

Table 5.1: Specimen's natural modes

Natural mode	Frequency [Hz]	Mode Type
1	103	1st flexural
2	291	2nd flexural
3	314	1st torsional

4	542	2nd torsional
5	550	3rd flexural
6	943	4th flexural

As it can be observed, at relatively low frequency, no transversal flexural modes can be excited; this is due to the higher transversal flexural stiffness if compared to the longitudinal one. As stated by Timoshenko [53] for uniform shells, the natural frequencies can be calculated as it follows:

$$f_{ij} = \frac{\lambda_{ij}^2}{2\pi a^2} D^{1/2} \tag{5.7}$$

where λ_{ij} are coefficients depending on boundary conditions and on the number of half-waves in longitudinal and transversal direction and D is flexural stiffness.

5.2.3 Specimen modal experimental analysis

From the results obtained by the afore mentioned FE analysis, steel plates have been tested by using the facilities described in Chapter 3.1.

In particular, the configuration shown in Fig. 5.10 have been selected as the most reliable and easy one to be investigated; two polyurethane rubber supports (Fig. 5.10b) have been lied in correspondence of the nodal line where the relative displacement of the first natural mode (Fig. 5.4) are equal to 0. Actually, the lower natural frequency of the specimen is the hardest to be excited by using a PCB Impact Hammer model 086D0.

Two piezoelectric mono-axial accelerometers have been placed at the extremities of the plates, one in the centre and one on the top (Fig. 10a); this configuration maximizes the number of natural frequencies that can be excited and so the response of the structure, both in terms of FRF and RT, is more reliable.

a)

b)

Figure 5.10: Experimental analysis configuration: (a) top view and (b) side view

The excitation of each specimen has been carried out with 15 hammer impacts in 3 different positions (Fig. 5.11): 5 on the stiffener's top, 5 in the centre and 5 in the bottom. In this way, a mean value of the FRF can be calculated, avoiding measurement's errors.

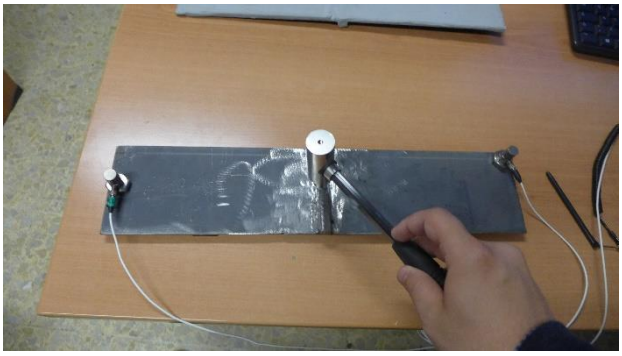

Figure 5.11: Excitation of the specimen

In this configuration, a complete series of tests have been carried out in order to calculate the DLF by using the four different methods herein exposed showing a perfect congruence among those methods.

In Fig. 5.12, the FRF with respect to the accelerometer placed on the left of Fig. 5.11 are visualized.

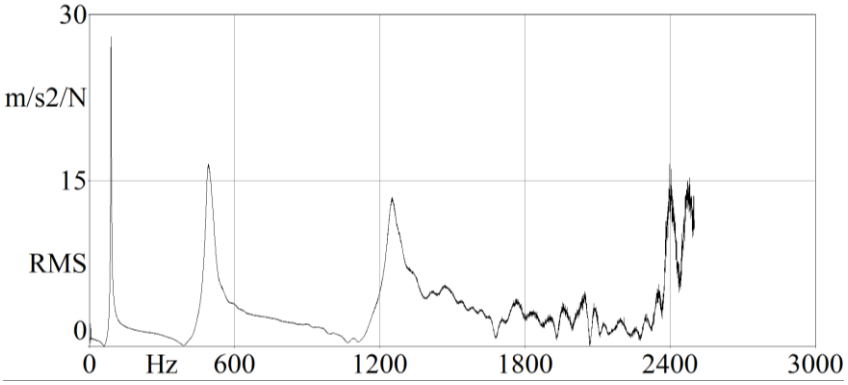

Figure 5.12: FRF of steel specimen

From Fig. 5.12, the calculation of α_{HPBM} have been carried out for the first and second natural modes of the specimen. Results are reported in Table 5.2

Table 5.2: Results obtained with half power bandwidth method for steel specimen

	Steel Specimen	
	f_r [Hz]	α_{HPBM}

1st Mode	100.7	0.0077
2nd Mode	542.6	0.0071

It can also be noted that for a frequency range higher than 1800 Hz, this configuration cannot be considered reliable because of the fluctuation of the FRF as shown in Fig. 5.12. It means that structure borne noise is more relevant than resonance.

The calculation of α_{LDM} have to be carried out by using the historical time signal (Fig. 5.13).

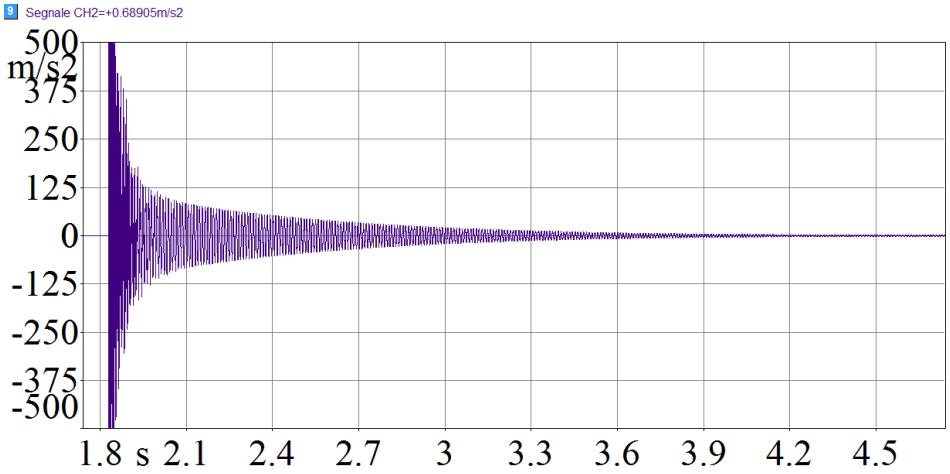

Figure 5.13: Historical time signal of steel specimen

From Fig. 5.13, the calculation of α_{LDM} have been carried out; as mentioned above, the DLF obtained by using this method cannot be calculated by a frequency based approach (Table 5.3).

Table 5.3: Results obtained with logarithmic decrement method for steel specimen

	Steel Specimen	
	f_r [Hz]	α_{LDM}
1st Mode	100.7	0.0069
2nd Mode	542.6	0.0074

The low level of DLF, graphically visible in the very long time decay, can also be verified by analysing the sonogram reported in Fig. 5.14.

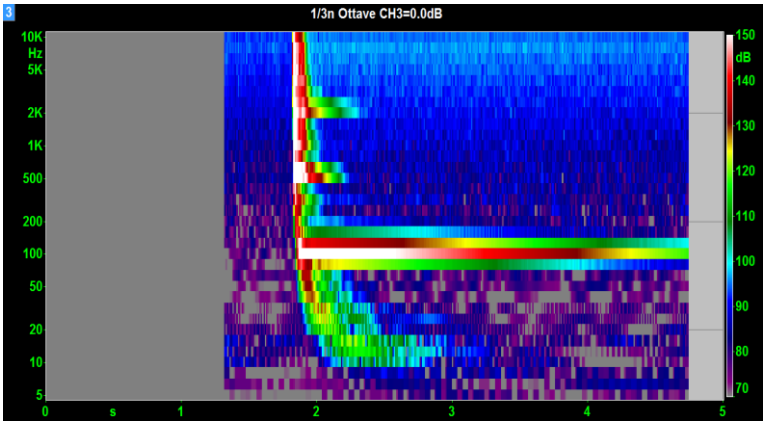

Figure 5.14: Sonogram of steel specimen

As it can be seen, the frequency with higher time decay is the one corresponding to the first natural mode, which is located in the 1/3 octave band 100 Hz centred.

The Nyquist plot have been reported in Fig. 5.15; the settings of the analyser have been changed in terms of trigger and number of lines in order to obtain visible circles for each normal modes of the specimen.

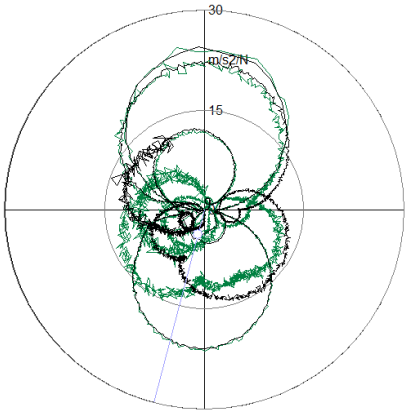

Figure 5.15: Nyquist plot of steel specimen

The results in terms of α_{CFM} are presented in Table 5.4 and, as expected, they are comparable with those obtained with different techniques.

Table 5.4: Results obtained with circle fit method for steel specimen

	Steel Specimen	
	f_r [Hz]	α_{CFM}
1st Mode	100.7	0.006
2nd Mode	542.6	0.0079

The last comparison have been carried out by comparing results obtained with FFT based techniques and the RT method. By studying the sonogram (Fig. 5.14), it can be clear that the most excited octave band is the one corresponding to 100 Hz, and so it should have the lower damping factor (Fig. 5.16).

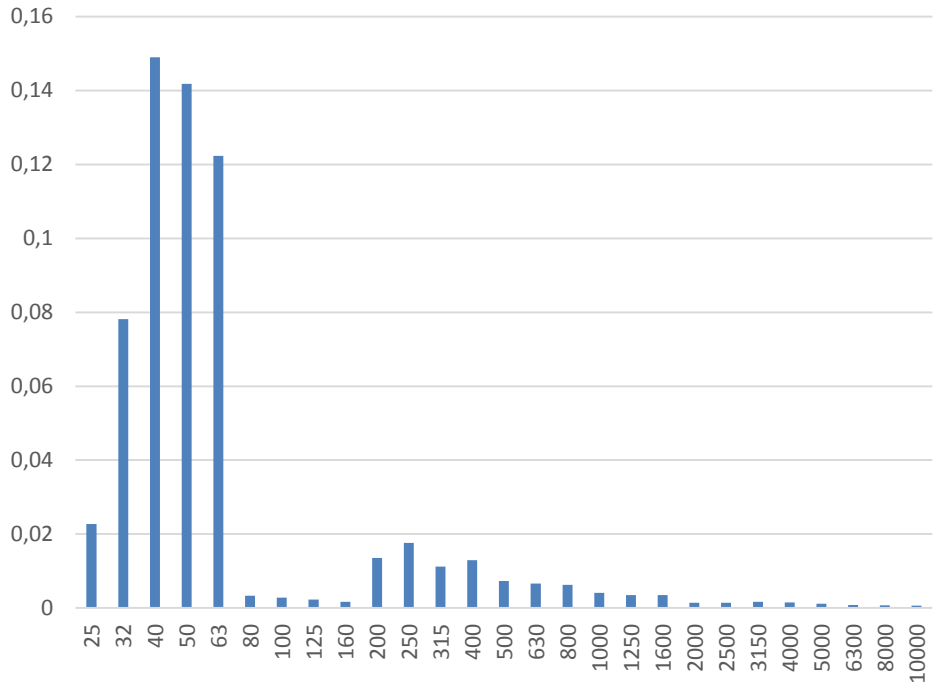

Figure 5.16: Results obtained with reverberation time method for steel specimen

The high damping value corresponding to the very low frequency range, says 25-80 Hz, cannot be considered reliable in accomplishment to the standard ISO 3382[67] that clarifies that if the BT value is lower than 16, the specimen is not able to respond with a significant energy that could be evaluated by the analyser.

By these comparisons, it appears clear that the four presented methods for the calculation of the damping loss factor are completely equivalent, as revealed also

for laminated glass in the next chapter; so, for the aims of this work, the RT60 method has been used, considering the above mentioned limitation due to the UNI EN ISO [67] threshold.

5.3 - EXPERIMENTAL ANALYSIS ON VISCOELASTIC MATERIALS

On the basis exposed in the previous chapter, several different specimen have been realized with the same dimension reported in Fig. 5.2.

They can be summarized in 3 different categories:

- Viscoelastic materials constrained by a metallic plate;
- Viscoelastic paints;
- Adhesive meta-materials composed by honeycomb plastics and metallic film glued by viscoelastic material.

A complete overview of all the specimens that have been studied in this research is presented in Fig. 5.17.

Figure 5.17: Specimen tested for the DLF estimation

The sonogram of the specimen "Visco constrained B" is reported in Fig. 5.18.

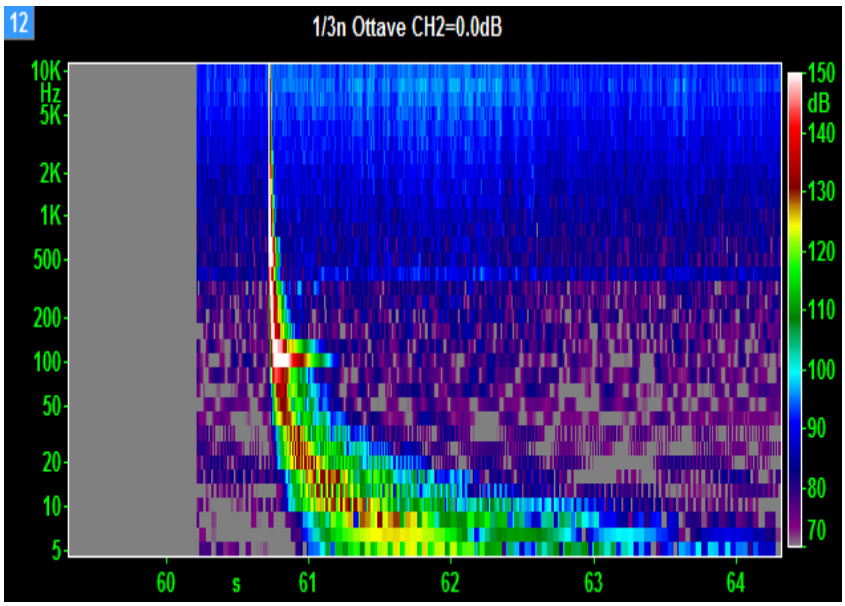

Figure 5.18: Sonogram of "Visco constrained B" specimen

By comparing the sonograms of Fig. 5.18 and Fig. 5.14, it can be easily highlighted the important reduction of the decay time for the first natural mode (@100 Hz), that corresponds to a significant increase in the damping loss factor.

The results of the experimental activity is reported in terms of DLF spectra in Fig. 5.19.

For each specimen, 10 different measurements have been carried out in order to reduce the deviation as much as possible and in order to avoid the ISO threshold by using different input forces. If all the measurements complies with the regulation, the mean decay time has been considered; if some measurements do not comply with ISO, only the correct one have been studied.

In the very low frequency range, say under 100 Hz, the DLF estimation cannot be considered as fully reliable because the specimen has no natural modes and so the decay time is too short, according to the UNI EN ISO [67]

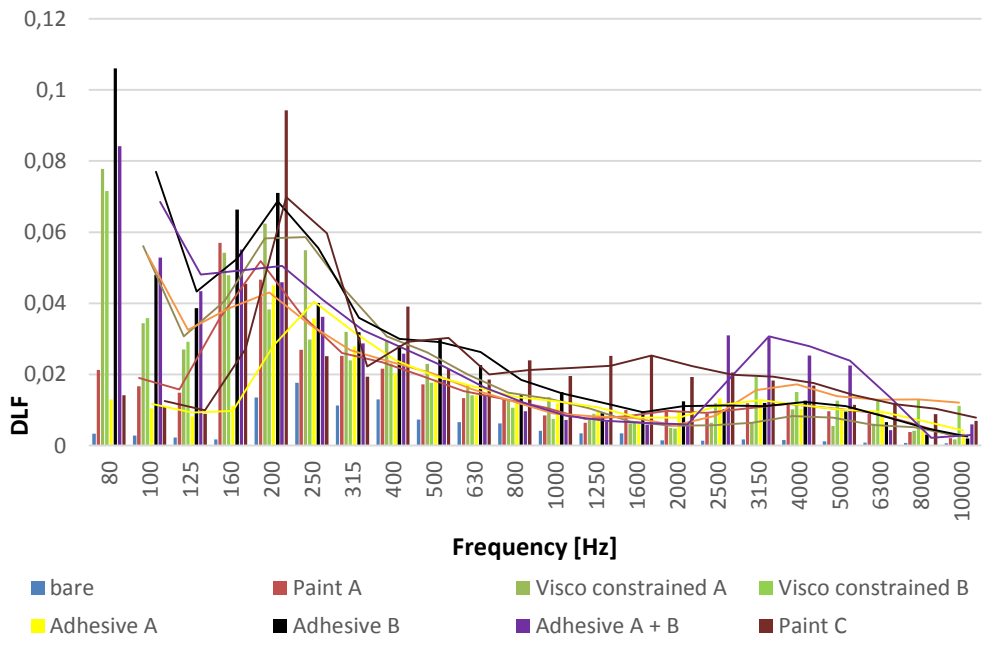

Figure 5.19: DLF spectrum for different viscoelastic specimens.

From a comprehensive analysis of DLF spectrum, some general considerations can be carried out:

- Adhesive meta-materials have the best performances for a wide frequency range. The unique limitations are the high material and installation costs and they can be used only for flat surfaces (e.g. yacht's side, beam's flanges) because the honeycomb plastic cannot be easily curved.
- Classic viscoelastic materials has an important inertia effect due the constraining plate and their performances improves especially for resonant frequencies; so, they can be used for zone that are excited by constant frequency forces, such as engine foundations.
- Viscoelastic paints have global lower DLF, but their effect is not affected by the frequency in which they operate, so they can be used for the treatment of random excitation sources such as waves, sloshing, etc.

5.3.1 – Experimental analysis on specimen of different shape and material

In order to be considered reliable, the method herein presented, has to be not dependent on the specimen, in terms of metallic material, shape and dimension.

This reliability have been achieved by testing 1200X1200 aluminium plates (Fig. 5.20), that have been treated by using "Visco constrained A" on the left part and by using "Visco constrained B" on the right part.

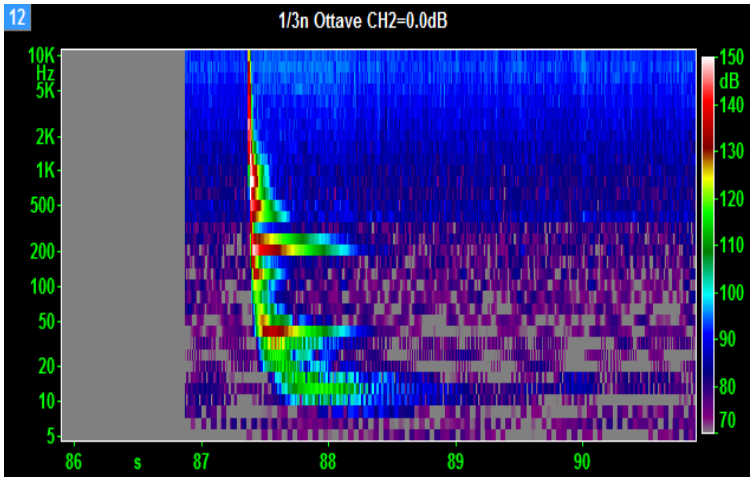

Figure 5.20: Sonogram of the treated aluminium specimen, "Visco Constrained B" side

By the way, this comparison cannot be carried out in terms of FFT, because the effect of the steel and aluminium plate is not comparable; so only the RT method can be used.

In Table 5.5, the final comparison between steel and aluminium supporting plate has been reported. As it can be clearly observed, the proposed method for the calculation of the DLF is independent from the dimension and construction material of the supporting plate.

Table 5.5: Comparison between DLF of steel supporting plate and aluminium bigger plate for "Visco constrained A" and "Visco Constrained B"

	"Visco Constrained A"	***"Visco Constrained B"***
Steel Specimen	0.034	0.035
Aluminium Specimen	0.036	0.035

5.4 - COMPARISON BETWEEN NUMERICAL AND EXPERIMENTAL DLF OF VISCOELASTIC MATERIALS

5.4.1 – Finite Element structural analysis

The damping properties of materials have a significant role in the numerical NVH assessment of yacht and naval structures, that is normally carried out by

using the Finite Element Method (Boote et al. 2013). As seen in Fig. 14 and Fig. 18, the viscoelastic treatment of a simple specimen can drastically modify both the FRF and the time response of the whole structure.

In FE analyses, the vibration response of complex structures is commonly carried out by evaluating the frequency response function that is calculated by the FFT [48].

This simplified approach does not allow to use the complete DLF spectrum as computed in Fig. 19, because the numerical solver use the Rayleigh approach, in which the damping effect is seen as a linear modification of the global stiffener's matrix:

$$[K] = (1 + iG)[K] + i \sum G_E [K_E] \tag{5.7}$$

in which G is a frequency dependant damping factor, that has to be calibrated with experimental analysis. The second term of Eq. 12 takes into account localized damping element, such as springs, dampers, bushes, etc.

In order to directly use the DLF spectrum as calculated in the previous part of this work, only explicit non-linear analyses has to be carried out, in which the solution is not given by the calculation of the inverse stiffness matrix, but the software solves directly the motion equation [48]:

$$[M][a_n] = [F_n^{est}] - [F_n^{int}] \tag{5.8}$$

In this framework, the computational times and costs required for this type of analysis are very expensive, even because the mesh size and the time step are strictly related by the Courant's convergence criterion:

$$\Delta t = \frac{SL}{c} \tag{5.9}$$

Then, this analysis could be useful only for very small specimens or in case of high non-linearity.

5.4.2 - Statistical Energy Analysis

For what concerns the mid to high frequency range, the deterministic approach of the Finite Element Method could not be considered reliable without the use of specific tools, such as the Monte Carlo Approach [68].

In this case, the NVH assessment can be carried out only by using statistical approaches, as the Statistical Energy Analysis (SEA), which can solve the power balance equation among different subsystems.

These equations are driven by the modal density n of each subsystem and, as stated by Lyon [69], the SEA could be considered reliable only for frequency bands with modal density greater than 2. For lower frequencies, an hybrid FEM-SEA model could be performed as seen in Fig. 5.21.

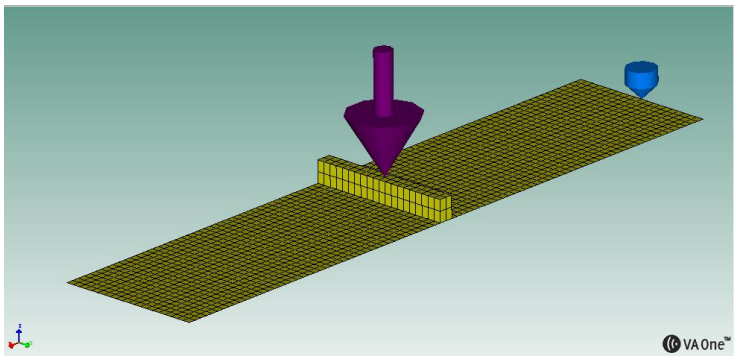

Figure 5.21: Hybrid FEM-SEA model of steel specimen

By using an hybrid approach, the modal density is no more calculated by theoretical formulations, but by using a FE solver and then the SEA software can easily compute the power balance without uncertainties.

For the validation of the DLF evaluation exposed in this paper, the steel specimen have been tested by the hybrid analysis. A constant (in frequency)

force (purple arrow in Fig. 5.21) have been applied in the same location of the experimental analysis and a velocity sensor (blue arrow in Fig. 21) has been located in correspondence of the accelerometer.

The DLF spectrum, as calculated in Fig. 5.19 by the RT method, has been used in the VaOne software. By the analysis of the velocity output spectrum in the 50-150 Hz frequency range (Fig. 5.22), the damping factor can be calculated with the HPBM method in correspondence of the peak of the first natural mode.

For this validation, two different DLF spectra has been tested: the steel specimen without any treatment and the "Visco Constrained B" specimen, in order to simulate the insulation material, and the results in term of DLF have been reported in Table 5.6.

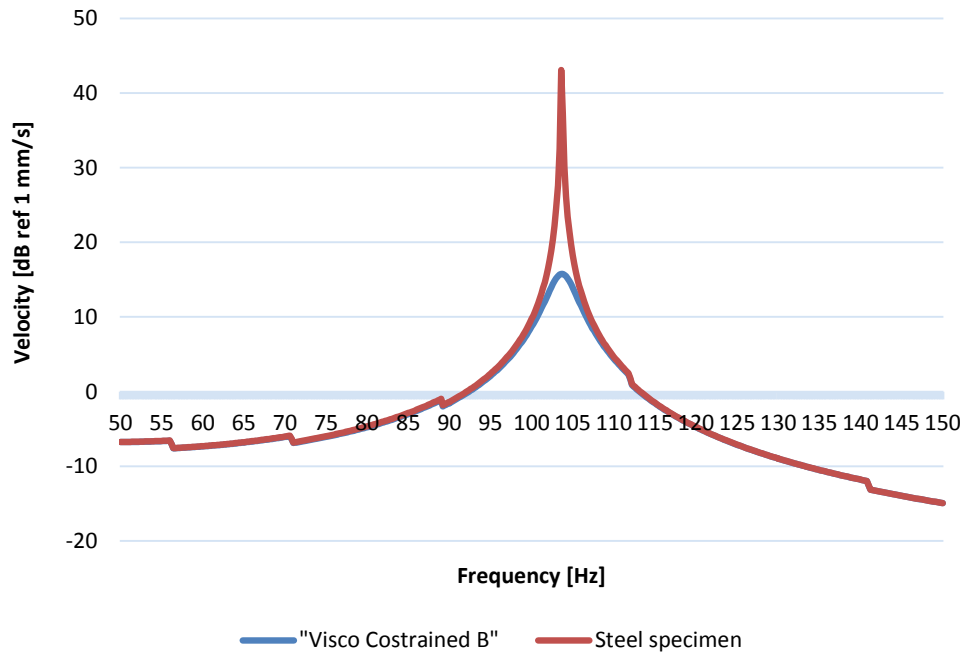

Figure 5.22: Velocity output spectrum of the steel specimen (red line) and "Visco Constrained B" specimen (blue line).

Table 5.6: Comparison between damping coefficient obtained by experimental tests and hybrid SEA-FEM analysis for the first natural mode

	Experimental activity	Numerical analysis
Steel Specimen	0.002	0.003
"Visco Constrained B"	0.035	0.038

Chapter 6

VIBROACOUSTIC CHARACTERIZATION OF LAMINATED GLASS

The aforementioned procedure has been adopting also for the estimation of the damping loss factor of laminated glass. In particular, two series of experimental tests have been carried out in this Chapter; in a first stage, the effect of different glass and interlayer thickness has been tested by 3 specimens. In a second stage, the role of an additional glass, passing from a 5 layer window to a 5 layer one, and the difference between a symmetrical lamination and an asymmetrical one has been assessed as well, in order to carry out a comprehensive study that would lead to a more refined use of different laminated glass in the superyacht NVH framework

6.1 – DLF EVALUATION ON 3 LAYER LAMINATED GLASSES

6.1.1 Test set up

Tests were performed on three samples of laminated glass plates, composed by two glass plies and an interlayer, that have the same planar dimensions (300x300 mm) but different thickness of the glass plies t_{glass} and of the PVB interlayer t_{PVB}:

- Sample 1: t_{glass}=6mm, t_{PVB}=1.52mm;
- Sample 2: t_{glass}=3mm, t_{PVB}=0.38mm;
- Sample 3: t_{glass}=8mm, t_{PVB}=0.38mm.

Tests was performed in free boundary condition, i.e. minimizing the interaction with the surrounding environment, in order to exclude external interferences as much as possible. In this sense, samples have been tested supported on vertexes

by very soft cushions made by polyurethane rubber supports (Fig. 6.1). The area of supports has been minimized in order to obtain a frequency response function not affected by shear leg effect [58], as for viscoelastic characterisation.

The hammer hits were given in the centre of samples for the modal analysis, in order to excite the third and the eighth mode of the free plates, and in seven different points to excite the maximum possible number of normal modes, as it can be seen in Fig. 6.1.

(a)

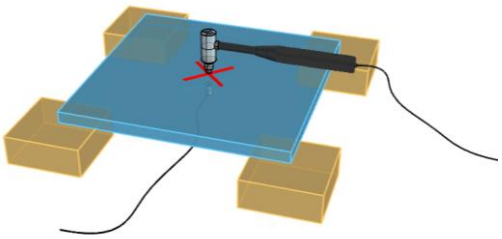

(b)

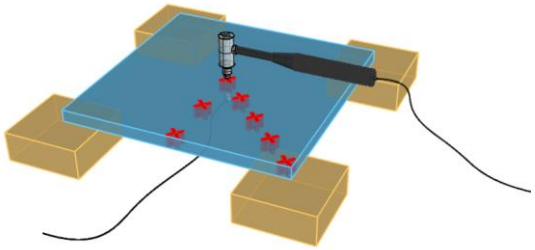

Figure 6.1: Configuration of modal tests (a) and reverberation time tests (b).

6.1.2 Experimental results

In order to confirm the results of Chapter 5, all the four methodology for the calculation of the damping loss factor have been tested also for laminated glass. Fig. 6.2 shows, as an example, the application of the HPBM method for sample 1. The full result set is summarized in Table 6.1.

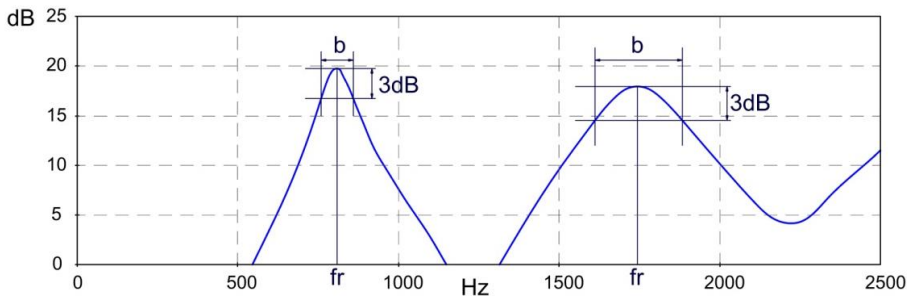

Figure 6.2: Application of the Half Power Bandwidth method to Sample 1.

Table 6.1: Results obtained with halfpower bandwidth method for sample 1, 2 and 3.

	Sample 1		Sample 2		Sample 3	
	f_r	α_{HPBM}	f_r	α_{HPBM}	f_r	α_{HPBM}
1st Mode	803	0.125	400	0.061	1000	0.1
2nd Mode	1743	0.144	1011	0.088	2256	0.115

The second studied method is the Logarithmic Decrement Method. The resampling of the time signal for sample 3 is shown in Fig. 6.3 while Table 3 summarizes the obtained results.

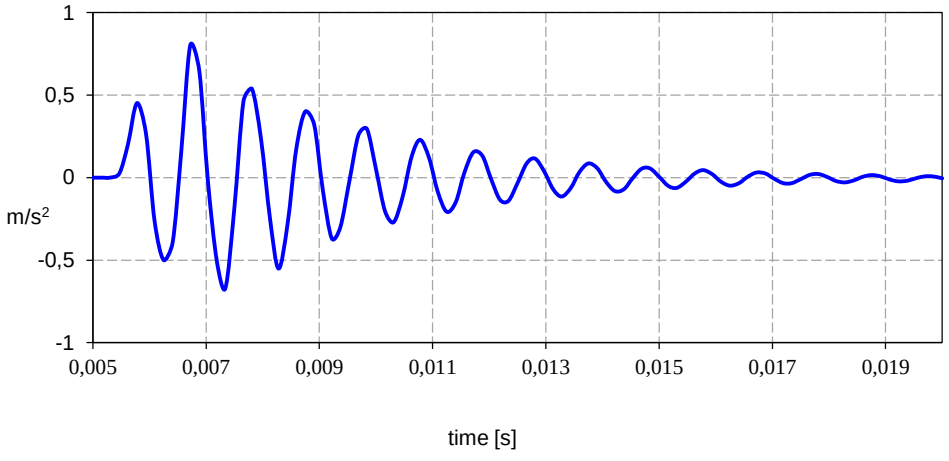

Figure 6.3: Resampling of the time signal of the accelerometer (sample 3).

Table 6.2: Application of logarithmic decrement method for the calculation of the damping loss factor for the first natural mode (sample 1, 2 and 3).

	Sample 1	Sample 2	Sample 3
α_{HPBM}	0.125	0.061	0.1
α_{LDM}	0.126	0.111	0.106

The third method under investigation is the Circle Fit Method [70]. The Nyquist plot as it can be seen in Fig. 6.4 has been used and the results are summarized in Table 6.3.

(a)

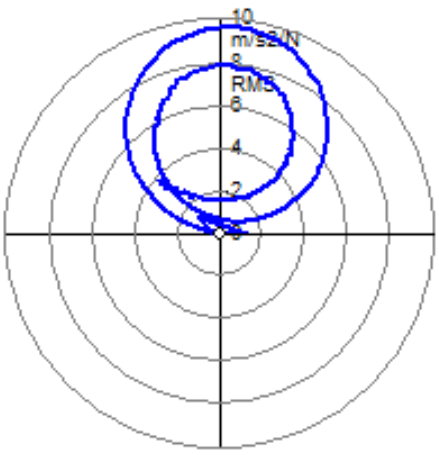

(b)

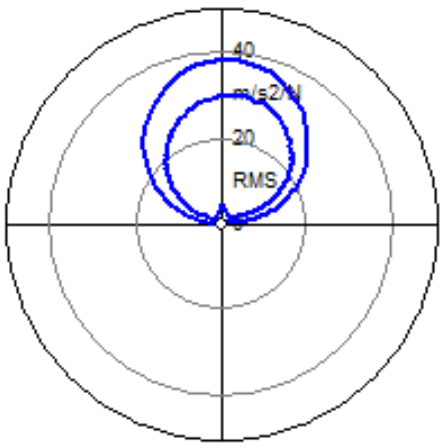

(c)

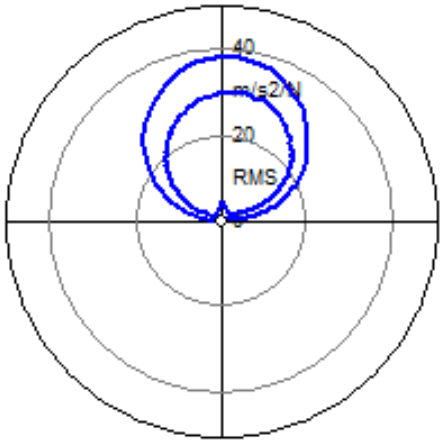

Figure 6.4: Nyquist plot obtained for (a) sample 1, (b) sample 2 and (c) sample 3.

Table 6.3: Application of the circle fit method for the calculation of the damping loss factor for sample 1, 2 and 3.

	Sample 1		Sample 2		Sample 3	
	f_r	α_{CFM}	f_r	α_{CFM}	f_r	α_{CFM}
1st Mode	800	0.130	398	0.060	993	0.103
2nd Mode	1731	0.171	1009	0.107	2250	0.124

The last applied method is the RT60 Method. The structural damping loss factor in one-third octave bands from 50 to 10000 Hz has been evaluated for each sample using the Time Decay procedure based on reverberation time (RT60) measurements. In order to ensure the correct evaluation of the time decay, measurements on shorter time signals have been performed. The decay has been considered linear and the time has been evaluated by a reverse integration method.

The trend of the EDT and the loss factor η in the frequency range under investigation for sample 2 is presented in Fig. 6.5.

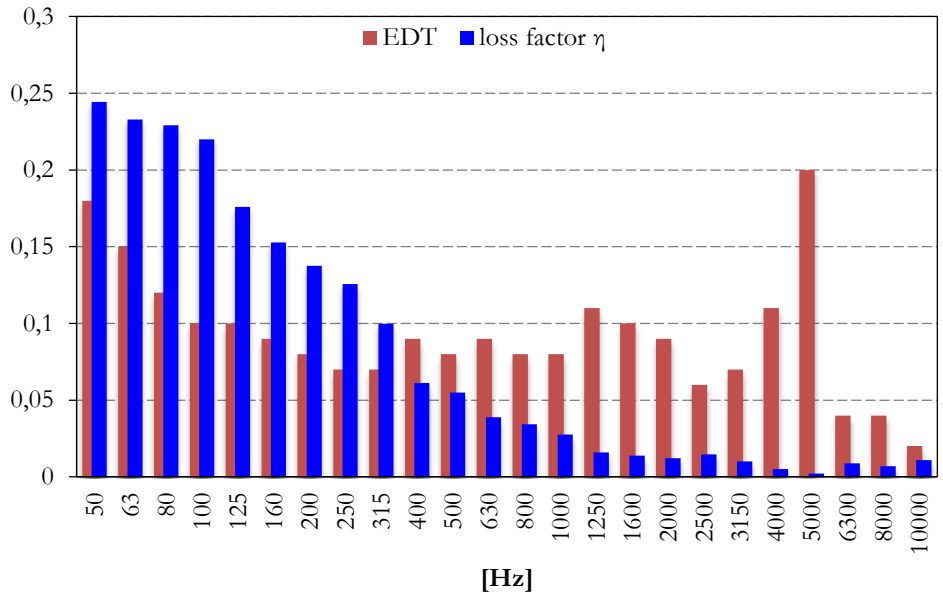

Figure 6.5: RT60 and loss factor values for sample 2.

Table 6.4 offers a comparison between loss factor values obtained by modal analysis and by reverberation time analysis.

Table 6.4: Damping loss factor calculation with different methods for the first natural mode.

	Sample 1	Sample 2	Sample 3
HPBM	0.125	0.061	0.1
LDM	0.126	0.111	0.106
CFM	0.13	0.060	0.103
RT60	0.092	0.061	0.11

As it can be observed the values of the loss factor obtained by different methods are really similar as observed for general viscoelastic materials in Chapter 5. Of course, when possible, it is better to perform a reverberation time analysis than a modal analysis, in order to get the trend of the loss factor for the frequency range of interest [71]. These data could then be entered in the model of the laminated window to take into account the damping properties of the structure.

6.2 – EFFECT OF THICKNESS IN THE VIBROACOUSTIC CHARACTERISTICS OF LAMINATED GLASS

A second series of experimental analysis have been carried out in order to evaluate the difference between a 3 layered laminated windows and a 5 layered one. The dimension of the specimen has been chosen of 800 x 1000 mm. In the following Fig. 6.6 and 6.7, the sonogram of the 3 layered and 5 layered specimen has been reported respectively.

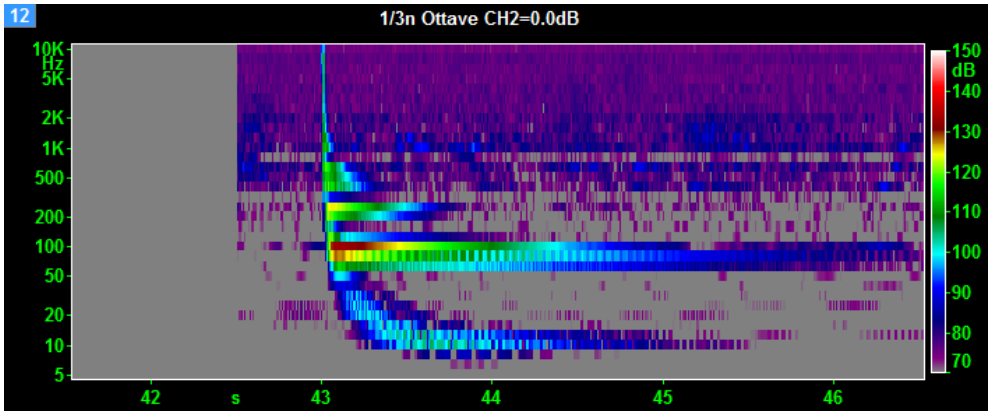

Figure 6.6: Sonogram of the 3 layered sample (centre of the panel)

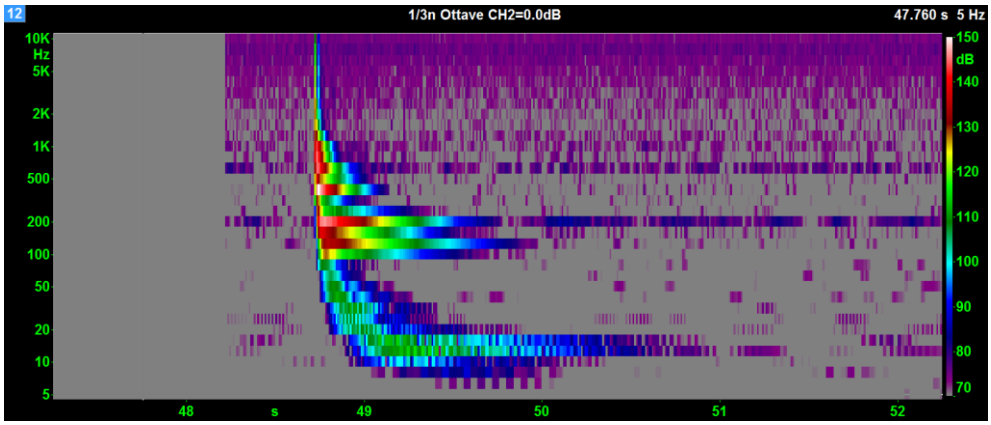

Figure 6.7: Sonogram of the 5 layered sample (centre of the panel)

As it appear clear from the previous figures, the 5 layered sample has an higher response in the mid frequency range (dark red areas), but the signal has a quicker

decay with respect to the 3 layered one. In Fig. 6.8, the DLF spectrum of the two specimens has been calculated by using Eq. 5.4.

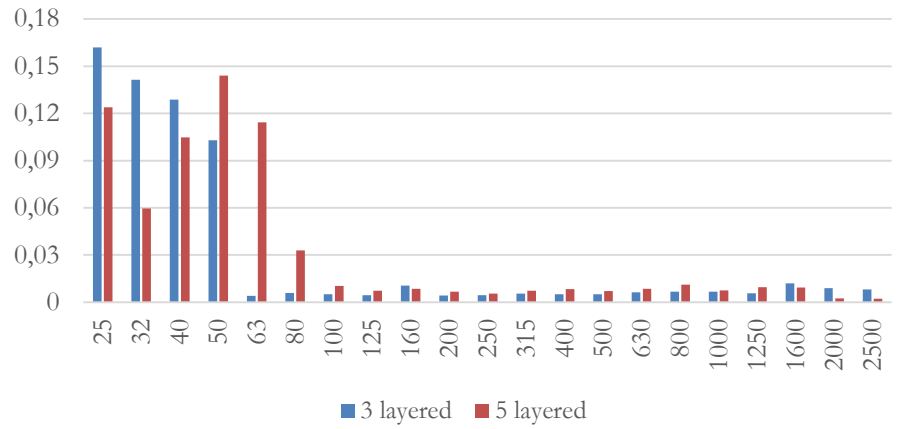

Figure 6.8: DLF of 3 and 5 layered laminated glass Samples

As it can be observed, in the low-mid frequency range, the 5 layered window has a better response then the 3 layered one; this is mainly due to the fact that the higher mass of the specimen has shifted the natural frequencies to the very low frequency range, where the 3 layered sample shows a better dynamic characteristic. In the high frequency range, where the modal bases are higher and the modal density increases, the two laminated glasses have a similar DLF spectrum.

So, for the common naval and nautical application, where the main excitation sources are in the low frequency range (say 80-200 Hz) the use of a 5 layered window, even though more expensive and heavier, should be more appropriate.

6.3 – EFFECT OF LAMINATION SIMMETRY IN THE VIBROACOUSTIC CHARACTERISTICS OF LAMINATED GLASS

In order to verify the effect of a symmetric or asymmetric lamination stack on the vibroacoustic characteristics of laminated glass, the ERP has been selected

as the more interesting parameter, since, by a numerical point of view, the asymmetric lamination stack shows the same natural frequency of the symmetric one, following Eq. 4.1 [53].

The window S1 of the superyacht study case selected in Chapter 8 has been chosen for this benchmark and the parametric model exposed in Section 4.1.2. In Fig. 6.9, the ERP [dB] as a function of narrow-band frequency has been reported; in Fig. 6.10, the spectrum has been transferred to third octave band centre frequencies. The asymmetric lamination sequence (11+3.04+13) has been generated by a difference in thickness of 2 mm between the glass plies, that is the maximum Δt that could be achieved without optical distortions of the image on the outer side of the windows[27].

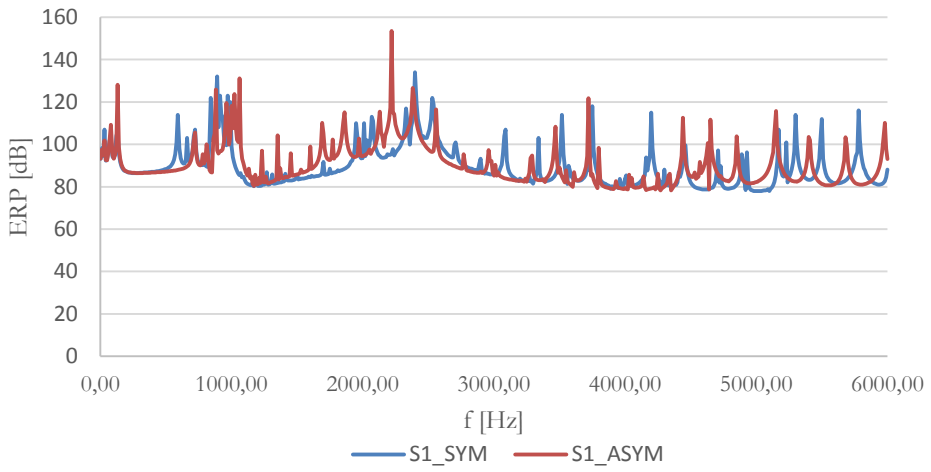

Figure 6.9: ERP for S1 windows in narrow band

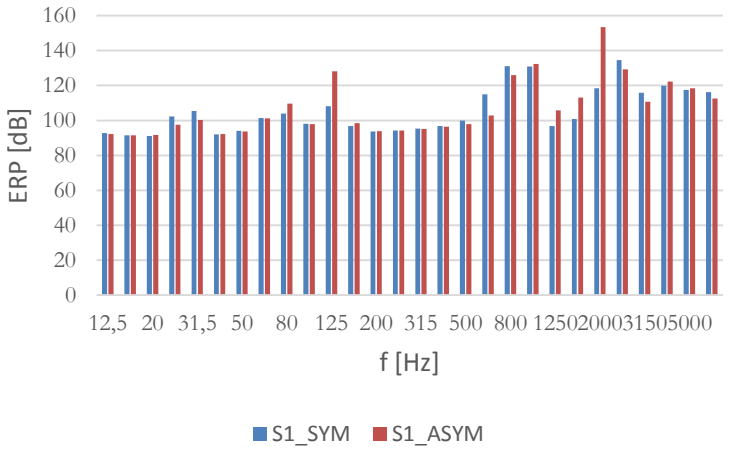

Figure 6.10: ERP for S1 windows in third octave band

As it can be seen from the previous graphs, the asymmetric window shows an higher energy transmission in the mid frequency range, especially in correspondence to the 125 Hz centred third octave band.

From a more general point of view, this result cannot be generalised, since the behaviour of the symmetric and asymmetric stack is strictly linked to the shear transfer mechanism of the interlayer, that could guarantee or avoid the collaboration of the outer glass ply. In this case, the PVB interlayer seems to uncouple the glass plies and so the natural frequencies of the two plates are different, generating a different modal density and so a different ERP.

Chapter 7

NUMERICAL VERTICAL HULL GIRDER VIBRATION ASSESSMENT OF A MEGAYACHT BY SUPERELEMENT ANALYSIS

In recent years, the definition of the dynamic assessment of a new vessel, beyond the static one, by the ship-owner and the builder has become a standard practice. The builder in this way assumes the task that vibration limits should not be exceeded and, if this does not happen, to identify and apply proper reliable solutions. In the preliminary design phase and during the subsequent construction phases, the yard performs a predictive study of the vibration levels of the structure or it can delegate this task to an independent technical office. The flow diagram in Figure 7.1 can synthesize the overall procedure [72].

For this scope, the assessment of hull girder vibration is mandatory; if local resonances are highlighted, the engineering solution could be somehow simple as stated by Pais[73] even if time and cost consuming. In the case of global resonances, the problem is more complicated since, as from Eq. 7.1, the unique way to modify the global ship vibration is to act on the weight (by increasing it, with obvious critical consequences) or on the cross section momentum of inertia.

For what concern the momentum of inertia of each cross section, as declared in Chapter 3, the presence of window panes in superstructures is crucial, because they extent for up to the 90% of the superstructure length itself. So, it must be evaluate if they can considered as collaborative at least in the hull girder vertical vibration, the most effective while dealing with comfort assessment.

In this Chapter, the effect of laminated glass on the vertical hull girder vibration has been assessed by using a FE model of a 80 meter superyacht, developed by the Technische Universität Hamburg (TUHH), that has been modified in order to be suitable for eigenvalue analysis.

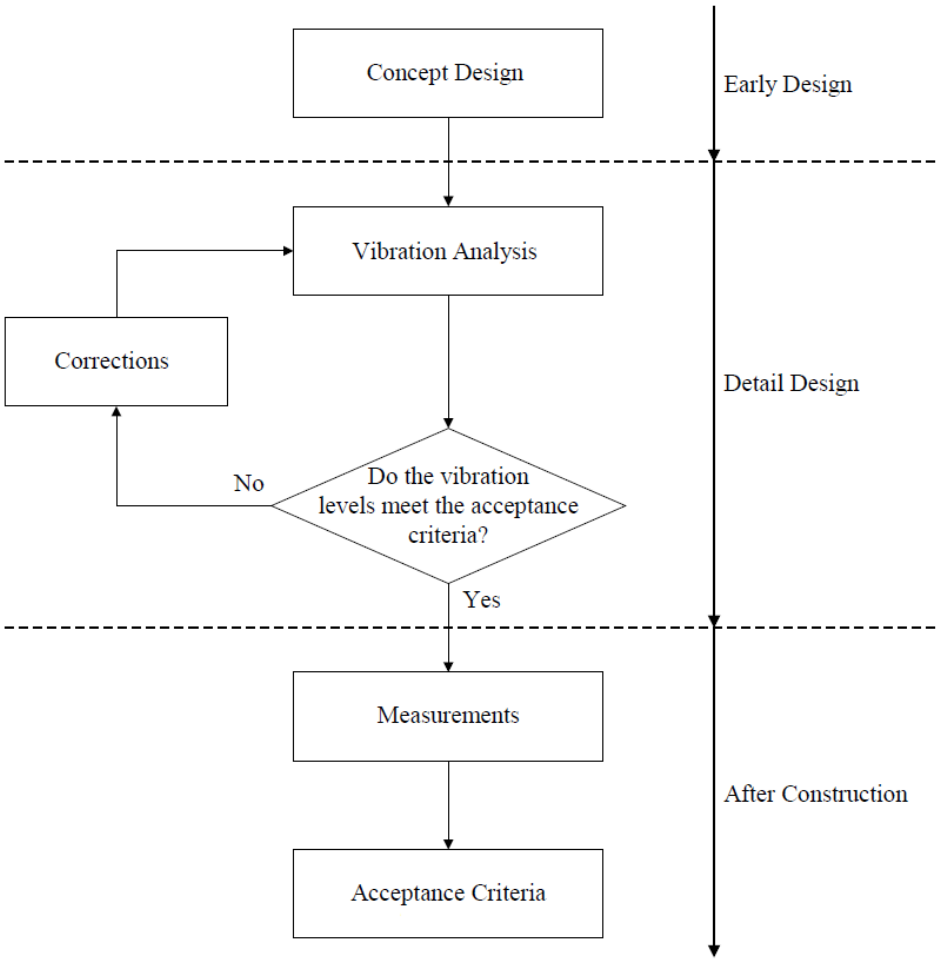

Figure 7.1: Flow diagram of vibration assessment [72]

7.1 – MODEL CREATION FOR HULL GIRDER VIBRATION ASSESSMENT

The model used for this analysis has been developed by the ship structure Department of the TUHH and it has been used to assess the contribution of glass pane to the global primary response of the yacht structure [9], [12] and to

verify the local behaviour of the glass pane in terms of reduction of corner stresses in the window recess.

The model has been created by using a coarse mesh (Fig. 7.2) for the steel and aluminium structure an it is based on the substructure technique[74].

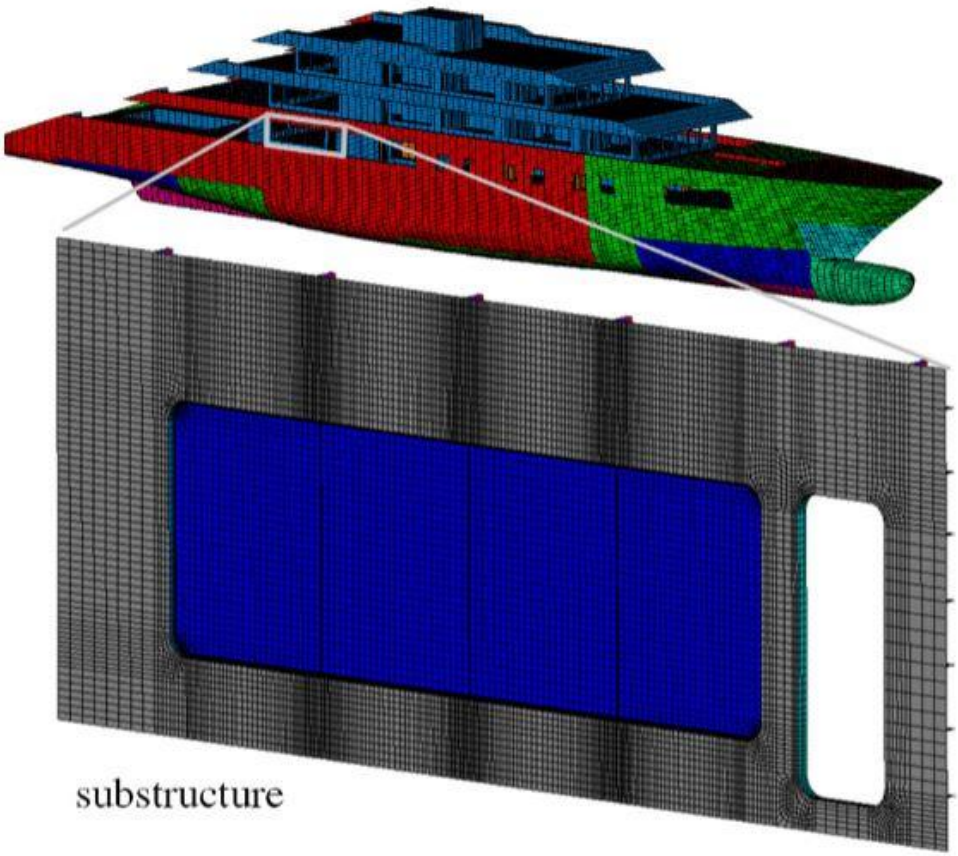

Figure 7.2: FE global model [12]

The substructure technique is able to simplify large complex FE models and thus reduce the computational time. For this purpose, the entire structure is divided into parts, the so-called substructures, of which a detailed FE model is created. In the subsequent "generation step", the nodes that are at the edges of this detailed FE model are defined as so-called master nodes and a stiffness and mass

matrix for the substructure is calculated with respect to these nodes. At this point, the substructure is considered as a unique superelement, having the stiffness and mass matrix as already calculated, that, in the so called "use steps", are merged with the ones obtained from the global FE model.

For what concerns the static analysis, by the expansion pass, it is possible to calculate stresses and deformation also in the substructures by the "expansion pass".

The superelement analysis scheme has been reported in Fig. (7.3).

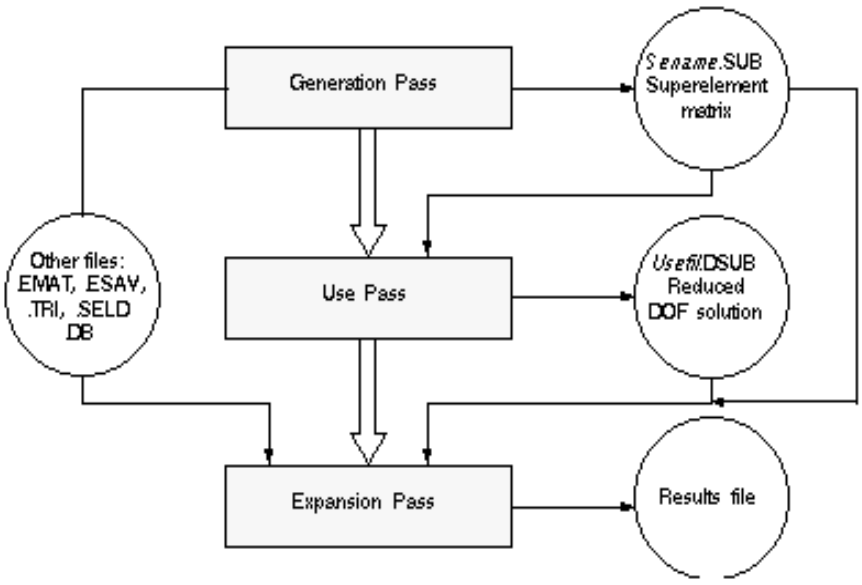

Figure 7.3: Superelement analysis in ANSYS Mechanical [74]

In Fig. 7.4, a detail of the submodel of the first order of superstructure is reported.

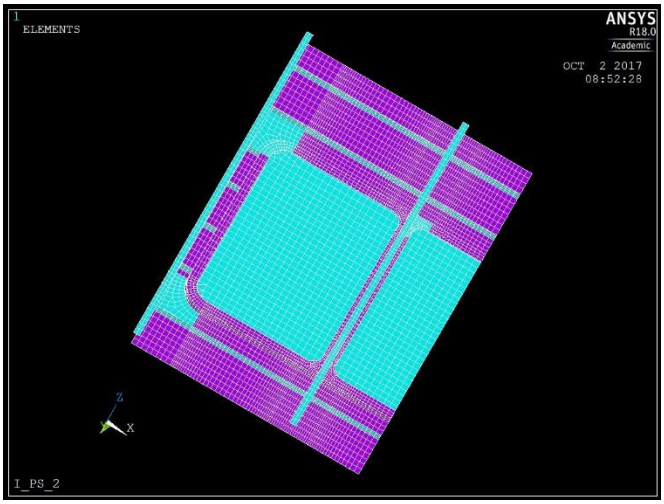

Figure 7.4: Window's submodel

The yacht under consideration, as it appears from the drawing of Fig. 7.5, has been designed with glued windows pane, mounted with an harder bonder on the internal window's recess and with a softer sealing to the transversal strut. With these scheme, the shear transfer is carried out by the internal bonding, and so the window pane and the metallic structure are not in the same plane; it could be expected that the contribution of window should be negligible, since the non co-planarity between windows and metal could somehow isolate the window pane.

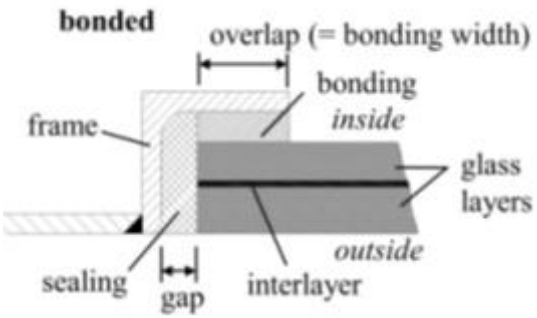

Figure 7.5: Bonding methodology used by the shipyard [12]

A detail of the FE modelling of the glass has been reported in Fig. 7.6; in this model, solid element has been used for the glass and interlayer. Two elements per thickness have been recommended by the authors[9] in order to achieve a correct stress distribution along the thickness.

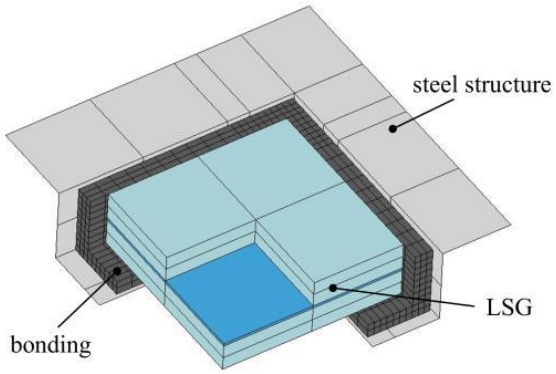

Figure 7.6: Numerical modelling of laminated glass[12]

For what concerns the eigenmodal analysis herein presented, the number of element per thickness is not so relevant, since the interest is focused on the vertical hull girder vibration, being it the most critical for the onboard comfort [75], that is governed only by the global momentum of inertia and mass, as it appears form Eq. 7.1[76].

$$N\nu = \varphi \cdot \sqrt{\frac{I}{(\Delta+\Delta_1)\cdot L^3\cdot(1+N\nu)}} \tag{7.1}$$

where:

- Nν frequency of the first mode of vertical vibration, expressed in cycles per minute
- I momentum of inertia of the main section, expressed in feet
- Δ displacement, expressed in tons
- Δ_1 fluid added mass
- L ship length between perpendiculars

- Ns shear correction factor of Lockwood Taylor
- φ empiric constant

As from Eq. 7.1, the structural discontinuity between metallic and glass pane should neglect the contribution of glazed structure to the global momentum of inertia, and the weight increase due to glass is negligible as well. So, it can be expected that, apart from a different mode shape, the frequency shift due to the presence of window pane should be almost negligible.

7.2 – RESULTS OF THE HULL GIRDER VERTICAL MODES

In the following Fig. 7.7 and 7.8, the two global FE model, without and with windows, are respectively presented. As it could be se, since the glass is present only in the substructure models, no visible difference are visible. The master nodes, on which the stiffness and mass matrix of superelements are transferred to the global models, have been plotted in magenta. No differences appear from the global model, since the master nodes are present both for the model without windows an in the model with windows; the presence of glazed surfaces can be appreciated in the submodel of each windows (see Fig. 7.4)

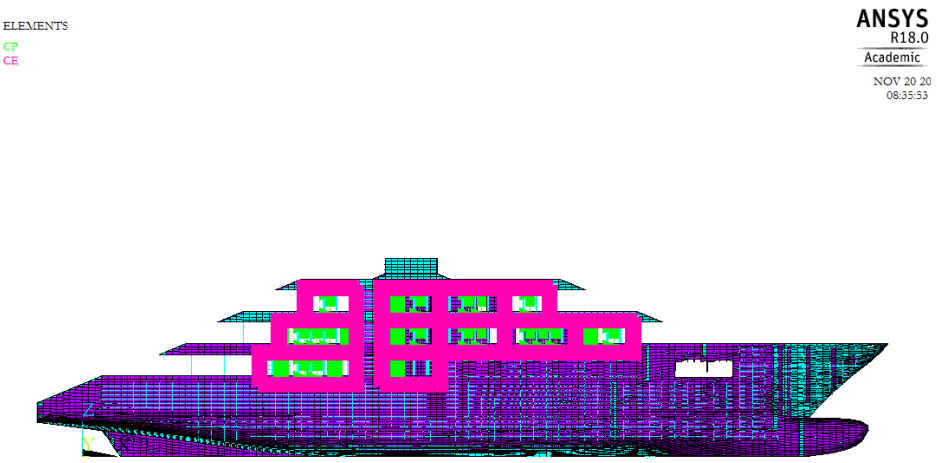

Figure 7.7: FE model without windows (master nodes in magenta)

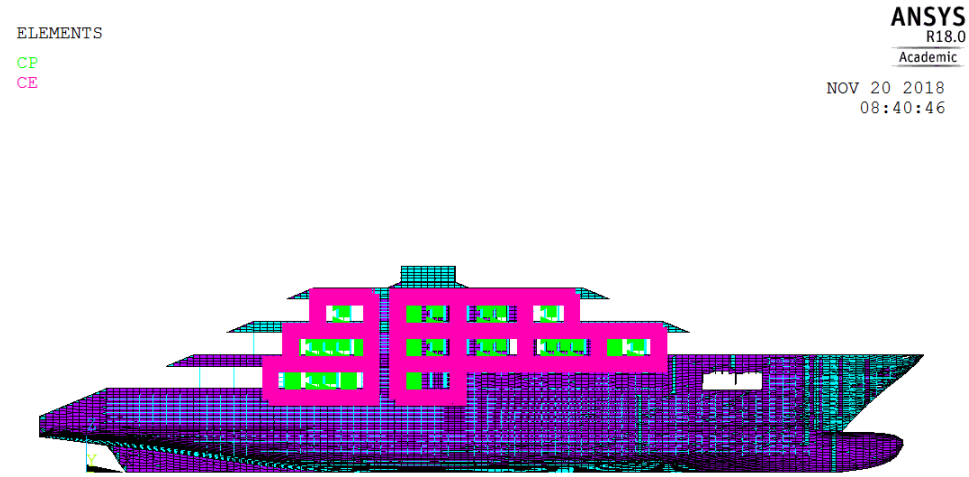

Figure 7.8: FE model with windows (master nodes in magenta)

The supernode modal solver [74] has been used; instead of computing each mode individually and working with mode shapes in the global model space, the supernode algorithm uses a mathematical approach based on substructuring to simultaneously determine all modes within a given frequency range and to manage data in a reduced model space.

In the following Fig. 7.9 and 7.10, the first vertical hull girder natural mode has been reported for the model without and with windows respectively. The effect of window panes shift the eigenfrequency from 2.45 Hz to 2.35 Hz, i.e. a reduction of 4%, that could be considered negligible.

This behaviour completely agree with the Burrill Eq. 7.1 [76] and with the results for the static analysis carried out in the Chapter 3 and discussed in literature[12], [49], where the non-contribution of glass has been assessed for the global response of yacht structures.

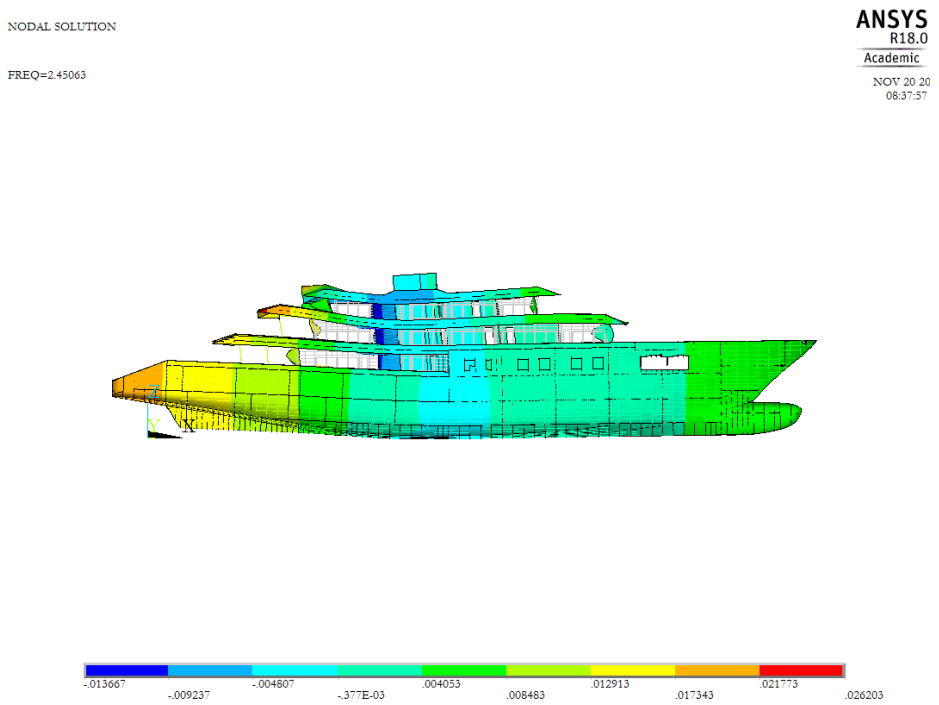

Figure 7.9: Deformed shape of the first vertical normal mode without windows

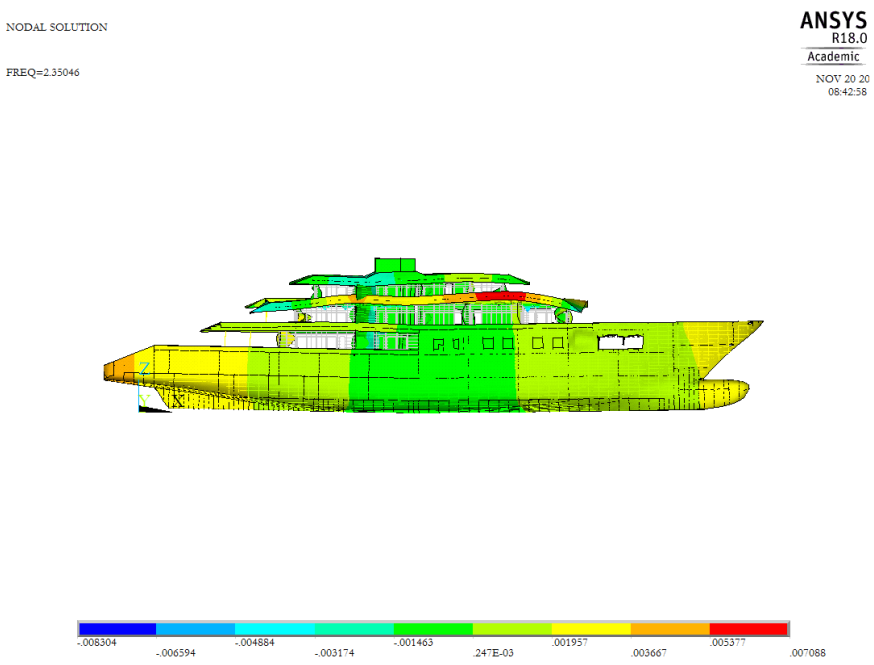

Figure 7.10: Deformed shape of the first vertical normal mode with windows

Chapter 8

THE INFLUENCE OF LAMINATED GLASS IN THE NVH ASSESSMENT OF A SUPERYACHT

Ship on-board noise propagation is one of the most important issues, which shipyards and ship-owners have to deal with. This issue begins during the early stage of designing a new vessel or rebuilding in order to reduce the costs[77] of any action that have to be carried out if the super or megayacht does not accomplish the CS rules [24] [59] or the owner requirements. Noise treatment and thermal insulation of walls, ceilings and floors are being selected in order to fulfil the noise criteria. This activity is done based on noise and vibration propagation analysis.

For what vibration analysis is concerned, numerical methods, based on the FE analysis, are widely available in literature [15], [47], [73] and are, nowadays, a common practice for naval architects; since this procedure is based on a traditional determinist approach, the reliability in the high frequency range [68] (> 150/200 Hz, see Fig. 1) cannot be fulfilled and it is necessary to shift to a non traditional Statistical Energy Analysis [78] (Fig. 8.1).

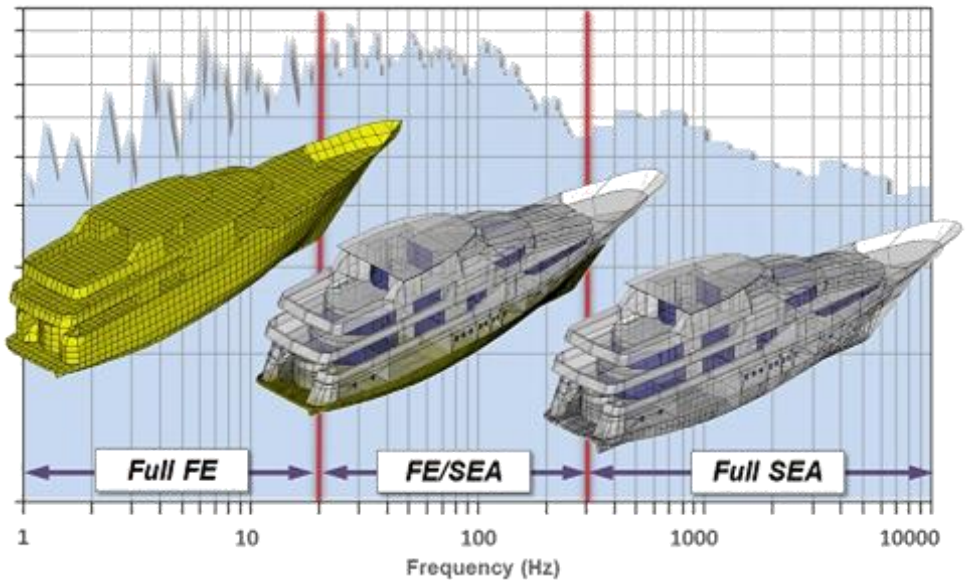

Figure 8.1: Reliable frequency range of NVH numerical procedure [79]

By the NVH assessment, it is possible to verify and predict the noise propagation onboard super and megayacht both in terms of structure borne noise (SBN) and air borne noise (ABN), as defined in Fig. 8.2.

For what concerns the onboard comfort, the ABN is completely cut off by the application of common insulation layers on room walls, so they are trivial to be confined.

The SBN, that is propagated directly by the ship structures, is the most effective problem for the comfort onboard, since it can be transmitted all along the motoryacht and it create problem of resonance between pure tonal components of excitation forces and any structural component. This aspect is particularly effective for glued laminated glass, that could have the natural frequency in the same frequency range (or, in worse cases, in the same octave or third octave band) of the excitation sources.

Moreover, as it will be explained in the next sections, SEA has the necessity of having larger subsystem if compared to traditional FE analysis, and so the role of equivalent method for the simplification of laminated glass is crucial.

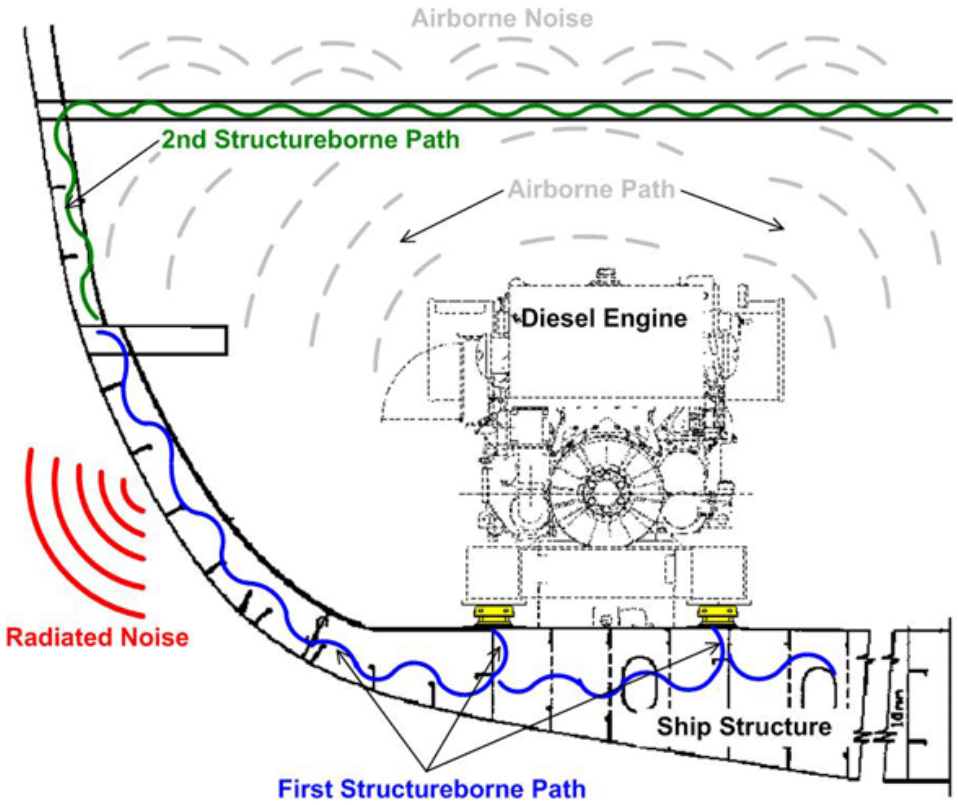

Figure 8.2: Noise paths on ship structures[80]

In this Chapter, the shortcomings of the previous Chapter in terms of vibroacoustic properties of laminated glass have been applied to a real superyacht studycase (under construction at the time being), that has been analysed by using the Statistical energy Analysis in order to perform a prognosis of the noise and vibration propagation onboard. The results, in terms of overall sound pressure level inside cavities and on specific plates, have been then compared with the experimental data obtained during the subsequent sea trial.

The real peculiarity of this work is the adoption of the simplified DEET proposed in Chapter 4 for the equivalent modelling of laminated glass, that, so far, has been simulated by adopting the approach proposed by CS (see Chapter 1) without considering the effect of those assumption on the different damping loss facto and natural modes. Moreover, the damping loss factor spectra used for damper materials have been calculated adopting the RT based methodology proposed in Chapter 5, avoiding the costly Oberst method.

8.1 – THE STATISTICAL ENERGY ANALYSIS

The SEA is a framework of study [69] for the prediction of sound and vibration for complex dynamic systems. The statistical aspect of this method emphasizes the differences between deterministic numerical approaches that are not able to predict the correct behaviour for high frequency ranges in which the mode shape and resonance frequencies are highly sensitive to small details of geometry and construction.

One of the basic advantages of SEA method is namely that the structures or acoustical cavities involved are represented by general geometrical and material data from which properties like average modal densities, average modal damping and average coupling data may be derived. Also the dynamic field variables are represented by simple spatial and temporal averages, corresponding to the total vibratory energy of the subsystems. The coupling leads to energy flow between subsystems in order to maintain an energy balance in the presence of dissipative losses [81].

The most obvious disadvantage of SEA in that the energy levels obtained for different subsystem are statistical estimates of the true levels, and therefore afflicted with some degree of uncertainty. Usually this problem will be less pronounced when the number of modes is sufficiently high for all subsystem. This will set limits for the practical use of SEA at low frequencies. However, no

physical limitations can be formulated as long as the subsystem can vibrate resonantly. The Statistical Energy Analysis from a purely theoretical point of view is a set of power balance equations, derived from the principle of conservation of energy.

Considering that a complex dynamic system can be divided into at least two simpler subsystems (Fig. 8.3) the set of power balance equations can be written as:

$$\begin{cases} \sum_1^2 \pi_{in,i} = \sum_1^2 \pi_{out,j} \\ \pi_{out,i} = \pi_{ij} + \pi_{diss,i} \end{cases} \tag{8.1}$$

Where $\pi_{in,i}$ is the power input in the i-th subsystem, $\pi_{out,i}$ is the power output, π_{ij} is the amount of power that is transmitted between i-th and j-th subsystem and $\pi_{diss,i}$ is the power that is dissipated by the i-th subsystem.

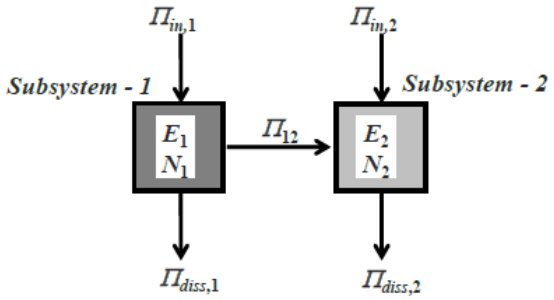

Figure 8.3: SEA system composed by 2 subsystems

In Fig. 8.3, the term E_i denotes the total energy of each subsystem and N_i is the modal density.

The dissipated power of each subsystem can be written as:

$$\pi_{diss,i}(\omega) = \omega \cdot \eta_i \cdot E_i \tag{8.2}$$

where η_i describes the damping loss factor (DLF) of the subsystem.

The last unknown term is the transmitted power that is depending on the energy of each subsystem as it follows:

$$\pi_{ij}(\omega) = \omega \cdot \eta_{ij} \cdot n_i \cdot \left(\frac{E_i}{n_i} - \frac{E_j}{n_j}\right) \tag{8.3}$$

The coupling loss factor η_{ij} depends on the type of subsystem (e.g. beam, shell, acoustic cavity) and on the transmission path (mass law, resonant, non-resonant or double wall) under consideration.

Under these assumptions, a SEA problem for a dynamic system composed of two subsystems could be written in matrix form as:

$$\begin{bmatrix}\pi_{in,1}\\ \pi_{in,2}\end{bmatrix} = \omega \cdot \begin{bmatrix} n_1(\eta_1 + \eta_{12}) & -n_1\eta_{12} \\ -n_2\eta_{21} & n_2(\eta_2 + \eta_{21})\end{bmatrix}\begin{bmatrix}\frac{E_1}{n_1}\\ \frac{E_2}{n_2}\end{bmatrix} \tag{8.4}$$

Generalizing Eq. 8.4 for an N-components dynamic system, the SEA matrix system is:

$$\begin{bmatrix}\pi_{in,1}\\ \vdots\\ \pi_{in,N}\end{bmatrix} = \omega \cdot \begin{bmatrix} n_1(\eta_1 + \sum_{i\neq 1}\eta_{1i}) & -n_1\eta_{12} & \cdots & -n_1\eta_{1N} \\ -n_2\eta_{21} & n_2(\eta_2 + \sum_{i\neq 2}\eta_{2i}) & \cdots & \cdots \\ \cdots & \cdots & \cdots & \cdots \\ -n_N\eta_{Ni} & \cdots & \cdots & n_N(\eta_N + \sum_{i\neq N}\eta_{Ni})\end{bmatrix} \cdot \begin{bmatrix}\frac{E_1}{n_1}\\ \vdots\\ \frac{E_N}{n_N}\end{bmatrix} \tag{8.5}$$

In the symmetric matrix system shown in Eq. 8.55, no information on mode shapes and on natural frequencies is requested for SEA computation; this implies that the analysis could be considered well-conditioned only for relative high value of n_i, typically higher than 2-3 modes per band [16].

The modal density is assessed statistically by using a statistical population based equation depending on the type of subsystem under consideration:

$$n(f) = \begin{cases} \frac{L}{\sqrt{2\pi f}} \sqrt[4]{\frac{\rho A}{EI}} \; for\ acoustic\ ducts \\ \frac{A}{2} \sqrt{\frac{12\rho(1-\upsilon^2)}{Et^2}} \; for\ thin\ flat\ plates \\ \frac{4\pi V}{c^3} f^2 \; for\ acoustic\ cavities \end{cases} \tag{8.6}$$

For lower n_i values, an hybrid approach is required; the information on natural modes and shapes are acquired from a preliminary FEM or BEM analysis as a precursor to the SEA computation.

8.2 – A REAL SUPERYACHT STUDYCASE

The statistical energy analysis has been applied to a prognosis study of noise propagation on a 54 meter pleasure vessel, whose characteristics have been reported in Table 8.1. The yacht, at the time of the calculation, was in the late construction stages, and the results obtained by the numerical calculation have been compared with the sound level obtained during the sea trials.

Table 8.1: Main characteristics of the vessel assumed as a study case

Length overall	54.60 m
Waterline length	52.14 m
Beam moulded	10.40 m
Depth	5.40
Scantling draft	2.55 m
Scantling displacement	687 t
Scantling speed	20 kn
Cruise speed	12 kn
Maximum speed	17 kn
Hull material	Aluminium light alloy
Superstructure material	Aluminium light alloy
CS	Lloyd's Register of Shipping

In Fig. 8.4, the general arrangements of the superyacht have been presented.

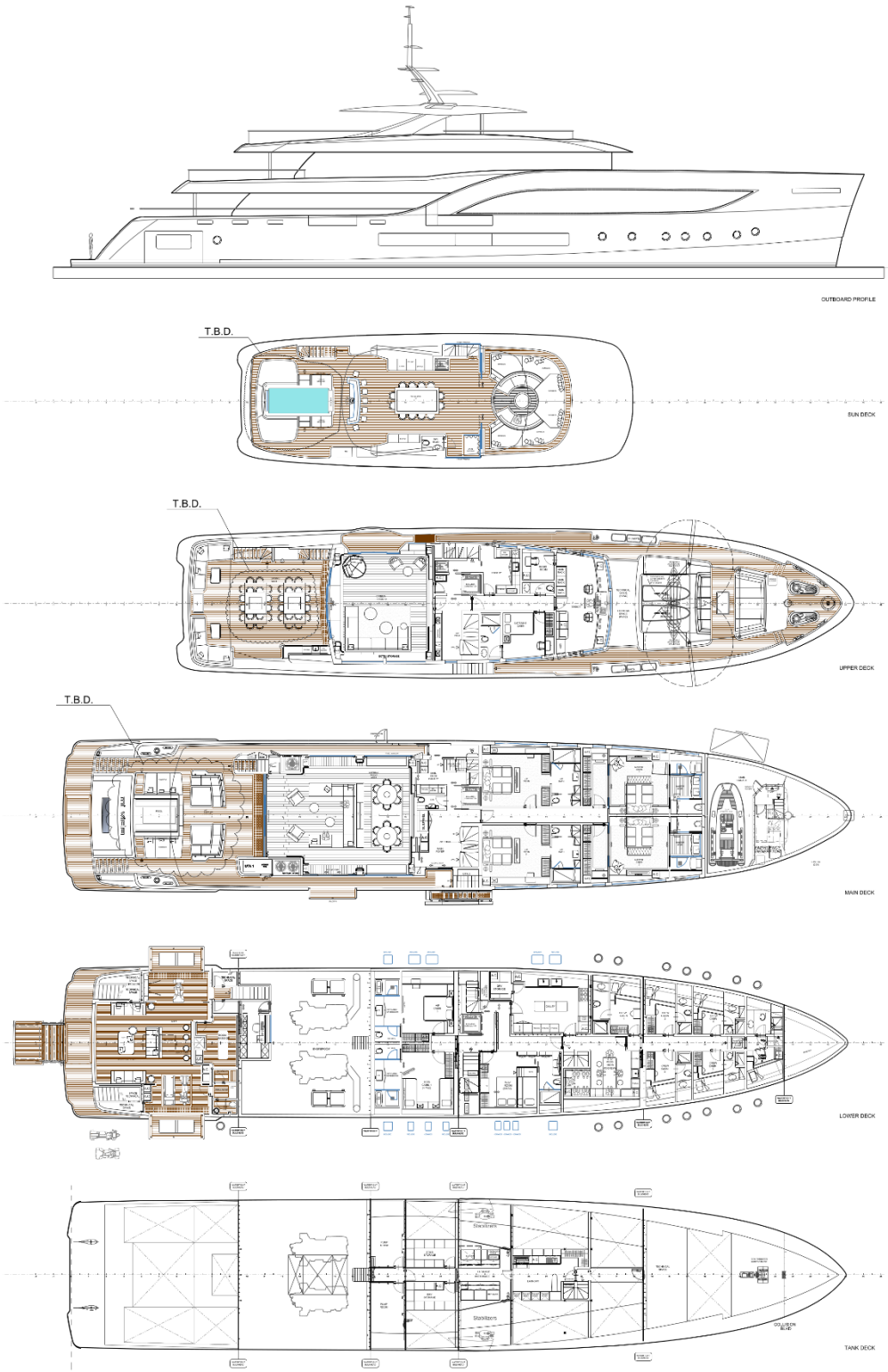

Figure 8.4: GA of the vessel assumed as a study case

As it can be seen from the GA of the Fig. 8.4, the engine room is just below the main saloon and aft the VIP Cabin; this internal layout could create problems in the internal sound pressure level if the noise control treatment of the structure surrounding the saloon and the VIP cabin is not properly designed.

Moreover, since the two aforementioned spaces are surrounded by windows, the glasses could act as harmonic speakers, if their natural frequencies are close to the main excitation own frequencies. The list main machineries installed onboard has been reported in Table 8.2.

Table 8.2: Main machineries installed onboard

Main engine	CATC32 T3
MCR Power	2x 1081 kW
Nominal revolution speed	2300 rpm
Gearbox	ZF5360
Propeller	5 blade @ 570 rpm
Generator set power	380 kW

8.2.1 Model creation

The software used for computing the SEA analysis of the yacht under consideration is VA One. It is an interactive software program for the analysis and design of vibroacoustic systems across the entire frequency range and it is based on proven vibroacoustic methods. The module used is the "Statistical Energy Analysis".

The vibro-acoustic system is described in terms of a source-path-receiver model. Sources inject energy into a vibro-acoustic system, this energy propagates along various transmission paths, before arriving at various receiving locations of interest. In general, the transmission paths in a vibro-acoustic system involve transmission through many different structural and acoustic components.

To reproduce this propagation scheme a VaOne model consists of three main model objects:

- subsystems, that are used to model the various structural and acoustic components that transmit energy through a vibro-acoustic system;
- junctions, that are used to model the connections between the various subsystems in a system. They are also used to describe the way in which energy is transmitted between the different subsystems in a system;
- sources, that are used to model the various sources that inject energy into the subsystems in a vibro-acoustic system.

In the next Fig. 8.5 and 8.6, the plate and cavity + plate model have been reported. In cyan, the laminated glasses have been plotted.

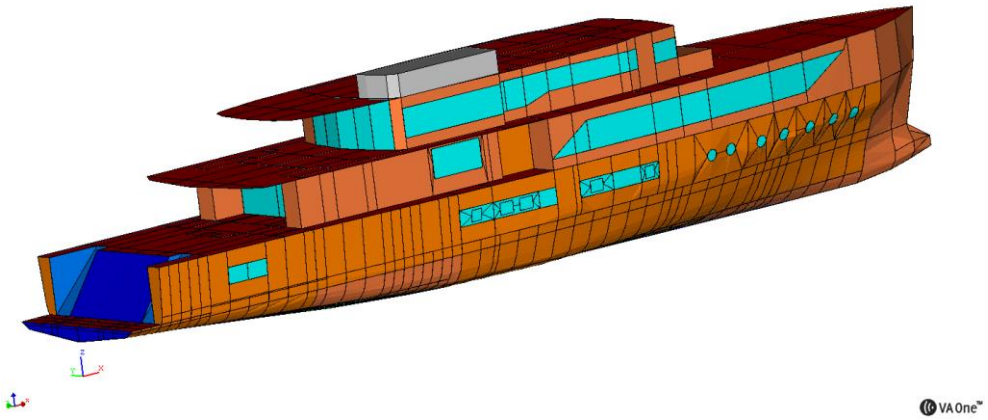

Figure 8.5: SEA model of the superyacht assumed a study case

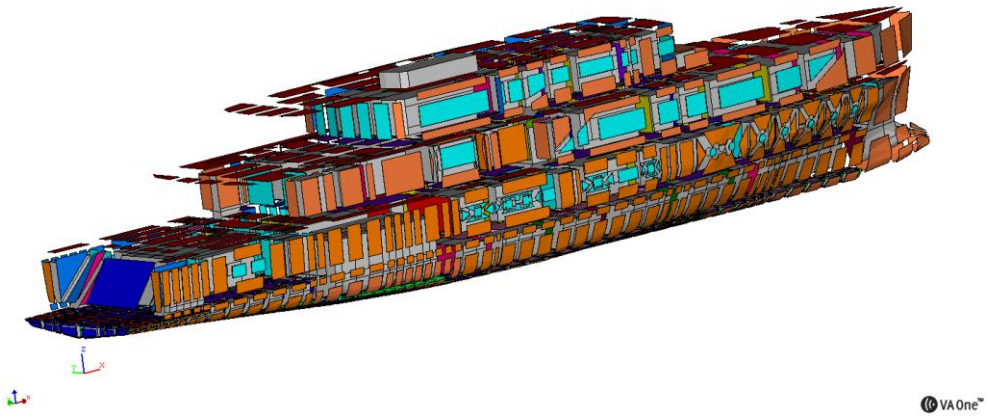

Figure 8.6: SEA model of the superyacht assumed a study case – shrink view

In order to numerically simulate the effect of sea, all the plates above the waterline has been connected to a semi-infinite fluid (SIF), as reported in Fig. 8.7. A SIF in VA One represents an unbounded exterior acoustic space. The acoustic waves radiated by a subsystem connected to a semi-infinite are not reflected back on the subsystem. The aim is to model the exterior acoustic radiation impedance on SEA subsystems, i.e. to add radiation damping to them; therefore, the SIF can be considered an energy-dissipating sink. It is defined by an acoustic fluid and a single 3D node location at which the radiated sound pressure level could be evaluated.

a)

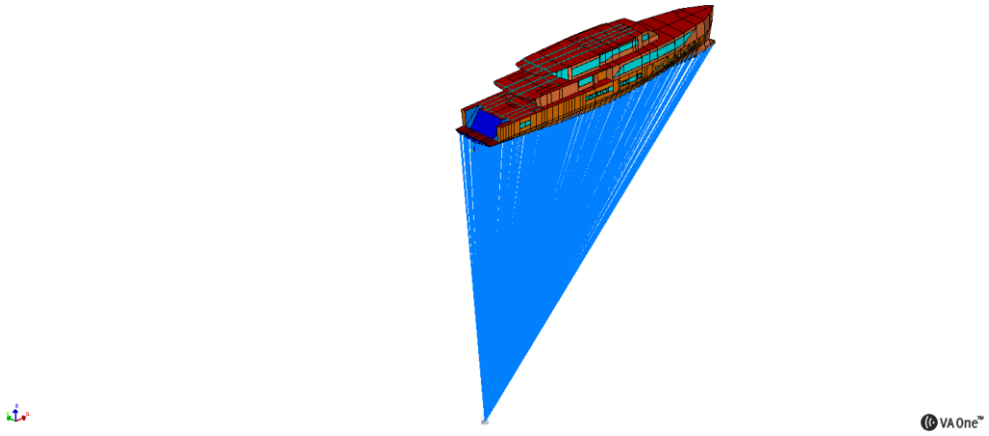

b)

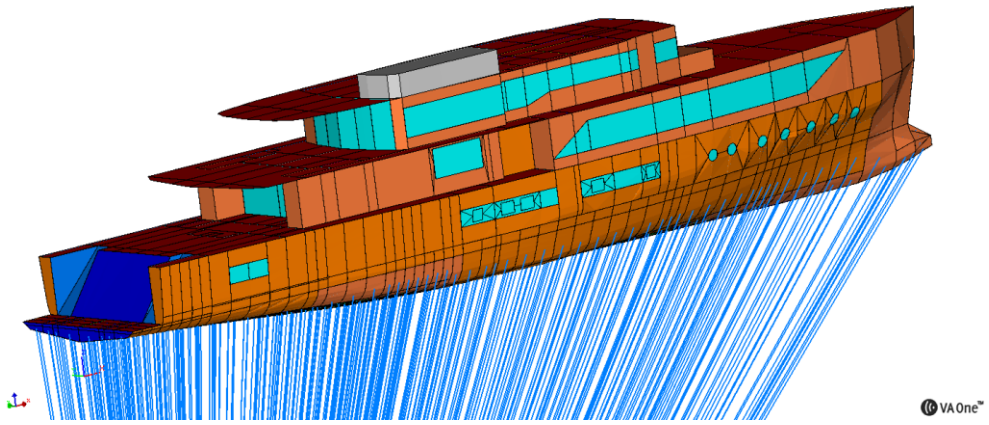

Figure 8.7: Application of Semi Infinite Fluid: a) general view and b) close up

The connection among subsystem is guarantee by the use of junctions, that describe different noise path depending on the subsystems they are connecting. In particular, in VaOne:

- Point junctions: they describe the transmission of vibration energy between two or more SEA subsystems coupled at a discrete point and connections between subsystems that are small compared with a wavelength;

- Line junctions: they describe the transmission of vibration energy between two or more SEA subsystems coupled along a line and connections between subsystems that are continuous and large compared with a wavelength;
- Area junctions: the represent acoustic energy transmission between a SEA plate and one or two acoustic cavities that share a common bounding area or face. The also could connect two cavities sharing a common face with no plate or shell in between them.

In Fig. 8.8, the use of SEA junctions in the study case has been reported.

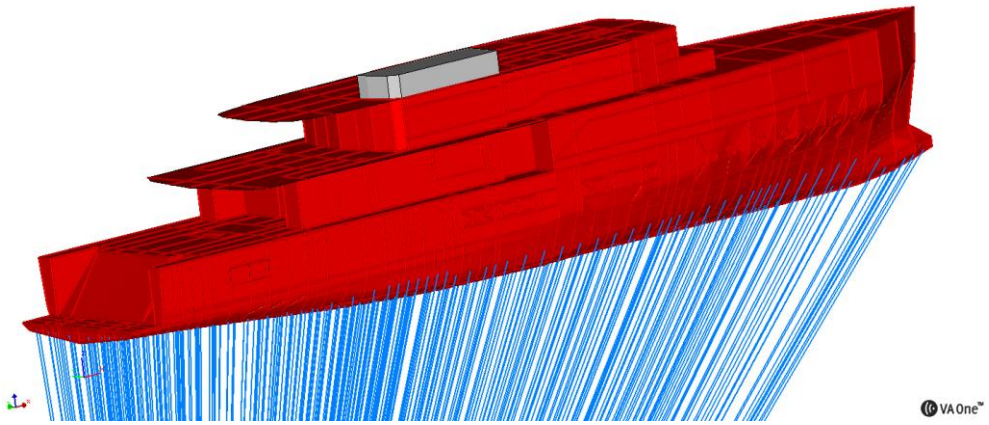

Figure 8.8: SEA junctions (red)

8.2.2 Procedure for the power input calibration

The SEA procedure requires a precise definition of the input power spectrum; for marine application, the principal sources are the propulsion engines[82] [83] that are directly connected to the hull's structure thorough the engine foundation, the propeller pressure pulse [84] and the generator sets.

The foundation, and in particular viscoelastic materials used for this application, are able to significantly modify the amount of energy transmitted to the hull's bottom and consequently the SBN propagation.

Therefore, the aim of this part of the thesis is to test a methodology to obtain the power source to input in the foundations, starting from standard vibration data for the main engine (usually given as a vibration velocity spectrum), on an already built superyacht, different from the study case studied in the next paragraph, since it is a vessel under construction and so no experimental data was available.

The procedure herein presented can be summarized by four main steps:

- Creation of an hybrid model composed of an FE model of structural foundation and SEA elements of the surrounding structures
- Calibration of input forces (narrow band) to obtain the measured velocity spectra;
- Calculation of the power input (1/3 octave band) representing the main engine action to input to the full SEA global model;
- Evaluation of the results in terms of sound pressure levels inside the vessel by means of SEA calculation with the computed power input.

For this porpoise, two input data are required:

- Velocity spectrum measured on the main engine foundation below and above the resilient mounting (Fig. 8.9);
- FE model of the structural foundation and SEA model of the whole vessel from which the hybrid model described at point 1 can be created.

(a)

(b)

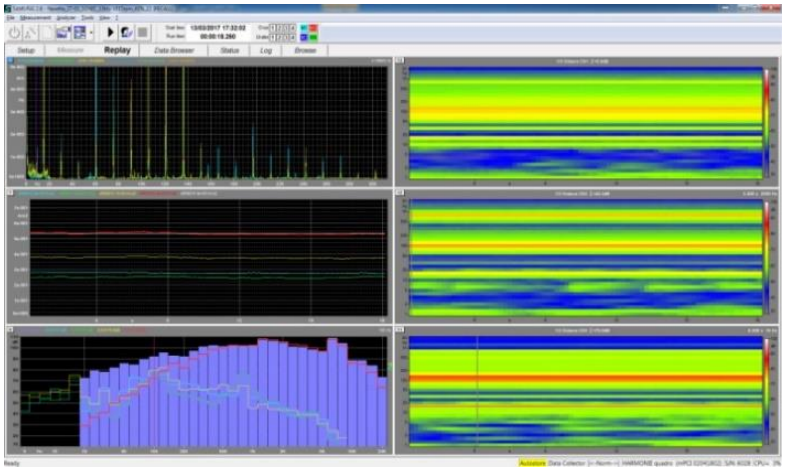

Figure 8.9: Velocity spectrum measurement, (a) accelerometers positioning and (b) response spectrum.

The velocity spectrum has been measured by the instrumentation shown in Fig. 8.10; it consists in an impact hammer and piezoelectric accelerometers for the calculation of the frequency response function and a microphone for the calculation of the SPL.

Figure 8.10: Instrumentation for N&V measurements on board.

The hybrid model of the engine foundation (Fig. 8.10) facilitates a reliable calculation even for the low frequency range, where a full SEA approach could lead to higher uncertainties. Moreover, the same testing condition could be created in the coupled SEA-FE model, by using forces and velocity sensor in the same place of the experimental activity.

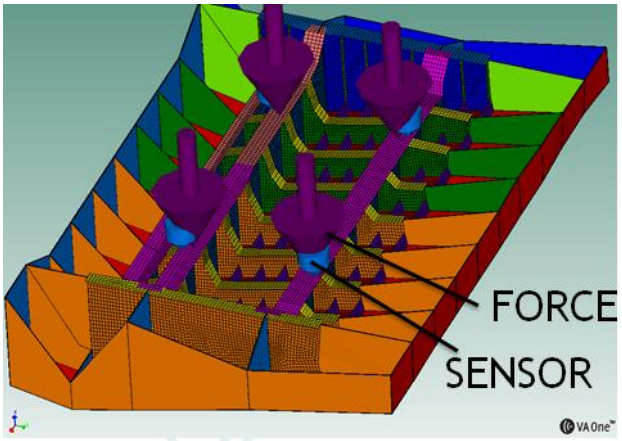

Figure 8.11: Hybrid model of the engine's foundation.

A local analysis of the hybrid model shown in Fig. 8.11 is carried out by applying a unit input force (F_{1N}). The velocity spectrum obtained by the numerical procedure (V_{1N}) has to be compared with the one obtained through the experimental measurements ($V_{measured}$).

Since the FE analysis is a linear static one, the superposition principle can be applied; so the correct input force (F_{INPUT}) can be calculated as:

$$F_{INPUT}(\omega) = F_{1N}(\omega) \cdot \frac{V_{measured}(\omega)}{V_{1N}(\omega)} \tag{8.7}$$

Once having found the total input force generated by the propulsion engines and the foundation's mobility (Y_z) (computed by the software), the power input spectrum can be easily calculated:

$$P_{INPUT}(\omega) = < F^2{}_{INPUT}(\omega) > \cdot Re(Y_z(\omega)) \tag{8.8}$$

The power input spectrum calculated by Eq. 5 can be applied to a global SEA model as shown in Fig. 8.12.

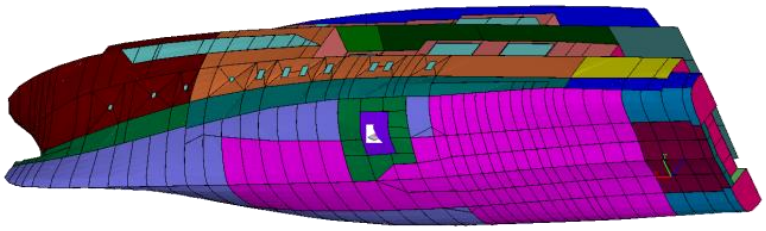

Figure 8.12: The global SEA model for the power input calibration.

A comparison between the measured velocity spectrum and the velocity spectrum obtained from different numerical models, applying Eq. 8.8, is shown in Fig. 8.13.

As it can be easily seen, the FE model alone (i.e. not integrated in a hybrid model with SEA plates) is not reliable for the mid and high frequency range where the oscillations are caused by local resonances of the mesh grid that are not corresponding to the real phenomenon.

Using the abovementioned hybrid model the reliability of the results increases if compared to the measured velocity spectrum.

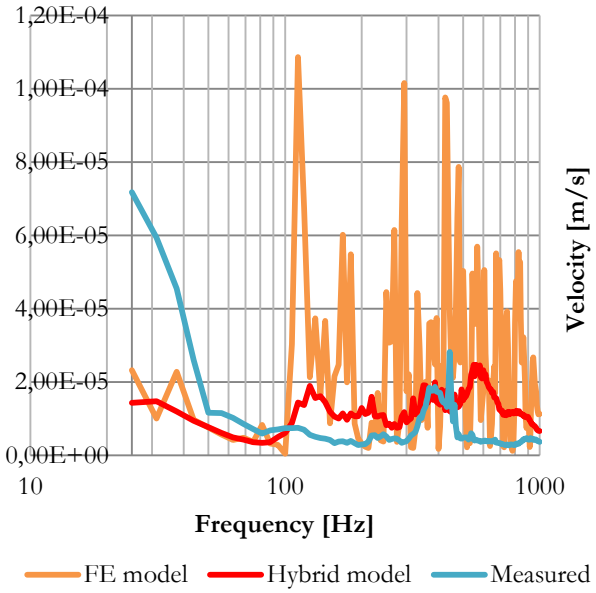

Figure 8.13: Velocity spectrum comparison

Fig. 8.14 shows a comparison between the SPL in the engine control room (adjacent to the engine room) measured onboard and the results of the SEA with the power input calculated using the described procedure.

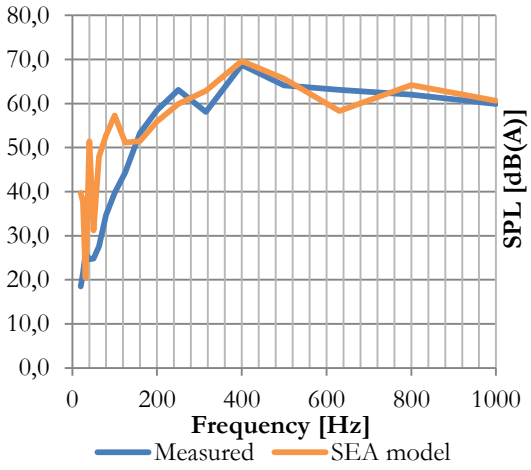

Figure 8.14: Comparison of the SPL in the engine control room

The general trend is similar; there is a discrepancy at low frequency but a good correspondence after 200 Hz. The same approach could be used for the power input calibration of any source of SBN. On the base of this experimental activities, a wide data set of power input has been collected in collaboration with RINA SpA and it can be used also for new vessel in the preliminary design stage, as it happened for this study case and presented in the next Paragraph.

8.2.3 ABN and SBN sources

The final step in the yacht model creation is the application of particular noise generating sources on the yacht. Noise spectra have been taken into consideration in accordance with the manufacturer data or estimated on the basis of RINA database and on board measurements of similar machineries. Therefore, the noise sources considered in this SEA analysis are in terms of airborne and structure borne noise sources. The scheme of the main ABN and SBN excitation sources has been reported in Fig. 8.15

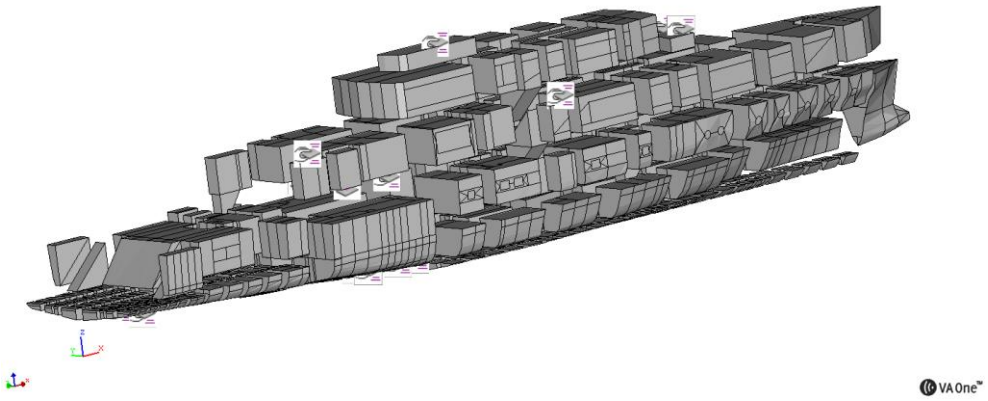

Figure 8.15: Loads applied to the SEA model (cavity view)

The ABN sources have been assigned as a pressure constrains, based on manufacturers data, in the room in which the machinery is installed. The ABN spectra have been reported in Fig. 8.16-8.17.

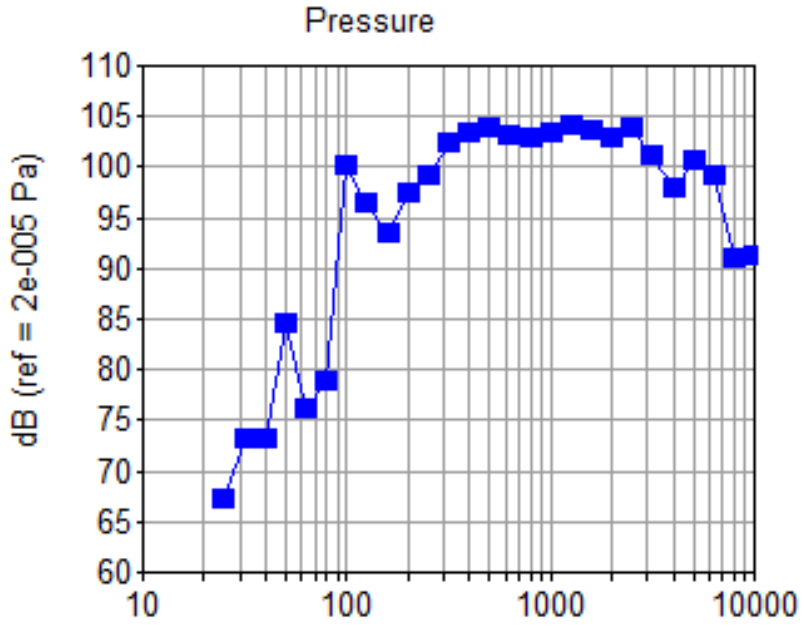

Figure 8.16: Main engine ABN spectrum

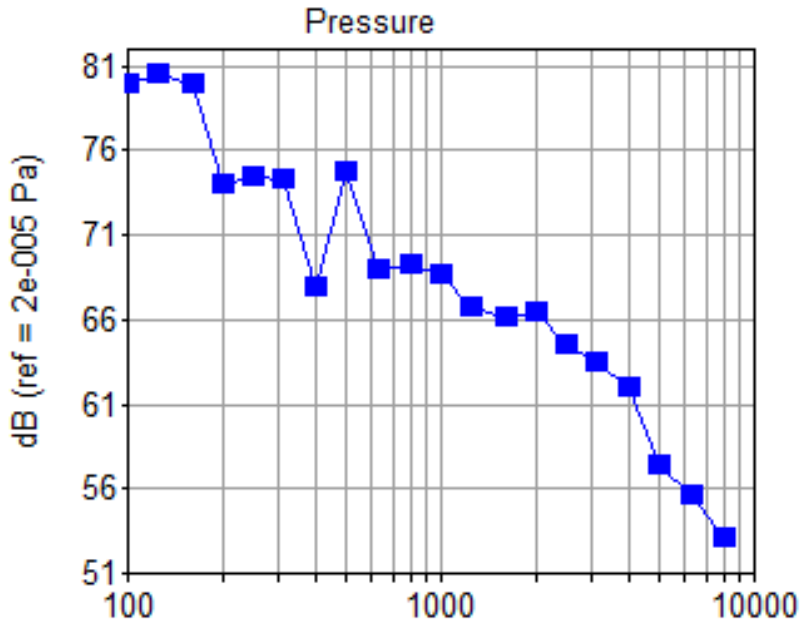

Figure 8.17: Genset ABN spectrum

Then, in order to reproduce the SBN, some energy constraints are applied directly on plates. The variable being constrained in the SEA equations is the energy level of a given wave field [51]. For this scope, the measurements carried out on similar vessel, with the same machineries installed onboard, could be transferred to a prognosis analysis on yachts in construction stages, as in the present research.

The engine and gearbox spectra, reported in the next Fig. 8.18-8.19, have been extrapolated from a similar vessel, built by the same shipyard, by using the procedure for the power input calibration as reported in Section 8.2.2. For what concerns the gearbox and the propeller SBN sources (Fig. 8.20-8.21), the velocity spectra, calculated onboard that similar ship have been used. These velocity/acceleration constrains have been applied directly to SEA plates and beams upon which the machinery is installed.

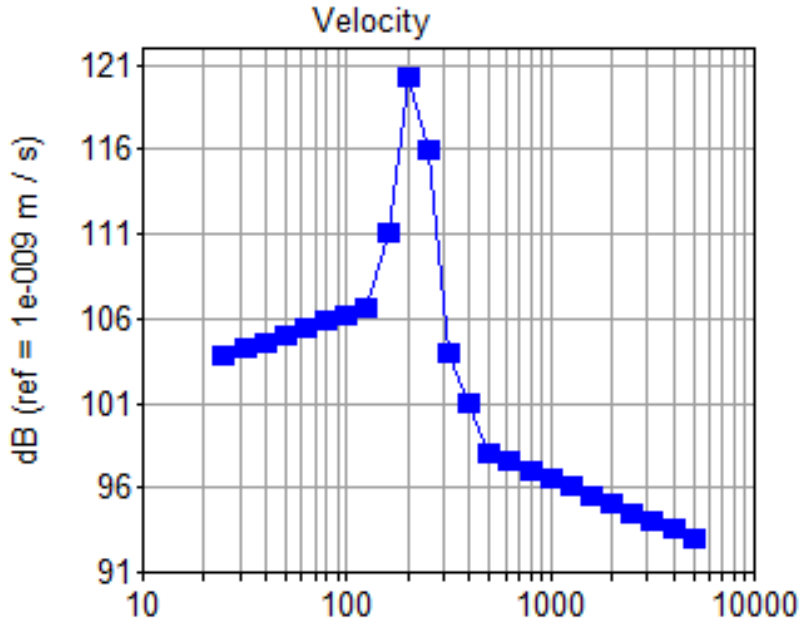

Figure 8.18: Engine SBN spectrum

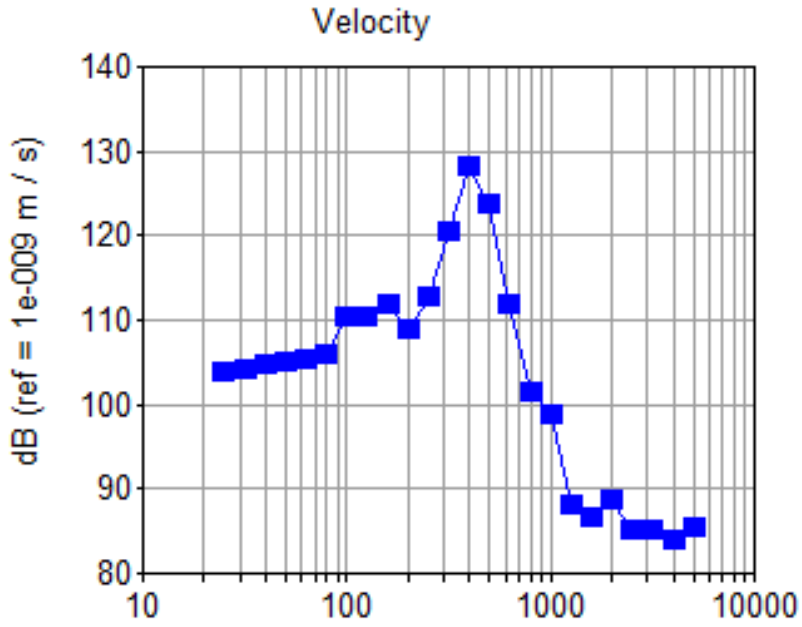

Figure 8.19: Gearbox SBN spectrum

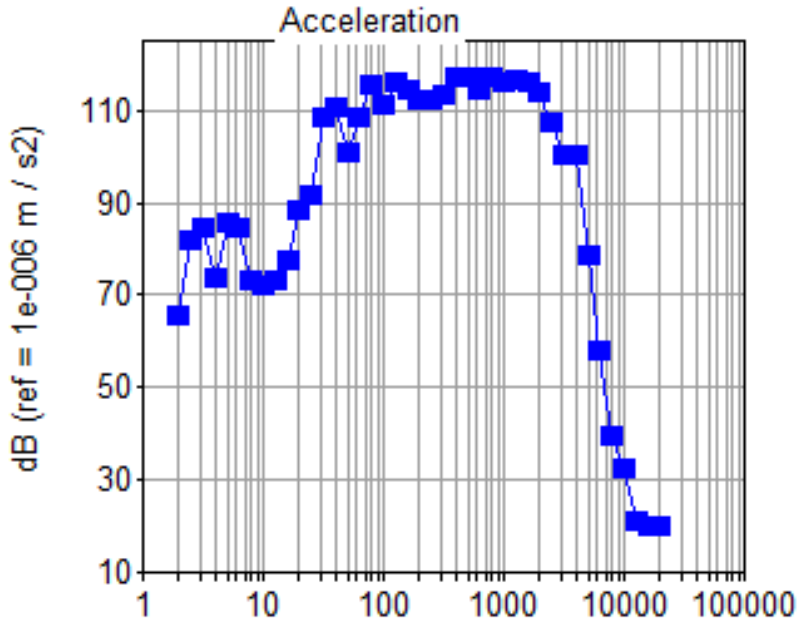

Figure 8.20: Propeller SBN spectrum

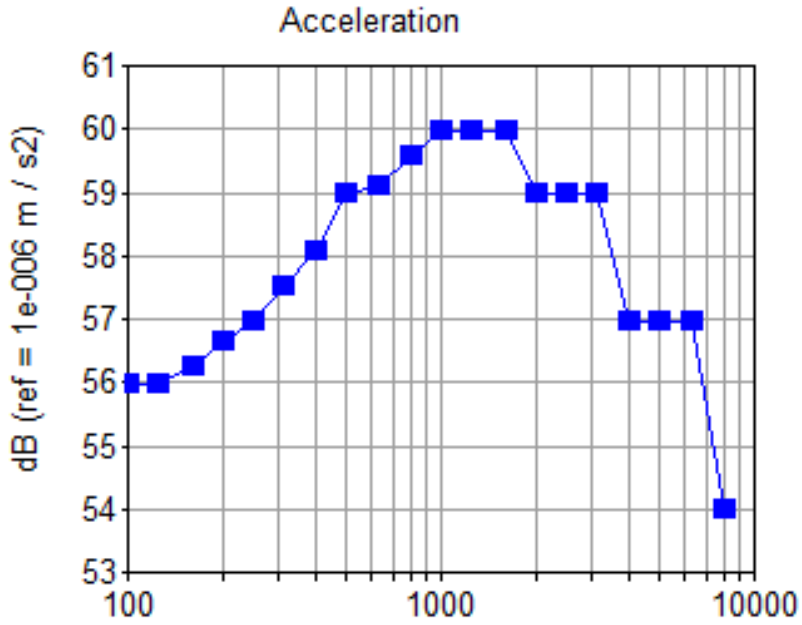

Figure 8.21: Genset SBN spectrum

8.2.4 Laminated glass modelling

Since the objective of this research was to assess the effect of laminated windows to the noise and vibration propagation, each window present onboard (Fig. 8.24, Table 8.2) has been studied separately.

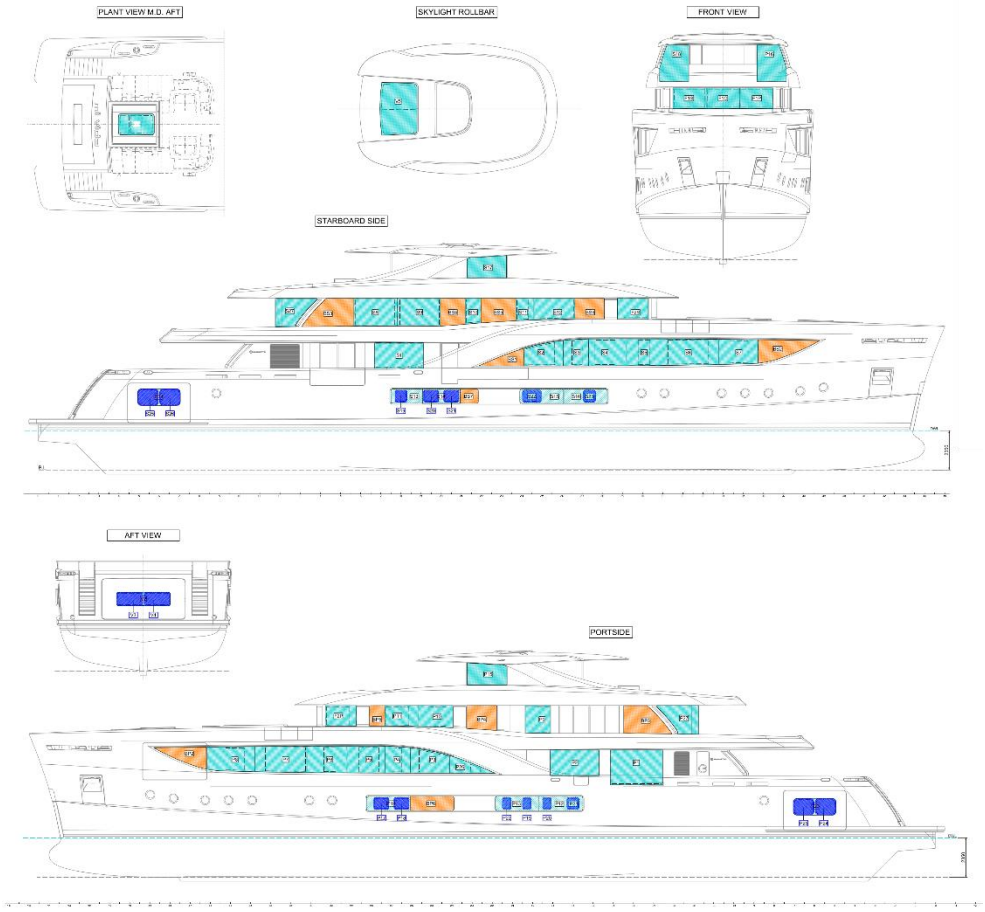

Figure 8.22: Window plan of the vessel assumed as a study case

The net opening and the lamination sequence have been used to create a specific model of each window by using the MSC Patran script as reported in Annex A.

Table 8.3: Windows' lamination sequences

Window	b	h	Net opening			Lamination sequence
S1	2900	1532	2760	x	1392	12+3.04+12
S2	2341	1330	1755	x	1140	8+3.04+8
S3	1505	1570	1430	x	615	8+3.04+8
S4	2265	1600	1195	x	1460	8+3.04+8
S5	2400	1585	700	x	1450	8+3.04+8
S6	3105	1540	2410	x	1405	12+3.04+12
S7	2330	1460	1100	x	1320	8+3.04+8

S8	2580	1645	2360	x	1510	12+3.04+12
S9	2580	1645	2360	x	1510	12+3.04+12
S10	940	1500	800	x	1360	8+3.04+8
S11	1080	1320	690	x	1175	8+3.04+8
S12	2440	1245	2050	x	1100	8+3.04+8
S13	1875	853		-		8+3.04+8
S14	2250	853		-		8+3.04+8
S15	2607	853		-		8+3.04+8
S16	2607	853		-		8+3.04+8
S17	2340	1310		-		8+3.04+8
S18	1745	2165		-		8+3.04+8
S19	720	720	600	x	600	10+3.04+10
S20	920	720	800	x	600	12+3.04+12
S21	920	720	800	x	600	12+3.04+12
S22	1120	720	1000	x	600	12+3.04+12
S23	720	720	600	x	600	10+3.04+10
S24	2540	990		-		8+3.04+8
S25	1220	970	1100	x	850	12+3.04+12
S26	1220	970	1100	x	850	12+3.04+12
P1	3100	2080	2960	x	1945	12+3.04+12
P2	2900	1532	2760	x	1392	12+3.04+12
P3	2341	1330	1755	x	1140	8+3.04+8
P4	1505	1570	1430	x	615	8+3.04+8
P5	2265	1600	1195	x	1460	8+3.04+8
P6	2400	1585	700	x	1450	8+3.04+8
P7	3105	1540	2410	x	1405	12+3.04+12
P8	2330	1460	1100	x	1320	8+3.04+8
P9	1510	1645	870	x	1505	8+3.04+8
P10	2035	1280	1035	x	1145	8+3.04+8
P11	2534	1225	1365	x	1085	8+3.04+8
P12	2607	853		-		8+3.04+8
P13	2607	853		-		8+3.04+8
P14	2607	853		-		8+3.04+8
P15	2340	1310		-		8+3.04+8
P16	1745	2165		-		8+3.04+8
P17	900	700	800	x	600	12+3.04+12
P18	900	700	800	x	600	12+3.04+12
P19	520	720	400	x	600	10+3.04+10
P20	520	720	400	x	600	10+3.04+10
P21	720	720	600	x	600	10+3.04+10

P22	520	720	400	x	600	10+3.04+10
P23	2540	990		-		8+3.04+8
P24	1220	970	1100	x	850	8+3.04+8
P25	1220	970	1100	x	850	12+3.04+12
P26	2695	1040	600	x	475	12+3.04+12

By calculating the natural frequencies of each windows and the most effective in terms of effective radiated power, the ERP based dynamic effective thickness has been computed as reported in Section 4.2.2, in order to obtain an equivalent uniform plate having the same dynamic properties of the laminated glass, but with an higher modal density and so a more reliable statistical response.

The calculation of the first natural mode of each panel has been reported in Table 8.4.

Table 8.4: Normal mode 11 of windows installed onboard

Window	Mode 11 [Hz]	Window	Mode 11 [Hz]
S1	67	**P1**	39.44
S2	76.53	**P2**	67
S3	196.19	**P3**	76.53
S4	79.88	**P4**	196.19
S5	161.8	**P5**	79.88
S6	68.65	**P6**	161.8
S7	93.43	**P7**	68.65
S8	62.46	**P8**	93.43
S9	62.46	**P9**	117.69
S10	136.45	**P10**	109.91
S11	174.54	**P11**	92.87
S12	75.72	**P12**	-
S13	113,87	**P13**	-
S14	-	**P14**	-
S15	-	**P15**	-
S16	-	**P16**	-
S17	-	**P17**	322.51
S18	-	**P18**	322.51

S19	341.76	**P19**	513.73
S20	322.51	**P20**	513.73
S21	322.51	**P21**	341.76
S22	193.72	**P22**	513.73
S23	341.76	**P23**	-
S24	-	**P24**	184.8
S25	184.8	**P25**	184.8
S26	184.8	**P26**	-

8.3 – NVH ASSESSMENT OF THE SUPERYACHT STUDYCASE

In Fig. 8.23, the overall sound pressure level (SPL) in dB(A) has been reported.

a)

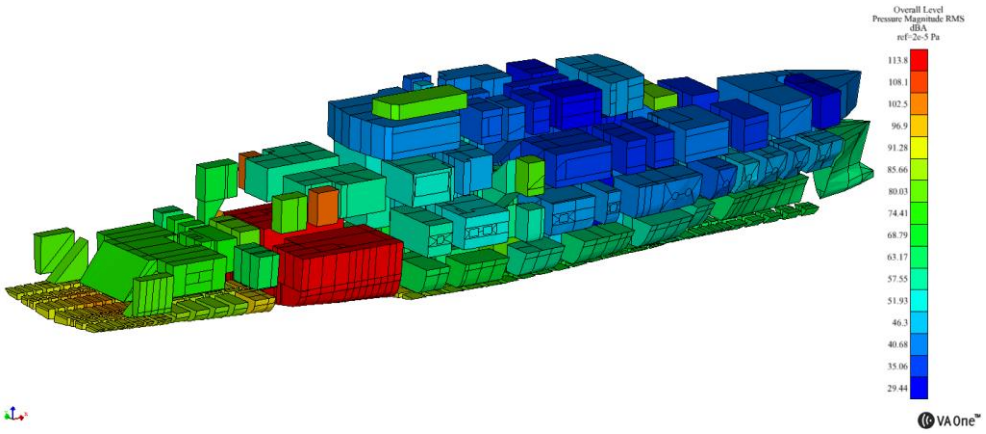

b)

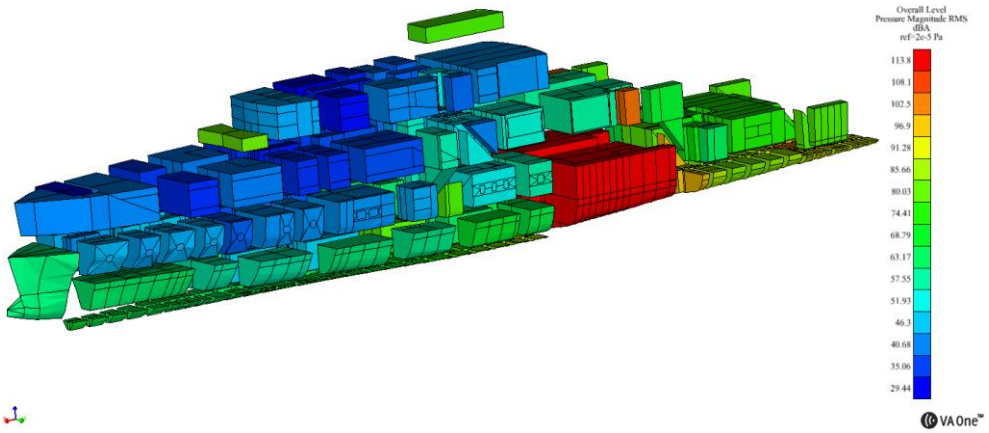

Figure 8.23: Sound Pressure Level [dB(A)]: a) starboard and b) port side view.

As it could be predicted the highest sound pressure level can be found in the engine room where the engine noise source are located; here the sound pressure level is about 114 dB(A). Then the energy propagates into adjacent cavities till the fore areas and the upper deck spaces that are the less noisy. The other areas interested by high SPL are the stern cavities that are located directly over the propellers; nevertheless, they are non-liveable spaces and so not interesting for the aim of this research.

The main saloon is affected by the short distance to the engine room. In order to verify the comfort level on that area, which, for calculation reasons, has been split in two different cavities (one for starboard side and one for portside), in Fig. 8.24, the SPL as a function of the centre frequency has been reported.

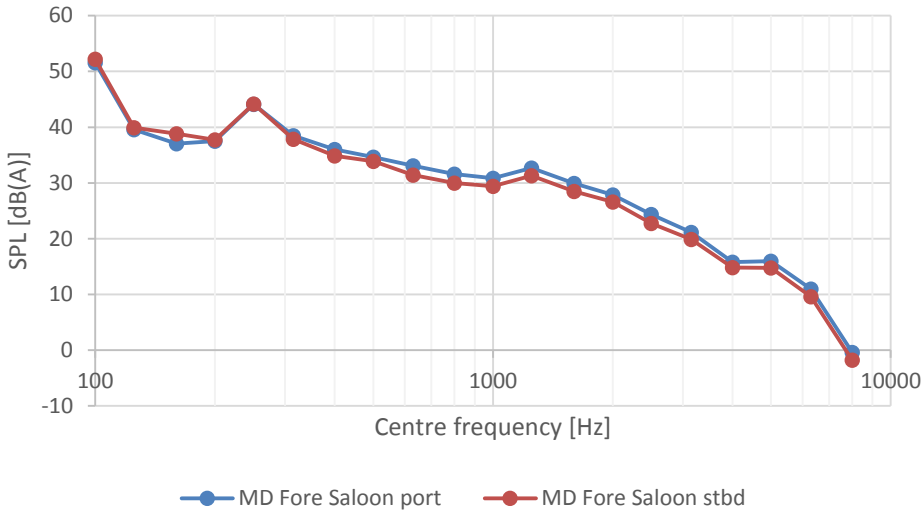

Figure 8.24: Numerical SPL in the MD Fore Saloon portside (blu) and starboardside (red)

As it can be seen, the small discrepancies are due to the non-symmetrical layout of internal spaces. In order to obtain the SPL in the entire MD fore saloon, the noise level in each abovementioned area have been sum and the final result has been reported in Fig. 8.25.

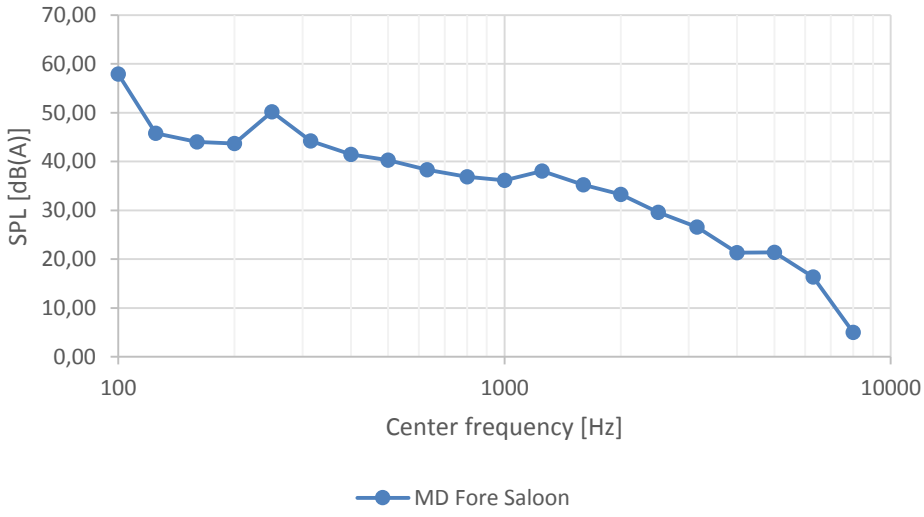

Figure 8.25: Numerical SPL in the MD Fore Saloon

By the way, the average sound pressure level L_P in the MD fore saloon has been calculated as:

$$L_P = 10 \log\left(\sum_{\Delta f} 10^{\frac{SPL(\Delta f)}{10}}\right) \tag{8.9}$$

and the final result was 59.49 dB(A).

In order to investigate the power contribution to the MD Fore Saloon (starboard side) in Fig. 8.26 the power inputs to the SEA cavity has been plotted.

As it can be seen, in the low frequency range, the major contribution to the SPL is due to plate 355-F, that is a wall panel on the superstructure side, and plate 353 that is a wall panel connected to the MD main foyer. In the mid frequency range (200-500 Hz) the noise is propagated by plate 355 and by the window S1, with continue increase with respect to frequency. In the very high frequency range, the power input graph shows that the two main source are again plate 353 and the window S1.

From this analysis, it could stated that the window S1 propagate a broadband noise, without showing a particular tonal component in correspondence to the energy firing frequency (75-100 Hz centred band), the propeller passing blade frequency (50-75 Hz centred band, not plotted in fig. 8.26) and the gearbox frequency (200 Hz centred band).

The total sound level in the MD fore saloon complies with the level B merit class required by RIA COMF additional class notation [85].

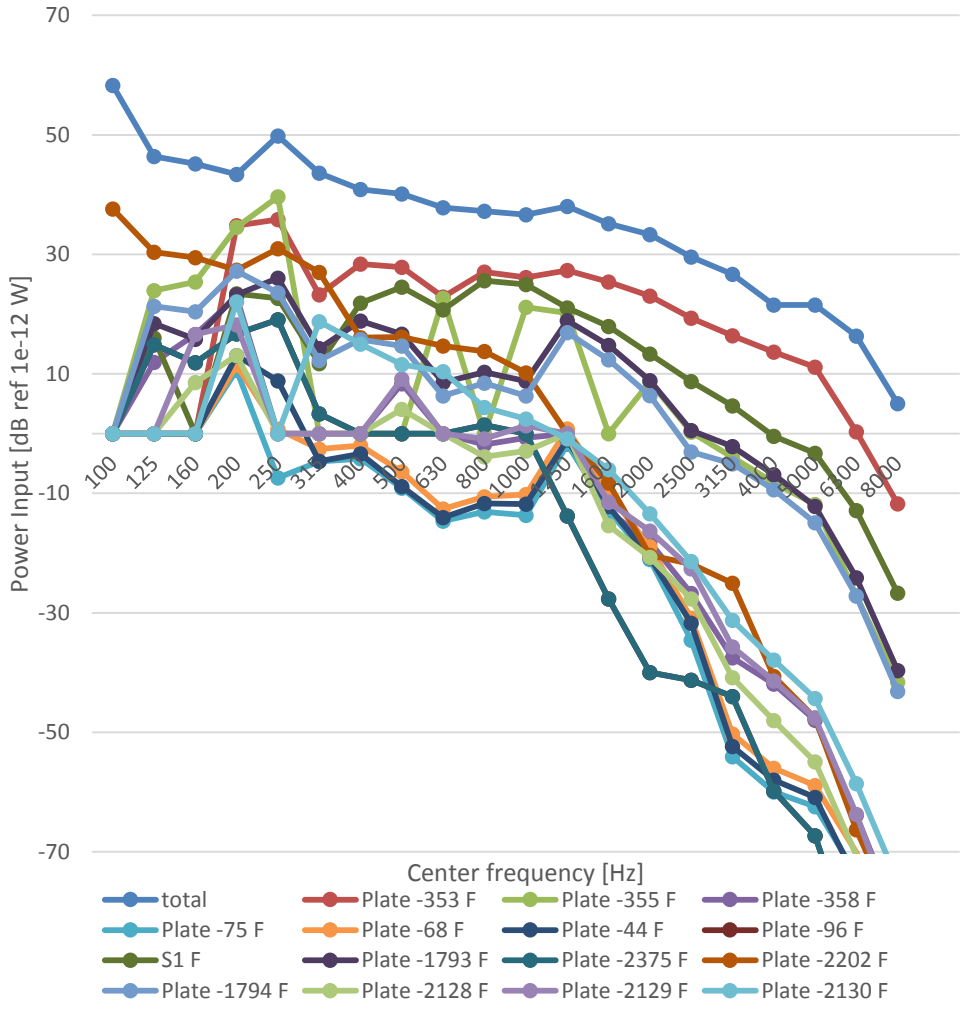

Figure 8.26: Power input in the MD Fore Saloon

In order to assess also the noise level in the owner cabin, the same procedure used for the MD fore saloon has been used and in Fig. 8.27, the SPL for the two separated cavities has been reported, since they are divided by an aluminium wall. The computation of the average sound pressure L_P has returned a value of 40.19 dB(A) that complies with the A merit class of RINA COMF notation[85].

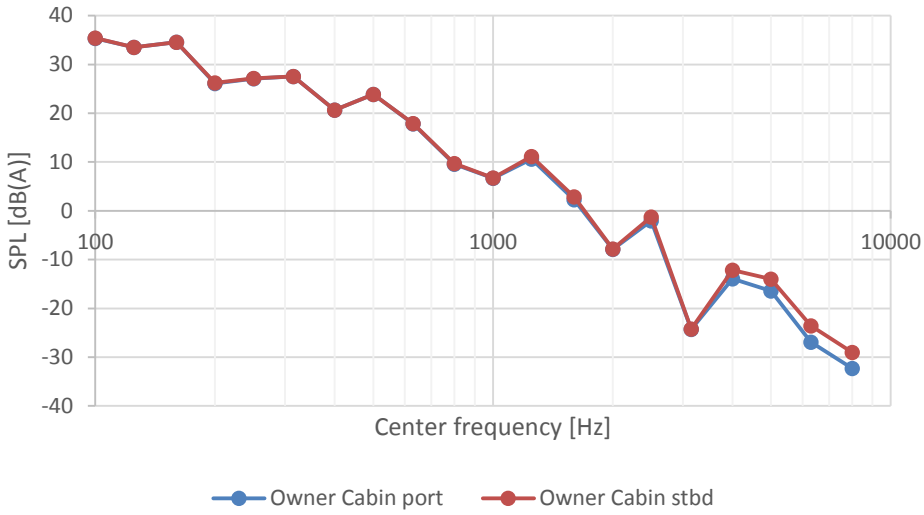

Figure 8.27: Numerical SPL in the owner cabin portside (blu) and starboardside (red)

8.4 – FULL SCALE EXPERIMENTAL RESULTS

The reliability of the SEA calculation has been verified by comparing the numerical results in terms of overall sound pressure level and the experimental campaign that was carried out during October 2018 in concurrently with the sea trials with sea state 1 and cruise speed of 12 kn.

The full scale tests have been performed together with the Italian CS RINA for the achievement of the COMF additional class notation. A microphone BSWA MP201 has been used for the noise measurements and a triaxial accelerometer PCB 356 has been adopted for the vibration assessment.

In particular, the piezoelectric accelerometer has been mounted on different windows in the cabin under investigation in order to assess the propagation of tonal mode of excitation sources. A difference of at least 3 dB in the signal received by the accelerometer between the adjacent third octave bands has been considered as a tonal component in the vibration spectrum. The microphone has been generally located in the middle of the room.

In Fig. 8.28 the results of the N&V measurement in the main saloon has been reported. Going into detail:

- Top left: velocity spectrum measured by the accelerometer;
- Top right: RMS acceleration spectrum measured by the accelerometer;
- Mid left: sound level on time;
- Mid right: slow response and equivalent sound level A-weighted;
- Bottom left: third octave spectrum. The blue bars represent the dB signal measured by the microphone, the cyan, green and yellow spectrum are the vibration level in dB measured by the accelerometer in x,y (on plane) and z (out of plane) direction respectively and the red curve is the microphone signal A-weighted.
- Bottom right, the FFT of the vibration level measured by the accelerometer in z direction.

For conciseness reasons, the MD fore saloon and the owner cabin has been analysed in this monograph.

For what concerns Fig. 8.29, related to the measurements carried out in the MD fore saloon, the triaxial accelerometer was placed in correspondence to the window S1.

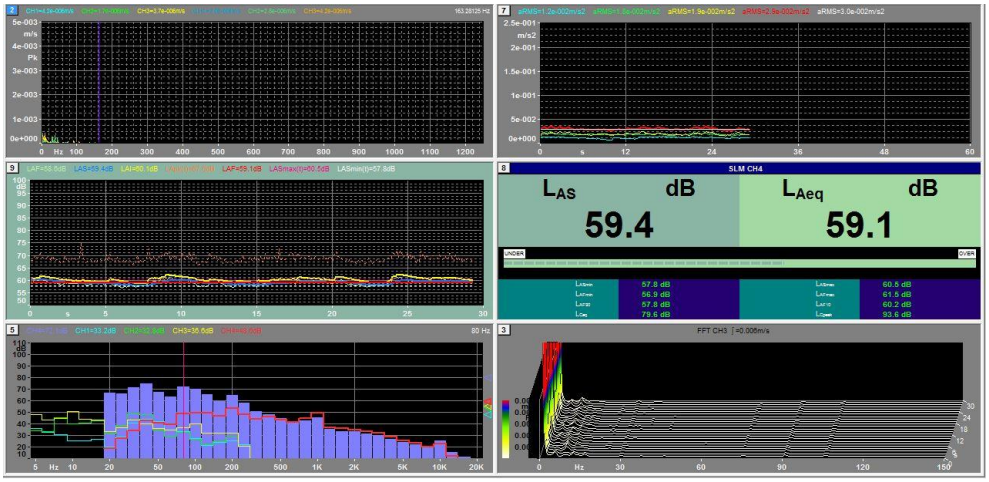

Figure 8.28:Noise measurement in the main saloon @ cruise speed

As it can be seen, the difference between the numerical calculation (59.49 dB(A)) and the experimental result (59.1 dB(A)) is very small. This is probably due to the fact that the main saloon is located very close to the engine room, where the majority of input sources are located and so the noise and vibration path is computed more precisely.

Moreover, in Fig. 8.29, a close up of the noise spectrum is reported. By analysing the signal registered by the microphone, it is possible to note that two main tonal components @ 200 Hz and @ 1000 Hz are propagated inside the main saloon; the first component is in the range of the first gearbox frequency and of an higher engine frequency. The tonal component propagated in the high frequency range, that is present in any measurement, was due to an erroneous mounting of the gearbox bearing causing a sort of "whistle" that can be heard in any space.

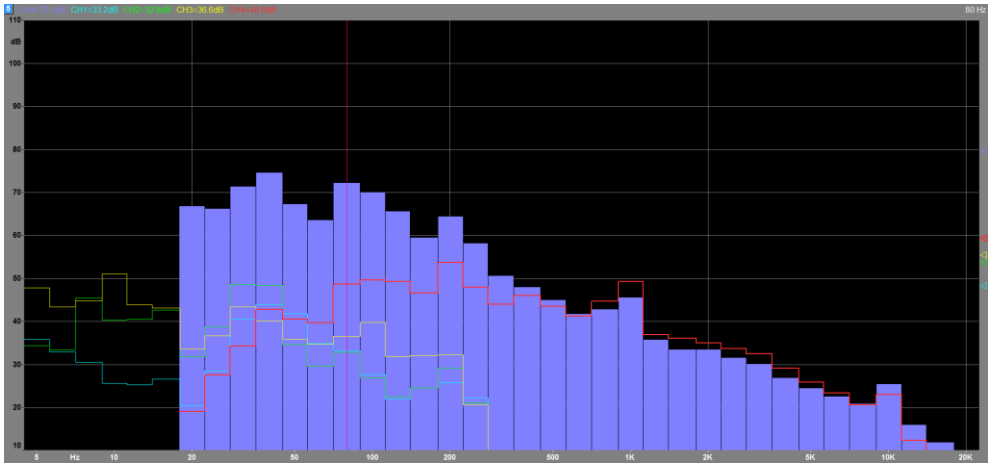

Figure 8.29: Noise spectrum in the MD fore saloon @ cruise speed

From the response of the accelerometer, neglecting the very low frequency range, where no modes of the window are excited, since the first one, as reported in Table 8.4, is @ 67 Hz, the highest tonal component has been measured in the third octave band centred @ 100 Hz, i.e. the range of the first firing frequency, very close to the first natural mode of the window pane.

The same analysis has been carried out for the owner room and the final Soundbook screen has been reported in Fig. 8.30. In this case, the discrepancies between numerical SPL (40.18 dB(A)) and experimental result (48 dB(A)) is a higher; this is probably due to the fact that the insertion loss of the path engine room-owner cabin has been overestimated.

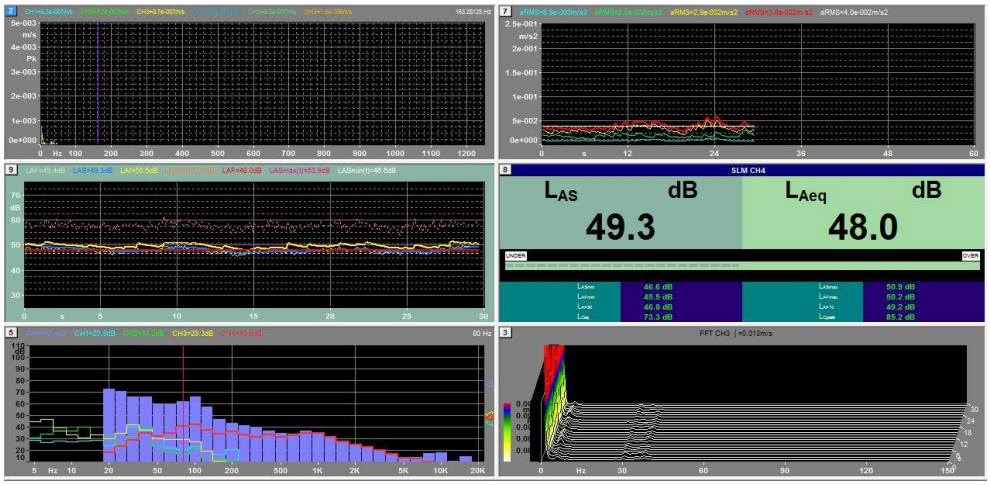

Figure 8.30: Noise measurement in the owner cabin @ cruise speed

In this case, the spectrum reported in Fig. 8.31, with the accelerometer placed in correspondence to the window S12 (first natural frequency: 75.72 Hz) shows a broadband noise in the low frequency range radiated by the window, without a significant tonal component, and the peak @ 1000 Hz due to the gearbox bearing.

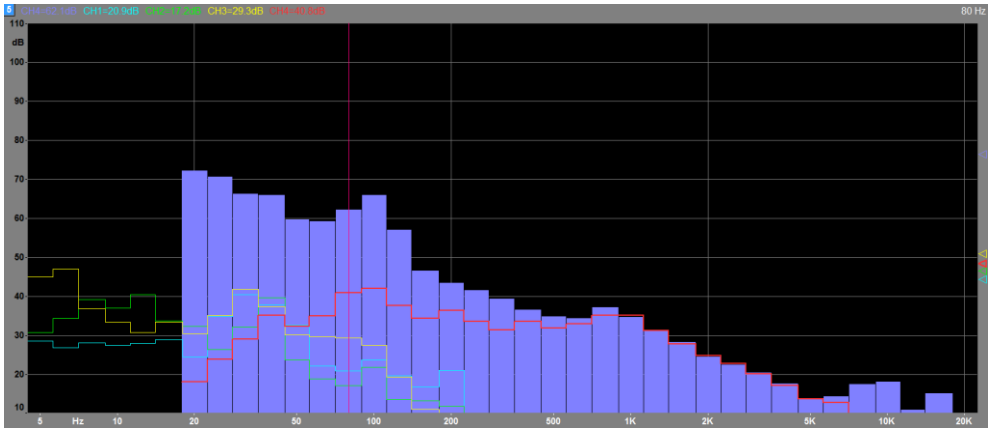

Figure 8.31: Noise spectrum in the owner cabin @ cruise speed

By the way, during the trials, the LD VIP cabin, located adjacent the engine room, highlighted very high noise levels (64 dB(A)) that has been investigated at the harbour with the only gensets on. In Fig. 8.32 and 8.33, the results of the

investigation in the LD VIP cabin @ berth has been reported, by locating the accelerometer on the window S13 (first natural frequency: 113 Hz)

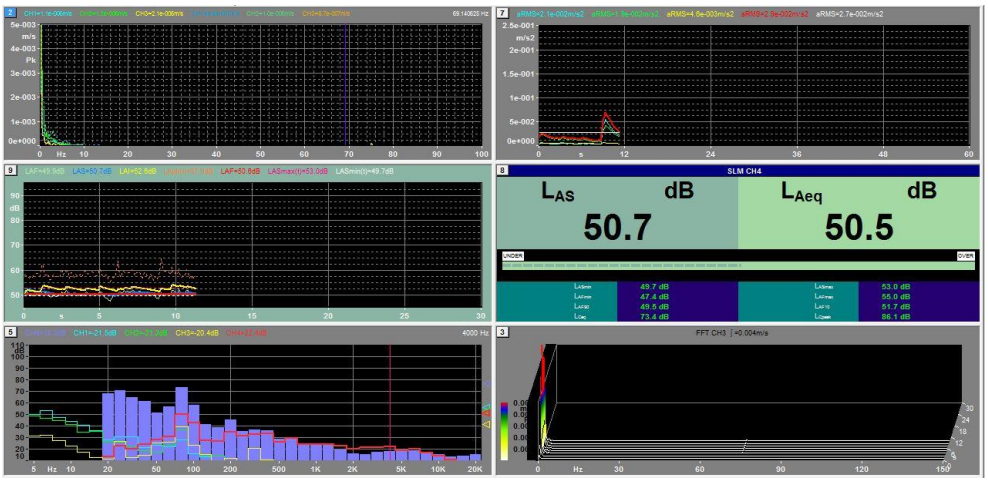

Figure 8.32: Noise measurement in the LD VIP cabin @ berth

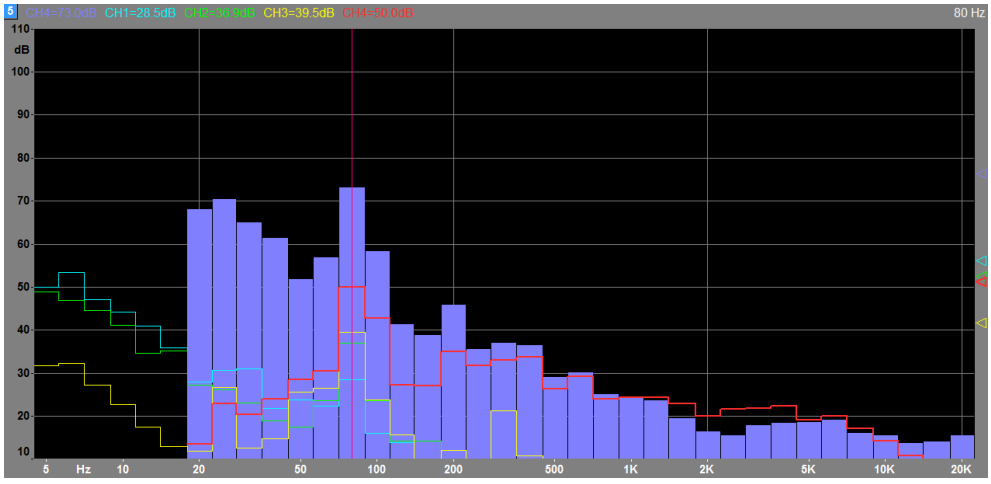

Figure 8.33: Noise spectrum in the LD VIP cabin @ berth

As it appear clear from the afore Fig. the window radiates a tonal component, measured in all the three direction, @ 75-100 Hz, where the firing frequency of the engine is present. Moreover, that window is also radiating the component of the gearbox self frequency, that is located in the 200 Hz centred third octave band. The first resonance acts exactly in correspondence to the first natural

frequency of the glass, that is the one having the higher ERP. In this case, being that resonance impossible to be modified by acting on the source (it should mean to change the engine or the engine foundation) or on the path (the engine room is adjacent the VIP cabin so the path is to short to be stiffened in an useful way), the unique solution is to act directly on the window. As results from this thesis, an increase in the mass of the glass should lead to a reduction of the first mode, so that to emphasize the problem, and so the best solution is to pass from a 3 layered window to a 5 layered one, that will also change the ERP from the glass pane (as shown in Section 6.2).

Chapter 9

CONCLUSIONS AND FUTURE DEVELOPMENTS

Laminated glass is nowadays a common composite material in the construction of yacht windows thanks to its capabilities of safety glass and its sound insulation properties. It has however a very complex structure since it is composed by materials, like glass and PVB, that have really different behaviour. Moreover, the PVB, characterized by viscoelastic properties, which depend on temperature, frequency and duration of loading, is very difficult to represent with a simple model.

Anyway, looking at the actual design trend of using larger and larger glass surfaces to make cabins and saloons more attractive for guests, it is important to verify the contribution of glass structure to the global response of the hull girder and to the noise radiation and vibration level of the areas under consideration.

Nowadays, the unique attention devoted by CS rules and backed up by scientific researches (but, mainly, for civil application) is to the structural capability of glazed panes to withstand external pressure loads, since they are considered as disconnected from the metallic frames. This approach has been adopted by the scientific community, that developed several equivalent model for static analysis and only one method for the dynamic simulation of laminated glass, that, although, is very complex and time consuming.

Moreover, only few studies have been carried out regarding the structural and dynamic integration of glass in global super and megayacht model, in order to validate the assumption made by CS.

In the study herein presented, after a complete overview of the rules proposed by the most common organization involved in yacht construction and the analytical formulation already developed in literature, the effect of laminated and monolithic glass to the primary response of a superyacht hull girder has been studied. That section of the thesis highlights that the common practice of gluing windows out of the side plane on superstructures has a twofold effect; from one side this prevents the glass from receiving loads from the metallic structure, both from the other side it is not able to cooperate with the hull to the primary response.

This phenomenon, that has been confirmed by some studies available in literature, is really dangerous having in mind the trend of enlarging the openings; for this reason, the study on the cooperation of large window panes to the primary response to global loads is currently undergoing in a joint project between the Polo Navale of DITEN – University of Genoa. CETENA and FINCANTIERI in the way to find a new solution for a more structural glass-metallic joint co-planar with the superstructure side that will somehow load the window in a way to guarantee its collaboration to the hull girder.

From Chapter 4, the vibroacoustic behaviour of laminated glass has been investigated, starting from the development of a simplified procedure for the determination of a dynamic equivalent monolithic glass with the same natural frequencies of the laminated one, simplifying, in this way, the complex algorithms proposed by Lopez – Aenlle Pelayo. For that porpoise, a parametric script in MSC Patran language has been developed.

Particular attention has been devoted to the damping loss factor of laminated glass; on that regard, a new RT based procedure, more simple with respect to

the standard Oberst test, has been proposed on viscoelastic materials and then extended to laminated glass. The herein proposed methodology, based on simple hammer tests, has the limitation imposed by ISO 3382-1 in terms of decay time and it is able only to excite the resonant modes. The development of this stage will be the use of a pink noise generator that will be able to excite also the non resonant modes of the glass, giving a more precise results even for the third octave band without any natural modes.

In Chapter 7, the results of a study carried out together with the Technische Universität Hamburg (TUHH) have been presented. A superelement model of a 80 meter yacht, prepared by TUHH, has been implemented and used for the influence of laminated glass in the first hull girder vibration. In particular, the shift in the first vertical eigenmode has been calculated. As it could be expected, since the vertical hull girder frequency is driven by the momentum of inertia of the main section and the total mass of the vessel, the out-of-plane glued window panes has a limited effect on the global vibration. This behaviour will be tested again by using the outcomes of the research on the new glass-metallic joint.

The last part of this monograph is devoted to the study of the noise propagation onboard a superyacht. In this stage, the main outcomes of the previous Chapter have been used; the DEET has driven the dynamic equivalence of laminated glass and the DLF spectra has been implemented in a SEA model of a 54 meter superyacht under construction at the time the model was developed.

As a matter of fact, many problems on laminated windows could be avoided by simple considerations in the preliminary design phase. Resonances of windows panes due to the excitation frequencies present on board such as the firing frequency of the main engines. In this sense the Equivalent Radiated Power is a useful tool to display the power radiated in the low frequency range where the resonances are the main causes of large variations in sound transmission. In some cases, the damping and noise control treatment applied onboard could prevent the problem and shift critical situations to other frequencies, but in other

cases (see Fig. 8.32) it does not happen, reflecting in very high sound pressure level radiated by the windows.

Nevertheless, the use of SEA is mainly based to the experience and to the experimental data available; moreover, the behaviour of the dynamic system in the low frequency range could not be achieved by a SEA model but it requires the computation of the modal density carried out in a deterministic way. On this regard, a benchmark on a superyacht is currently being developed tighter with MSC Software Company in order to test a new virtual SEA solver for Actran that should use complex FRF on a Fe based model in order to enlarge its range of applicability.

[1] A. Ivaldi, "Growing length in the megayacht industry and structure-related design topics," *Ships Offshore Struct.*, 2015.

[2] D. Truelock *et al.*, *Committee II.2 Dynamic Response*, vol. II, no. Proceedings of the 20th International Ship and Offshore Structures Congress (ISSC 2018). 2018.

[3] A. Ergin *et al.*, *Committee V.5 Dynamic Response*, vol. II, no. Proceedings of the 20th International Ship and Offshore Structures Congress (ISSC 2018). 2018.

[4] T. Pais, "Influence of comfort requirements on the structural layout of superyachts."

[5] F. Verbaas, "Foundations for a code for Maritime Structural Design of Glass Components," in *24 th International HISWA Symposium on Yacht Design and Yacht Construction*, 2016, no. November, pp. 1–15.

[6] F. Verbaas, "USE OF GLASS AND THE REGULATIONS," in *22 nd International HISWA Symposium on Yacht Design and Yacht Construction International HISWA Symposium on Yacht Design and Yacht Construction*, 2012.

[7] K. M. Jansen, "Glass as a load bearing material in yacht industries," in *22 nd International HISWA Symposium on Yacht Design and Yacht Construction*, 2012.

[8] DNV-GL, "Glass stiffnes in ship structures," 2018.

[9] W. Fricke and B. Gerlach, "Effect of large openings without and with windows on the shear stiffness of side walls in passenger ships," *Ships Offshore Struct.*, 2015.

[10] F. Albertoni, A. Barbato, and A. Ivaldi, "Hull – superstructure interaction. A naval ship case – study," in *Proceedings of IMAM*, 2012.

[11] V. Zanic, J. Andric, and P. Prebeg, "Superstructure deck effectiveness of the generic ship types - A concept design methodology," in *Proceedings of the 12th International Congress of the International Maritime Association of the Mediterranean, IMAM 2005 - Maritime Transportation and Exploitation of Ocean and Coastal Resources*, 2005.

[12] B. Wiegard, S. Ehlers, O. Klapp, and B. Schneider, "Bonded window panes in strength analysis of ship structures," *Sh. Technol. Res.*, vol. 65, no. 2, pp. 102–121, May 2018.

[13] S. Semrau and C. Weißenborn, "Radiation of Ship Windows Induced by Structure-borne Sound," *Proc. NAG/DAGA 2009*, pp. 285–288, 2009.

[14] B. Van Antwerpen, D. Udekem, C. Weißenborn, F. Field, and T. Sa, "Vibro-Acoustic simulation of structure-borne induced radiation of ship windows," in *NAG/DAGA 2009 International Conference on Acoustics*, 2009, no. 1, pp. 216–219.

[15] D. Boote, T. Pais, and E. Camporese, "Numerical and experimental analysis of the dynamic behaviour of large yacht superstructures," in *RINA, Royal Institution of Naval Architects - International Conference on Design*

and Construction of Super and Mega Yachts, 2013, pp. 141–148.
[16] D. Blanchet and A. Caillet, "Full frequency noise and vibration control onboard ships," in *21st International Congress on Sound and Vibration 2014, ICSV 2014*, 2014.
[17] M. López-Aenlle and F. Pelayo, "Dynamic effective thickness in laminated-glass beams and plates," *Compos. Part B Eng.*, 2014.
[18] L. Galuppi and G. Royer-Carfagni, "The Effective Thickness of Laminated Glass Plates," *J. Mech. Mater. Struct.*, 2012.
[19] A. Zemanová, J. Zeman, T. Janda, J. Schmidt, and M. Šejnoha, "On modal analysis of laminated glass: Usability of simplified methods and Enhanced Effective Thickness," *Compos. Part B Eng.*, 2018.
[20] H. Koruk and K. Sanliturk, "On measuring dynamic properties of damping materials using Oberst beam method," in *Proceedings of the ASME 2010 10th Biennial Conference on Engineering Systems Design and Analysis ESDA2010*, 2010, pp. 1–8.
[21] IMO, *SOLAS, Consolidated Edition 2014*. 2014.
[22] Lloyd´s Register, "Rules and Regulations for the Classification of Special Service Craft," 2018.
[23] A. A. B. for Shipping, "Guide for Building and Classing of Yachts," 2018.
[24] Registro Italiano Navale, "Rules for the classification of pleasure craft," 2017.
[25] International Standard Organization, "ISO 11336-1," *Int. Organ. Stand.*, 2012.
[26] Code Vessel Safety Branch and Maritime and Coastguard Agency, "Large Commercial Yacht Code."
[27] C. N. delle Ricerche, "CNR-DT 210/2013 Istruzioni per la Progettazione, l'Esecuzione ed il Controllo di Costruzioni con Elementi Strutturali di Vetro," 2013.
[28] C. Vallabhan, Y. Das, and M. Ramasamudra, "Properties of PVB Interlayer Used in Laminated Glass," *J. Mater. Civ. Eng.*, 1992.
[29] C. Fors, "Mechanical properties of interlayers in laminated glass. Experimental and Numerical Evaluation," 2014.
[30] N. G. McCrum, C. P. Buckley, and C. B. Bucknall, *Principles of polymer engineering*. 1988.
[31] D. Gutierrez-Lemini, *Engineering viscoelasticity*. 2014.
[32] S. J. Bennison, M. H. X. Qin, and P. S. Davies, "High-performance laminated glass for structurally efficient glazing," in *Innovative Light-weight Structures and Sustainable Facades*, 2008.
[33] I. Calderone, P. S. Davies, S. J. Bennison, H. Xiaokun, and L. Gang, "Effective laminate thickness for the design of laminated glass," *Glas. Process. Days*, 2009.
[34] E. H. Lee, "Stress analysis for linear viscoelastic materials," *Rheol. Acta*, 1961.
[35] W. T. Read, "Stress analysis for compressible viscoelastic materials," *J. Appl. Phys.*, 1950.
[36] J. D. Ferry, *Viscoelastic Properties of Polymers, 3rd Edition*. 1980.

[37] L. Galuppi and G. F. Royer-Carfagni, "Effective thickness of laminated glass beams: New expression via a variational approach," *Eng. Struct.*, 2012.
[38] L. Galuppi, G. Manara, and G. Royer Carfagni, "Practical expressions for the design of laminated glass," *Compos. Part B Eng.*, 2013.
[39] J. Romanoff *et al.*, "Hull-superstructure interaction in optimised passenger ships," *Ships Offshore Struct.*, 2013.
[40] Y. Okumoto, Y. Takeda, M. Mano, and T. Okada, *Design of ship hull structures: A practical guide for engineers*. 2009.
[41] M. Heder and A. Ulfvarson, "Hull beam behaviour of passenger ships," *Marine structures : Design, Construction & Safety*, vol. 4, no. 1. London, pp. 17–34, 1991.
[42] R. Toming, E.-H. Kerge, H. Naar, K. Tabri, J. Romanoff, and H. Remes, "Hull and superstructure interaction using coupled beam method," in *PRADS 2016 - Proceedings of the 13th International Symposium on PRActical Design of Ships and Other Floating Structures*, 2016.
[43] J. B. Caldwell, "The effect of superstructures on the longitudinal strength of ships," *Trans. R. Inst. Nav. Archit.*, 1957.
[44] A. J. Johnson, "Stresses in deckhouse and superstructure," *Trans. R. Inst. Nav. Archit.*, 1957.
[45] J. C. Chapman, "The interaction between a ship hull and a long superstructures," *Trans. R. Inst. Nav. Archit.*, 1957.
[46] M. D. A. Mackney and C. T. F. Foss, "Superstructure effectiveness in the preliminary assessment of the hull behavior," *Mar. Technol.*, vol. 36, no. 1, 1999.
[47] A. Alaimo, A. Milazzo, and D. Tumino, *Modal and structural fem analysis of a 50 ft pleasure yacht*. 2012.
[48] Anon, "NASTRAN USER'S GUIDE - LEVEL 15.," *NASA Contract. Reports*, 1975.
[49] B. Gerlach and W. Fricke, "Experimental and numerical investigation of the behavior of ship windows subjected to quasi-static pressure loads," *Mar. Struct.*, 2016.
[50] D. Boote, T. Pais, G. Vergassola, A. Tonelli, and L. Gragnani, "On the damping coefficient of laminated glass for yacht industry," *Int. Shipbuild. Prog.*, vol. 64, no. 1–2, 2017.
[51] L. Gragnani, "Dynamic characterization of lamianted glass for megayachts windows."
[52] D. Ross, E. E. Ungar, and E. M. Kerwin, "Damping of Plate Flexural Vibrations by Means of Viscoelastic Laminae," in *Structural Vibrations*, 1960.
[53] S. Timoshenko, *Theory of Plates and Shells*. 1941.
[54] A. W. Leissa, "The free vibration of rectangular plates," *Top. Catal.*, 1973.
[55] S. Marburg, E. Lösche, H. Peters, and N. Kessissoglou, "Surface contributions to radiated sound power," *J. Acoust. Soc. Am.*, 2013.
[56] V. V. Krylov, "Acoustic black holes and their applications for vibration damping and sound absorption," *Proc. Int. Conf. Noise Vib. Eng. / Int. Conf.*

Uncertain. Struct. Dyn., 2012.
[57] V. Krylov, "Acoustic black holes: Recent developments in the theory and applications," *IEEE Trans. Ultrason. Ferroelectr. Freq. Control*, 2014.
[58] T. Pais, D. Boote, and P. Kaeding, "Experimental and numerical analysis of absorber materials for steel decks," in *Proceedings of the International Offshore and Polar Engineering Conference*, 2016.
[59] D. Boote, T. Pais, and S. Dellepiane, "Vibrations of superyacht structures: Comfort rules and predictive calculations," in *Analysis and Design of Marine Structures - Proceedings of the 4th International Conference on Marine Structures, MARSTRUCT 2013*, 2013.
[60] T. D. Rossing, "Shock and vibration handbook , 2nd ed.," *Am. J. Phys.*, 1977.
[61] R. E. Blake, "Basic vibration theory," *Harris Shock Vib. handbookshock Vib. Handb.*, 2010.
[62] Clarence W De Silva, "Frequency Response," *Vibration*, p. 943, 2000.
[63] C. W. De Silva, *Vibration Monitoring, Testing, and Instrumentation*. 2007.
[64] M. Carfagni, E. Lenzi, and M. Pierini, "The loss factor as a measure of mechanical damping," in *1998 IMAC XVI - 16th International Modal Analysis Conference*, 1998.
[65] N. Srikanth and M. M. Gupta, "Damping characterization of magnesium based composites using an innovative circle-fit approach," *Compos. Sci. Technol.*, 2003.
[66] L. Komzsik, "Numerical Methods User's Guide," *MSC/NASTRAN*, 1998.
[67] International Standard Organization, "Iso 3382-1," *Int. Organ. Stand.*, 2009.
[68] J. Zhang, C. Wan, and T. Sato, "Advanced Markov Chain Monte Carlo approach for finite element calibration under uncertainty," *Comput. Civ. Infrastruct. Eng.*, vol. 28, no. 7, pp. 522–530, 2013.
[69] R. H. Lyon and R. G. DeJong, *Theory and Application of Statistical Energy Analysis*. 1995.
[70] L. L. Beranek and I. L. Ver, "Noise and vibration control engineering," *IEEE Power Engineering Review*. 1992.
[71] M. R. Schroeder, "Frequency-Correlation Functions of Frequency Responses in Rooms," *J. Acoust. Soc. Am.*, 1962.
[72] ABS, "Guidance notes on ship vibration," *Abs*, no. April, pp. 1–96, 2006.
[73] T. Pais, D. Boote, and G. Vergassola, "Vibration analysis for the comfort assessment of a superyacht under hydrodynamic loads due to mechanical propulsion," *Ocean Eng.*, vol. 155, no. February, pp. 310–323, May 2018.
[74] ANSYS, "Theory Reference for ANSYS Mechanical APDL," *ANSYS Inc*, 2013.
[75] T. Pais, "Analytical and numerical computation of added mass in vibration analysis for a superyacht," *Ships Offshore Struct.*, vol. 13, no. 4, pp. 443–450, 2017.
[76] L. Burrill, "Ship vibration; simple methods of estimating critical frequencies," *North East Coast Inst. Eng. Shipbuild.*, 1934.

[77] I. Asmussen, W. Menzel, and H. Mumm, "Ship Vibration," *GL Technol.*, p. 52, 2001.
[78] D. N. Manik, "Statistical energy analysis (SEA) applications in vibration and noise," *20th Int. Congr. Sound Vib. 2013, ICSV 2013*, vol. 4, no. July, pp. 3639–3654, 2013.
[79] ESI Group, "Marine application made easy with VaOne." 2018.
[80] Noise Control Engineering, "http://www.noise-control.com/airbornenoiseanalysis.php." .
[81] J. Plunt, *Methods for predicting noise levels in ships – experiences from empirical an sea calculation methods*. 1980.
[82] G. Vergassola, T. Pais, and D. Boote, "Numerical tools and experimental procedures for the prediction of noise propagation on board superyachts," *Trans. R. Inst. Nav. Archit. Part B Int. J. Small Cr. Technol.*, vol. 160, no. B1, pp. B9–B16, 2018.
[83] M. Biot, L. Moro, and P. N. Mendoza Vassallo, "Prediction of the structure-borne noise due to marine diesel engines on board cruise ships," in *21st International Congress on Sound and Vibration 2014, ICSV 2014*, 2014.
[84] Z.-Q. Rao and C.-J. Yang, "Numerical prediction of tonal noise for non-cavitating propellers in effective wake," *Ships Offshore Struct.*, vol. 13, no. 5, pp. 551–560, 2018.
[85] Registro Italiano Navale, "COM Yacht Additional Class Notation," 2017.

Annex A

MSC PATRAN SCRIPT FOR ERP CALCULATION

```
set_current_dir( "C:\Users\G_Vergassola\Desktop\S1_ERP" )
parametric_modeling_util.define_user_config_file ("Variabili_Modello_3l.dat")
#
#-------------------------------------------------------------------
# Imposto i Paramatri del modello
#-------------------------------------------------------------------
#
parametric_modeling_util.create_variable( "L", "Real", "", "", "1500",        @
        "Lunghezza" )
$# Real L = 1500; em_sf_comment_previous_line()
parametric_modeling_util.reset_variable( "L" )
$# Real L = 1500; em_sf_comment_previous_line()
#
#-------------------------------------------------------------------
#
parametric_modeling_util.create_variable( "B", "Real", "", "", "1000",        @
        "Altezza" )
$# Real B = 1000; em_sf_comment_previous_line()
parametric_modeling_util.reset_variable( "B" )
$# Real B = 1000; em_sf_comment_previous_line()
#
#-------------------------------------------------------------------
#
```

```
parametric_modeling_util.create_variable( "t_1", "Real", "", "", "10",        @
        "Spessore Vetro interno" )
$# Real t_1 = 10; em_sf_comment_previous_line()
parametric_modeling_util.reset_variable( "t_1" )
$# Real t_1 = 8; em_sf_comment_previous_line()
#
#--------------------------------------------------------------------
#
parametric_modeling_util.create_variable( "t_int", "Real", "", "", "10",      @
        "Spessore interlayer" )
$# Real t_int = 10; em_sf_comment_previous_line()
parametric_modeling_util.reset_variable( "t_int" )
$# Real t_int = 0.64; em_sf_comment_previous_line()
#
#--------------------------------------------------------------------
#
parametric_modeling_util.create_variable( "t_2", "Real", "", "", "10",        @
        "Spessore vetro esterno" )
$# Real t_2 = 10; em_sf_comment_previous_line()
parametric_modeling_util.reset_variable( "t_2" )
$# Real t_2 = 8; em_sf_comment_previous_line()
#
#--------------------------------------------------------------------
#
parametric_modeling_util.create_variable( "t_tot", "Real", "", "", "10",      @
        "Spessore totale" )
$# Real t_tot = 10; em_sf_comment_previous_line()
parametric_modeling_util.reset_variable( "t_tot" )
$# Real t_tot = 16.64; em_sf_comment_previous_line()
#
#--------------------------------------------------------------------
```

```
#
#
parametric_modeling_util.create_variable( "E_vetro", "Real", "", "", "10",    @
      "Modulo di Young del vetro" )
$# Real E_vetro = 10; em_sf_comment_previous_line()
parametric_modeling_util.reset_variable( "E_vetro" )
$# Real E_vetro = 70000; em_sf_comment_previous_line()
#
#-----------------------------------------------------------------
#
parametric_modeling_util.create_variable( "ni_vetro", "Real", "", "", "10",   @
      "Coefficiente di poisson del vetro" )
$# Real ni_vetro = 10; em_sf_comment_previous_line()
parametric_modeling_util.reset_variable( "ni_vetro" )
$# Real ni_vetro = 0.22; em_sf_comment_previous_line()
#
#-----------------------------------------------------------------
#
parametric_modeling_util.create_variable( "rho_vetro", "Real", "", "", "10",  @
      "Coefficiente di poisson del vetro" )
$# Real rho_vetro = 10; em_sf_comment_previous_line()
parametric_modeling_util.reset_variable( "rho_vetro" )
$# Real rho_vetro = 2.7E-9; em_sf_comment_previous_line()
parametric_modeling_util.create_variable( "E_inter", "Real", "", "", "10",    @
      "Modulo di Young del interlay" )
$# Real E_inter = 10; em_sf_comment_previous_line()
parametric_modeling_util.reset_variable( "E_inter" )
#
#-----------------------------------------------------------------
#
parametric_modeling_util.create_variable( "ni_inter", "Real", "", "", "10",   @
```

```
      "Coefficiente di poisson del interlay" )
$# Real ni_inter = 10; em_sf_comment_previous_line()
parametric_modeling_util.reset_variable( "ni_inter" )
$# Real ni_inter = 0.22; em_sf_comment_previous_line()
#
#-----------------------------------------------------------------
#
parametric_modeling_util.create_variable( "rho_inter", "Real", "", "", "10",   @
      "Densita del interlay" )
$# Real rho_inter = 10; em_sf_comment_previous_line()
parametric_modeling_util.reset_variable( "rho_inter" )
$# Real rho_inter = 2.7E-9; em_sf_comment_previous_line()
#
#-----------------------------------------------------------------
#
parametric_modeling_util.create_variable( "v_z", "Real", "", "", "10",        @
  "Velocita perpendicolare al vetro" )
$# Real v_z = 10; em_sf_comment_previous_line()
parametric_modeling_util.reset_variable( "v_z" )
$# Real v_z = 10; em_sf_comment_previous_line()
#
#-----------------------------------------------------------------
#
parametric_modeling_util.create_variable( "gel", "Real", "", "", "10",        @
  "Global edge lenght" )
$# Real gel = 10; em_sf_comment_previous_line()
parametric_modeling_util.reset_variable( "gel" )
$# Real gel = 50; em_sf_comment_previous_line()
#
#-----------------------------------------------------------------
#
```

```
parametric_modeling_util.create_variable( "f_inf", "Real", "", "", "10",      @
    "Frequenza limite inferiore" )
$# Real f_inf = 10; em_sf_comment_previous_line()
parametric_modeling_util.reset_variable( "f_inf" )
$# Real f_inf = 2; em_sf_comment_previous_line()
#
#--------------------------------------------------------------------
#
parametric_modeling_util.create_variable( "f_sup", "Real", "", "", "10",      @
    "Frequenza limite superiore" )
$# Real f_sup = 10; em_sf_comment_previous_line()
parametric_modeling_util.reset_variable( "f_sup" )
$# Real f_sup = 6000; em_sf_comment_previous_line()
#
#--------------------------------------------------------------------
#
parametric_modeling_util.create_variable( "f_step", "Real", "", "", "10",      @
     "Step di frequenze" )
$# Real f_step = 10; em_sf_comment_previous_line()
parametric_modeling_util.reset_variable( "f_step" )
$# Real f_step = 100; em_sf_comment_previous_line()
#
#--------------------------------------------------------------------
#
parametric_modeling_util.create_variable( "rhocp", "Real", "", "", "10",      @
    "Coefficiente di scala" )
$# Real rhocp = 10; em_sf_comment_previous_line()
parametric_modeling_util.reset_variable( "rhocp" )
$# Real rhocp = 2E9; em_sf_comment_previous_line()
#
#--------------------------------------------------------------------
```

```
#
parametric_modeling_util.create_variable( "erpc", "Real", "", "", "10",       @
   "Velocita del fluido di contorno" )
$# Real erpc = 10; em_sf_comment_previous_line()
parametric_modeling_util.reset_variable( "erpc" )
$# Real erpc = 3.4E5; em_sf_comment_previous_line()
#
#-----------------------------------------------------------------
#
parametric_modeling_util.create_variable( "erprho", "Real", "", "", "10",     @
    "densita del fluido di contorno" )
$# Real erprho = 10; em_sf_comment_previous_line()
parametric_modeling_util.reset_variable( "erprho" )
$# Real erprho = 1.0E-12; em_sf_comment_previous_line()
#-----------------------------------------------------------------
# Genero il gruppo "Vetro_esterno"
#-----------------------------------------------------------------
#
sys_poll_option( 2 )
ga_group_create( "Vetro_esterno" )
ga_group_current_set( "Vetro_esterno" )
sys_poll_option( 0 )
#
#-----------------------------------------------------------------
# Genero la geometria per il vetro esterno
#-----------------------------------------------------------------
#
STRING asm_create_patch_xy_created_ids[VIRTUAL]
asm_const_patch_xyz( "1", "<`L` `B` 0>", "[`-L/2` `-B/2` `0`]", "Coord 0",
@
asm_create_patch_xy_created_ids )
```

```
$# 1 Patch created: Patch 1
#
#-------------------------------------------------------------------
# Genero la geometria per i vincoli
#-------------------------------------------------------------------
#
STRING asm_create_grid_xyz_created_ids[VIRTUAL]
asm_const_grid_xyz( "5", "[`L/2` `B/2+100` 0 ]", "Coord 0",  @
asm_create_grid_xyz_created_ids )
STRING asm_create_grid_xyz_created_ids[VIRTUAL]
asm_const_grid_xyz( "6", "[`L/2` `-B/2-100` 0 ]", "Coord 0",  @
asm_create_grid_xyz_created_ids )
STRING asm_create_grid_xyz_created_ids[VIRTUAL]
asm_const_grid_xyz( "7", "[`-L/2` `-B/2-100` 0 ]", "Coord 0",  @
asm_create_grid_xyz_created_ids )
STRING asm_create_grid_xyz_created_ids[VIRTUAL]
asm_const_grid_xyz( "8", "[`-L/2` `B/2+100` 0 ]", "Coord 0",  @
asm_create_grid_xyz_created_ids )
STRING asm_create_grid_xyz_created_ids[VIRTUAL]
asm_const_grid_xyz( "9", "[`L/2+100` `B/2+100` 0 ]", "Coord 0",  @
asm_create_grid_xyz_created_ids )
STRING asm_create_grid_xyz_created_ids[VIRTUAL]
asm_const_grid_xyz( "10", "[`L/2+100` `-B/2-100` 0 ]", "Coord 0",  @
asm_create_grid_xyz_created_ids )
STRING asm_create_grid_xyz_created_ids[VIRTUAL]
asm_const_grid_xyz( "11", "[`-L/2-100` `-B/2-100` 0 ]", "Coord 0",  @
asm_create_grid_xyz_created_ids )
STRING asm_create_grid_xyz_created_ids[VIRTUAL]
asm_const_grid_xyz( "12", "[`-L/2-100` `B/2+100` 0 ]", "Coord 0",  @
asm_create_grid_xyz_created_ids )
STRING sgm_create_surface__created_ids[VIRTUAL]
```

```
sgm_const_surface_vertex( "2", "Point 9", "Point 5", "Point 6", "Point 10",  @
sgm_create_surface__created_ids )
$# 1 Surface Created: Surface 2
sgm_const_surface_vertex( "3", "Point 5", "Point 3", "Point 2", "Point 8",  @
sgm_create_surface__created_ids )
$# 1 Surface Created: Surface 3
sgm_const_surface_vertex( "4", "Point 6", "Point 4", "Point 1", "Point 7",  @
sgm_create_surface__created_ids )
$# 1 Surface Created: Surface 4
sgm_const_surface_vertex( "5", "Point 11", "Point 7", "Point 8", "Point 12",  @
sgm_create_surface__created_ids )
$# 1 Surface Created: Surface 5
#
#---------------------------------------------------------------------
# Creo il materiale vetro
#---------------------------------------------------------------------
#
material.create( "Analysis code ID", 1, "Analysis type ID", 1, "vetro", 0,   @
"Date: 31-Mar-16          Time: 10:34:59", "Isotropic", 1, "Directionality",  @
 1, "Linearity", 1, "Homogeneous", 0, "Linear Elastic", 1,   @
"Model Options & IDs", ["", "", "", "", ""], [0, 0, 0, 0, 0], "Active Flag",   @
1, "Create", 10, "External Flag", FALSE, "Property IDs", ["Elastic Modulus",
@
"Poisson Ratio", "Density"], [2, 5, 16, 0], "Property Values", ["`E_vetro`",   @
"`ni_vetro`", "`rho_vetro`", ""] )
#
#---------------------------------------------------------------------
# Creo la shell vetro esterno
#---------------------------------------------------------------------
#
elementprops_create( "vetro_esterno", 51, 25, 35, 1, 1, 20, [13, 20, 36, 4037, @
```

```
 4111,  4118, 4119, 8111, 4400, 4401, 4402, 4403, 4404, 4405, 4406, 4407,  @
4408, 4409],  [5, 9, 1, 1, 1, 1, 1, 4, 4, 4, 1, 1, 1, 1, 1, 1, 4, 4], [ @
"m:vetro", "",  "`t_1`","", "`t_1/2`", "", "", "", "", "", "", "", "", "", "", @
 "",    "", ""], "Surface 1" )
$# Property Set "vetro_esterno" created.
#
#------------------------------------------------------------------
# Creo la shell vetro esterno_aux
#------------------------------------------------------------------
#
elementprops_create( "vetro_esterno_aux", 51, 25, 35, 1, 1, 20, [13, 20, 36, 4037,
@
 4111,  4118, 4119, 8111, 4400, 4401, 4402, 4403, 4404, 4405, 4406, 4407,  @
4408, 4409],  [5, 9, 1, 1, 1, 1, 1, 4, 4, 4, 1, 1, 1, 1, 1, 1, 4, 4], [ @
"m:vetro", "",  "`t_1`","", "`t_1/2`", "", "", "", "", "", "", "", "", "", "", @
 "",    "", ""], "Surface 2:5" )
$# Property Set "vetro_esterno_aux" created.
#
#------------------------------------------------------------------
# Genero la mesh del vetro esterno
#------------------------------------------------------------------
#
INTEGER fem_create_mesh_surfa_num_nodes
INTEGER fem_create_mesh_surfa_num_elems
STRING fem_create_mesh_s_nodes_created[VIRTUAL]
STRING fem_create_mesh_s_elems_created[VIRTUAL]
fem_create_mesh_surf_4(  "IsoMesh",  49152,  "surface  1:5",  1,  ["`gel`"],
"Quad4",  @
 "#", "#", "Coord 0", "Coord 0", fem_create_mesh_surfa_num_nodes,   @
fem_create_mesh_surfa_num_elems, fem_create_mesh_s_nodes_created,   @
fem_create_mesh_s_elems_created )
```

```
#
#-----------------------------------------------------------------
# Genero il gruppo "interlayer"
#-----------------------------------------------------------------
#
sys_poll_option( 2 )
ga_group_create( "interlayer" )
ga_group_current_set( "interlayer" )
sys_poll_option( 0 )
#
#-----------------------------------------------------------------
# Genero la geometria interlayer
#-----------------------------------------------------------------
#
STRING sgm_sweep_solid_ext_created_ids[VIRTUAL]
sgm_const_solid_extrude( "1", "<0 0 `-t_int`>", 1., 0., "[0 0 0]", "Coord 0",  @
"srf 1:5", sgm_sweep_solid_ext_created_ids )
#
#-----------------------------------------------------------------
# Creo il materiale interlayer
#-----------------------------------------------------------------
#
material.create( "Analysis code ID", 1, "Analysis type ID", 1, "interlay", 0,  @
 "Date: 31-Mar-16          Time: 10:34:59", "Isotropic", 1, "Directionality", @
  1, "Linearity", 1, "Homogeneous", 0, "Linear Elastic", 1,   @
"Model Options & IDs", ["", "", "", "", ""], [0, 0, 0, 0, 0], "Active Flag",   @
1, "Create", 10, "External Flag", FALSE, "Property IDs", ["Elastic Modulus",
@
"Poisson Ratio", "Density"], [2, 5, 16, 0], "Property Values", ["`E_inter`",   @
"`ni_inter`", "`rho_inter`", ""] )
#
```

```
#-----------------------------------------------------------------
# Creo il solido interlay
#-----------------------------------------------------------------
#
elementprops_create( "interlay", 71, 25, 30, 1, 1, 20, [13, 21, 4124, 4126,  @
4125, 8111, 4401, 4402, 4403, 4404, 4405, 4406, 4407, 4410, 4411], [5, 4, 4,  @
4, 4, 4, 4, 1, 1, 1, 1, 1, 1, 1, 6], ["m:interlay", "", "", "", "", "", "",  @
"","", "", "", "", "", "", ""], "Solid 1" )
$# Property Set "interlay" created.
#
#-----------------------------------------------------------------
# Creo il solido interlay_aux
#-----------------------------------------------------------------
#
elementprops_create( "interlay_aux", 71, 25, 30, 1, 1, 20, [13, 21, 4124, 4126,  @
4125, 8111, 4401, 4402, 4403, 4404, 4405, 4406, 4407, 4410, 4411], [5, 4, 4,  @
4, 4, 4, 4, 1, 1, 1, 1, 1, 1, 1, 6], ["m:interlay", "", "", "", "", "", "",  @
"","", "", "", "", "", "", ""], "Solid 2:5" )
$# Property Set "interlay_aux" created.
#
#-----------------------------------------------------------------
# genero la mesh del interlayer
#-----------------------------------------------------------------
#
INTEGER fem_create_mesh_solid_num_nodes
INTEGER fem_create_mesh_solid_num_elems
STRING fem_create_mesh_s_nodes_created[VIRTUAL]
STRING fem_create_mesh_s_elems_created[VIRTUAL]
fem_create_mesh_sol_5( "solid 1", "IsoMesh", "Hex8", 1, ["`gel`"], 49152, 0, 1,
@
 0, 1, 0., "", "#", "#", "Coord 0", "Coord 0",  @
```

```
fem_create_mesh_solid_num_nodes, fem_create_mesh_solid_num_elems,  @
fem_create_mesh_s_nodes_created, fem_create_mesh_s_elems_created )
fem_create_mesh_sol_5( "solid 2", "IsoMesh", "Hex8", 1, ["`gel`"], 49152, 0, 1,
@
 0, 1, 0., "", "#", "#", "Coord 0", "Coord 0",  @
fem_create_mesh_solid_num_nodes, fem_create_mesh_solid_num_elems,  @
fem_create_mesh_s_nodes_created, fem_create_mesh_s_elems_created )
fem_create_mesh_sol_5( "solid 3", "IsoMesh", "Hex8", 1, ["`gel`"], 49152, 0, 1,
@
 0, 1, 0., "", "#", "#", "Coord 0", "Coord 0",  @
fem_create_mesh_solid_num_nodes, fem_create_mesh_solid_num_elems,  @
fem_create_mesh_s_nodes_created, fem_create_mesh_s_elems_created )
fem_create_mesh_sol_5( "solid 4", "IsoMesh", "Hex8", 1, ["`gel`"], 49152, 0, 1,
@
 0, 1, 0., "", "#", "#", "Coord 0", "Coord 0",  @
fem_create_mesh_solid_num_nodes, fem_create_mesh_solid_num_elems,  @
fem_create_mesh_s_nodes_created, fem_create_mesh_s_elems_created )
fem_create_mesh_sol_5( "solid 5", "IsoMesh", "Hex8", 1, ["`gel`"], 49152, 0, 1,
@
 0, 1, 0., "", "#", "#", "Coord 0", "Coord 0",  @
fem_create_mesh_solid_num_nodes, fem_create_mesh_solid_num_elems,  @
fem_create_mesh_s_nodes_created, fem_create_mesh_s_elems_created )
#
#-----------------------------------------------------------------
# Genero il gruppo "Vetro_interno"
#-----------------------------------------------------------------
#
sys_poll_option( 2 )
ga_group_create( "Vetro_interno" )
ga_group_current_set( "Vetro_interno" )
sys_poll_option( 0 )
```

```
#
#-----------------------------------------------------------------
# Genero la geometria per il vetro interno
#-----------------------------------------------------------------
#
STRING sgm_transform_surf__created_ids[VIRTUAL]
sgm_transform_translate_v1( "6", "surface", "<0 0 `-t_int`>", `t_int`,   @
FALSE, "Coord 0", 1, FALSE, "srf 1", sgm_transform_surf__created_ids )
STRING sgm_transform_surf__created_ids[VIRTUAL]
sgm_transform_translate_v1( "7", "surface", "<0 0 `-t_int`>", `t_int`,   @
FALSE, "Coord 0", 1, FALSE, "srf 2:5", sgm_transform_surf__created_ids )
#
#-----------------------------------------------------------------
# Creo la shell vetro interno
#-----------------------------------------------------------------
#
elementprops_create( "vetro_interno", 51, 25, 35, 1, 1, 20, [13, 20, 36, 4037, @
 4111,  4118, 4119, 8111, 4400, 4401, 4402, 4403, 4404, 4405, 4406, 4407,  @
4408, 4409],  [5, 9, 1, 1, 1, 1, 1, 4, 4, 4, 1, 1, 1, 1, 1, 1, 4, 4], [ @
"m:vetro", "",  "`t_2`","", "`-t_2/2`", "", "", "", "", "", "", "", "", "", "" @
, "",    "", ""], "Surface 6" )
$# Property Set "vetro_interno" created.
#
#-----------------------------------------------------------------
# Creo la shell vetro interno_aux
#-----------------------------------------------------------------
#
elementprops_create( "vetro_interno_aux", 51, 25, 35, 1, 1, 20, [13, 20, 36, 4037,
@
 4111,  4118, 4119, 8111, 4400, 4401, 4402, 4403, 4404, 4405, 4406, 4407,  @
4408, 4409],  [5, 9, 1, 1, 1, 1, 1, 4, 4, 4, 1, 1, 1, 1, 1, 1, 4, 4], [ @
```

```
"m:vetro", "",  "`t_2`","", "`-t_2/2`", "", "", "", "", "", "", "", "", "", "" @
, "",    "", ""], "Surface 7:10" )
$# Property Set "vetro_interno_aux" created.
#
#-----------------------------------------------------------------
# Genero la mesh del vetro interno
#-----------------------------------------------------------------
#
INTEGER fem_create_mesh_surfa_num_nodes
INTEGER fem_create_mesh_surfa_num_elems
STRING fem_create_mesh_s_nodes_created[VIRTUAL]
STRING fem_create_mesh_s_elems_created[VIRTUAL]
fem_create_mesh_surf_4( "IsoMesh", 49152, "surface 6:10", 1, ["`gel`"],
"Quad4", @
 "#", "#", "Coord 0", "Coord 0", fem_create_mesh_surfa_num_nodes,  @
fem_create_mesh_surfa_num_elems, fem_create_mesh_s_nodes_created,  @
fem_create_mesh_s_elems_created )

#
#-----------------------------------------------------------------
# Faccio equivalence
#-----------------------------------------------------------------
#
REAL fem_equiv_all_x_equivtol_ab
INTEGER fem_equiv_all_x_segment
fem_equiv_all_group4( [" "], 0, "", 1, 1, 10., FALSE,  @
fem_equiv_all_x_equivtol_ab, fem_equiv_all_x_segment )
#
#-----------------------------------------------------------------
# Applico i carichi
#-----------------------------------------------------------------
```

```
#
loadsbcs_create2( "velocity", "Velocity", "Nodal", "", "Static", [ @
"Surface 2:5"], "Geometry", "Coord 0", "1.", ["<0,0,`-v_z`>",  @
"<    >", "<    >", "<    >"], ["", "", "", ""] )
$# Load/BC set "velocity" created.
#
#---------------------------------------------------------------------
# Creo il sistema di vincoli
#---------------------------------------------------------------------
#
loadsbcs_create2( "fixity", "Displacement", "Nodal", "", "Static", [ @
"Surface 2:5"], "Geometry", "Coord 0", "1.", ["<0,0,0>", "< 0,0 ,0 >" @
 , "<    >", "<    >"], ["", "", "", ""] )
$# Load/BC set "fixity" created.
#
#---------------------------------------------------------------------
# Creo il load case
#---------------------------------------------------------------------
#
loadcase_create2( "erp", "Time Dependent", "", 1., ["fixity", "velocity"], [0, @
 0], [1., 1.], "", 0., TRUE )
#
#---------------------------------------------------------------------
# Creo il subcase
#---------------------------------------------------------------------
#
mscnastran_subcase.create( "111", "Default", "This is a default subcase." )
mscnastran_subcase.create_char_param( "LOAD CASE", "erp" )
mscnastran_subcase.create_char_param( "SUBCASE TITLE",  @
"This is a default subcase." )
mscnastran_subcase.create_char_param( "SUBCASE SUBTITLE", "Default" )
```

```
mscnastran_subcase.create_char_param( "SUBCASE LABEL",  @
"This load case is the default load case that always appears" )
mscnastran_subcase.create_char_param( "SUBCASE TITLE FLAG", "OFF" )
mscnastran_subcase.create_char_param( "SUBCASE SUBTITLE FLAG",
"ON" )
mscnastran_subcase.create_char_param( "SUBCASE LABEL FLAG", "OFF"
)
mscnastran_subcase.create_char_param( "Default", "STRUCTURAL" )
mscnastran_subcase.create_char_param( "DISPLACEMENTS", "1" )
mscnastran_subcase.create_char_param( "DISPLACEMENTS 1",  @
"DISPLACEMENT(SORT1,REAL)=0" )
mscnastran_subcase.create_char_param( "CONSTRAINT FORCES", "1" )
mscnastran_subcase.create_char_param( "CONSTRAINT FORCES 1",  @
"SPCFORCES(SORT1,REAL)=0" )
mscnastran_subcase.create_char_param( "SUBCASE WRITE", "ON" )
mscnastran_subcase.create_char_param( "SUBCASE DIRECT TEXT POS",
"OFF" )
mscnastran_subcase.create_int_param( "SUBCASE INPUT 0", 0 )
mscnastran_subcase.create_matrix_param( "FREQUENCY RESPONSE
DATA", 5, 1, [[1.] @
 [`f_inf`][`f_sup`][`f_step`][-1.]] )
mscnastran_subcase.create_char_param( "ROTOR DYNAMICS", "OFF" )
mscnastran_subcase.create_char_param( "ALL EXPLICIT MPCS", "ON" )
#
#-----------------------------------------------------------------
# Lancio l'analisi (Full Run deve essere abilitato)
#-----------------------------------------------------------------
#
jobfile.open( "erp", "ANALYZE NO JOBFILE" )
jobfile.write_spl( "/* Jobfile for PATNAS created %A% at %A% */", ["04-Apr-
18" @
```

```
, "09:57:01"] )
jobfile.writec( "", "TRANSLATOR = pat3nas" )
jobfile.writec( "DATABASE", "C:\Users\G_Vergassola\Desktop\S1_ERP" )
jobfile.writec( "JOBNAME", "erp" )
jobfile.writec( "ANALYSIS TITLE", "MSC.Nastran job created on 31-Mar-16
at" // @
" 11:24:56" )
jobfile.writec( "ANALYSIS SUBTITLE", "" )
jobfile.writec( "ANALYSIS LABEL", "" )
jobfile.writec( "", "" )
jobfile.writec( "OBJECT", "Entire Model" )
jobfile.writec( "METHOD", "Analysis Deck" )
jobfile.writec( "", "" )
jobfile.writec( "MODEL SUFFIX", ".bdf" )
jobfile.writec( "RESULTS SUFFIX", ".op2" )
jobfile.writec( "", "" )
jobfile.writec( "", "/*" )
jobfile.writec( "", " * File Search Path Declaration" )
jobfile.writec( "", " */" )
jobfile.writec( "", "" )
jobfile.writec( "File Search Path", "C:\Users\G_Vergassola" )
jobfile.writec( "File Search Path", "C:\MSC.Software\Patran_x64\20160" )
jobfile.writec( "File Search Path", "C:\MSC.Software\Patran_x64\20160\help"
// @
"files" )
jobfile.writec( "File Search Path",
"C:\MSC.Software\Patran_x64\20160\alters" )
jobfile.writec( "File Search Path",
"C:\MSC.Software\Patran_x64\20160\icons" )
jobfile.writec( "File Search Path", "C:\MSC.Software\Patran_x64\20160\icon"
// @
```

```
"s\RibbonIcons" )
jobfile.writec( "File Search Path", "C:\MSC.Software\Patran_x64\20160\bin" )
jobfile.writec( "File Search Path",
"C:\MSC.Software\Patran_x64\20160\bin\exe" )
jobfile.writec( "File Search Path",
"C:\MSC.Software\Patran_x64\20160\msce" // @
"xplore_files\" )
jobfile.writec( "File Search Path",
"C:\MSC.Software\Patran_x64\20160\mscp" // @
"rocor_files\dmap" )
jobfile.writec( "File Search Path",
"C:\MSC.Software\Patran_x64\20160\mscp" // @
"rocor_files\plb" )
jobfile.writec( "File Search Path",
"C:\MSC.Software\Patran_x64\20160\mscp" // @
"rocor_files\lib" )
jobfile.writec( "File Search Path",
"C:\MSC.Software\Patran_x64\20160\mscp" // @
"rocor_files\icons" )
jobfile.writec( "File Search Path", "C:\MSC.Software\Patran_x64\20160\shar"
// @
"eware\msc\unsupported\utilities\icons" )
jobfile.writec( "File Search Path", "C:\MSC.Software\Patran_x64\20160\shar"
// @
"eware\msc\unsupported\utilities\plb" )
jobfile.writec( "File Search Path", "C:\MSC.Software\Patran_x64\20160\shar"
// @
"eware\msc\unsupported\utilities\extra_files" )
jobfile.writec( "", "" )
jobfile.writec( "", "/*" )
jobfile.writec( "", " * Translation Parameters" )
```

```
jobfile.writec( "", " */" )
jobfile.writec( "", "" )
jobfile.writec( "DATA OUTPUT", "XDB+PRINT" )
jobfile.writec( "OUTPUT2 REQUESTS", "P3 Built In" )
jobfile.writec( "OUTPUT2 FORMAT", "Binary" )
jobfile.writec( "DIVISION TOLERANCE", "1.0e-08" )
jobfile.writec( "NUMERICAL TOLERANCE", "1.0e-04" )
jobfile.writec( "WRITING TOLERANCE", "1.0e-21" )
jobfile.writec( "GEOM CHECK", "INFORM" )
jobfile.writec( "SORTED BULK", "NO" )
jobfile.writec( "CARD FORMAT", "either" )
jobfile.writec( "NODE COORDINATES", "reference frame" )
jobfile.writec( "COORD COORDINATES", "global" )
jobfile.writec( "MSC.Nastran VERSION", "2017." )
jobfile.writec( "WRITE STORED PRECISION", "TRUE" )
jobfile.writec( "PROPS ON ELEM ENTRY", "FALSE" )
jobfile.writec( "CONTINUATION ENTRY", "FALSE" )
jobfile.writec( "PCOMPG ENTRY", "TRUE" )
jobfile.writec( "CONVERT CBAR CBEAM", "FALSE" )
jobfile.writec( "ITERATIVE SOLVER", "FALSE" )
jobfile.writei( "SUPER ELEMENT 0", 0 )
jobfile.writec( "SEALL WRITE", "FALSE" )
jobfile.writec( "PART SUPERELEMENT CREATE", "TRUE" )
jobfile.writec( "AUTOQSET", "FALSE" )
jobfile.writec( "FIXEDB", "FALSE" )
jobfile.writei( "SUPER TREE COUNT", 0 )
jobfile.writec( "MODEL TOLERANCE", "0.0049999999" )
jobfile.writec( "ELEMENT PROPERTY OFFSET", "0" )
jobfile.writec( "MATERIAL PROPERTY OFFSET", "0" )
jobfile.writec( "TABLE OFFSET", "0" )
jobfile.writec( "LOAD SET OFFSET", "0" )
```

```
jobfile.writec( "LOAD CASE OFFSET", "0" )
jobfile.writec( "CONTROL SET OFFSET", "0" )
jobfile.writec( "RIGID ELEMENT OFFSET", "0" )
jobfile.writec( "SCALAR POINT OFFSET", "0" )
jobfile.writec( "BEGINNING CONTINUATION MARKER", "+      A" )
jobfile.writec( "NUMBER ONLY", "ON" )
jobfile.writec( "BEGINNING NUMBER", "OFF" )
jobfile.writec( "TRAILING NUMBER", "OFF" )
jobfile.writec( "SYNTAX NUMBER", "ON" )
jobfile.writec( "SYNTAX MARKER", "." )
jobfile.writec( "EXTERNAL SUPERELEMENT METHOD", "NONE" )
jobfile.writec( "GRID COORDINATES ROUNDING", "15" )
jobfile.writec( "COORD DATA PRECISION ROUNDING", "15" )
jobfile.writec( "MPC DATA PRECISION ROUNDING", "15" )
jobfile.writec( "LBC DATA PRECISION ROUNDING", "7" )
jobfile.writec( "MAT DATA PRECISION ROUNDING", "7" )
jobfile.writec( "PROP DATA PRECISION ROUNDING", "7" )
jobfile.writec( "", "" )
jobfile.writec( "", "/*" )
jobfile.writec( "", " * Solution Parameters" )
jobfile.writec( "", " */" )
jobfile.writec( "", "" )
jobfile.writec( "SOLUTION TYPE", "FREQUENCY RESPONSE" )
jobfile.writei( "SOLUTION SEQUENCE", 111 )
jobfile.writec( "DATABASE RUN", "ON" )
jobfile.writec( "FORMULATION", "Modal" )
jobfile.writec( "CYCLIC SYMMETRY", "OFF" )
jobfile.writec( "AUTOMATIC CONSTRAINTS", "ON" )
jobfile.writec( "SHELL NORMAL TOLERANCE", "" )
jobfile.writec( "MASS CALCULATION", "Lumped" )
jobfile.writec( "DATA DECK ECHO", "None" )
```

```
jobfile.writec( "PLATE RZ STIFFNESS FACTOR", "100.0" )
jobfile.writec( "MAXIMUM PRINTED LINES", "" )
jobfile.writec( "MAXIMUM RUN TIME", "" )
jobfile.writec( "WT-MASS CONVERSION", "1.0" )
jobfile.writec( "NODE ID FOR WT-GENER", "" )
jobfile.writec( "RIGID ELEMENT TYPE", "LINEAR" )
jobfile.writec( "STRUCTURAL DAMPING COEFF.", "" )
jobfile.writec( "RESIDUAL VECTOR", "Nastran Default" )
jobfile.writec( "REAL EIGENVALUE EXTRACTION METHOD", "Lanczos" )
jobfile.writec( "LOWER FREQUENCY RANGE", "" )
jobfile.writec( "UPPER FREQUENCY RANGE", "" )
jobfile.writec( "REAL EIGNVALUE NUMBER OF DESIRED ROOTS", "10" )
jobfile.writec( "DIAGNOSTIC OUTPUT LEVEL", "0" )
jobfile.writec( "USE CONTACT TABLE", "OFF" )
jobfile.writec( "INITIAL CONTACTPAIR LOADCASE NAME", "" )
jobfile.writei( "MDOF DATA", 0 )
jobfile.writec( "CELL WRITE", "ON" )
jobfile.writei( "CELL INPUT 0", 0 )
jobfile.writec( "FMS WRITE", "ON" )
jobfile.writei( "FMS INPUT 0", 1 )
jobfile.writec( "FMS INPUT 1", "ASSIGN USERFILE=erp.csv UNIT=30 FORMATTED " // @
"NEW DELETE" )
jobfile.writec( "EXEC WRITE", "ON" )
jobfile.writei( "EXEC INPUT 0", 0 )
jobfile.writec( "CASE WRITE", "ON" )
jobfile.writei( "CASE INPUT 0", 2 )
jobfile.writec( "CASE INPUT 1", "ERP(SORT2,PRINT,FILTER=0.0, SOLUTION=ALL," // @
```

```
" CSV=30,RHOCP=2.0E9," )
jobfile.writec( "CASE INPUT 2", ", ERPC=3.4E5, ERPRHO=1.0E-12) =
ALL" )
jobfile.writec( "BULK WRITE", "ON" )
jobfile.writei( "BULK INPUT 0", 2 )
jobfile.writec( "BULK INPUT 1", "ERPPNL,PANEL,101" )
jobfile.writec( "BULK INPUT 2", "SET3,101,PROP,1" )
jobfile.writec( "CELL DTI POSITION", "START" )
jobfile.writec( "FMS DTI POSITION", "START" )
jobfile.writec( "EXEC DTI POSITION", "START" )
jobfile.writec( "CASE DTI POSITION", "START" )
jobfile.writec( "BULK DTI POSITION", "START" )
jobfile.writec( "", "END" )
jobfile.close( )
mscnastran_job.associate_subcases( "111", "erp", 1, ["Default"] )
analysis_submit_2( "MSC.Nastran", "erp" )
```

List of figures

List of tables